Microwave-assisted Solid State Synthesis of Cathode Materials Incorporating Chitin for Lithium Iron Phosphate Batteries

Ekawat Ratchai

A Thesis Submitted in Fulfillment of the Requirements for the
Doctor of Philosophy in Sustainable Energy Management
Prince of Songkla University
2022

Microwave-assisted Solid State Synthesis of Cathode Materials Incorporating Chitin for Lithium Iron Phosphate Batteries

Ekawat Ratchai

A Thesis Submitted in Fulfillment of the Requirements for the

Doctor of Philosophy in Sustainable Energy Management

Prince of Songkla University

2022

Thesis Title   Microwave-assisted Solid State Synthesis of Cathode Materials

                          Incorporating Chitin for Lithium Iron Phosphate Batteries

Author   Mr. Ekawat Ratchai

Major Program Sustainable Energy Management

Major Advisor

....
(Asst. Prof. Dr. Montri Luengchavanona)

Co-advisor

....
(Assoc. Prof. Dr. Kua-anan Techatoa)

Examining Committee:

....Chairperson
(Assoc. Prof. Dr. Chitnarong Sirisathitkul)

....Committee
(Assoc. Prof. Dr. Suchada Chantrapromma)

....Committee
(Assoc. Prof. Dr. Kua-anan Techatoa)

....Committee
(Asst. Prof. Dr. Montri Luengchavanona)

....Committee
(Asst. Prof. Dr. Khamphe Phoungthong)

        The Graduate School, Prince of Songkla University, has approved this thesis as fulfillment of the requirements for the Doctor of Philosophy Degree in Sustainable Energy Management

....
(Prof. Dr. Damrongsak Faroongsarng)
Dean of Graduate School

This is to certify that the work here submitted is the result of the candidate's own investigations. Due acknowledgement has been made of any assistance received.

....Signature

(Asst. Prof. Dr. Montri Luengchavanona)

Major Advisor

....Signature

(Assoc. Prof. Dr. Kua-anan Techatoa)

Co-advisor

....Signature

(Mr. Ekawat Ratchai)

Candidate

I hereby certify that this work has not been accepted in substance for any degree, and is not being currently submitted in candidature for any degree.

....Signature

(Mr. Ekawat Ratchai)

Candidate

ชื่อวิทยานิพนธ์	การสังเคราะห์วิธีโซลิตสเตตโดยใช้ไมโครเวฟช่วยในการผลิตวัสดุแคโทดร่วมกับไคตินสำหรับแบตเตอรี่ลิเทียมไอรอนฟอสเฟส
ผู้เขียน	เอกวัฒน์ ราชไชย
สาขาวิชา	การจัดการพลังงานอย่างยั่งยืน
ปีการศึกษา	2565

บทคัดย่อ

วัสดุแคโทดเป็นส่วนประกอบที่สำคัญสำหรับแบตเตอรี่ลิเทียมไอรอนฟอสเฟต (LFP) เนื่องด้วยต้นทุนในการผลิตต่ำ, มีความปลอดภัยสูง, ไม่เป็นพิษและเป็นมิตรต่อสิ่งแวดล้อม อย่างไรก็ตามวัสดุแคโทดที่ผลิตจากลิเทียมไอรอนฟอสเฟตมีข้อเสียคือมีการนำไฟฟ้าที่ไม่ดีและมีความหนาแน่นของพลังงานต่ำ ซึ่งข้อเสียดังกล่าวสามารถปรับปรุงและแก้ไขได้ด้วยกระบวนการสังเคราะห์และการเคลือบคาร์บอนที่วัสดุแคโทด วิทยานิพนธ์ฉบับนี้มีวัตถุประสงค์เพื่อปรับปรุงประสิทธิภาพของวัสดุแคโทดสำหรับแบตเตอรี่ลิเทียมไอรอนฟอสเฟต โดยใช้ไมโครเวฟช่วยวิธีโซลิดสเตตร่วมกับไคติน (LFPM) เพื่อสังเคราะห์วัสดุแคโทดสำหรับแบตเตอรี่ลิเทียมไอรอนฟอสเฟต ผลการศึกษาพบว่า 1) ปริมาณคาร์บอนจากไคตินที่เคลือบวัสดุ LFPM เท่ากับ 19.80 wt% และเป็นเนื้อเดียวกันกับวัสดุ LFPM มีขนาดอนุภาคเฉลี่ยประมาณ 380 nm, 2) เวลาที่เหมาะสมที่สุดในการสังเคราะห์วัสดุแคโทด LFPM โดยการใช้ไมโครเวฟช่วยวิธีโซลิดสเตต คือ 5 นาที ทำให้วัสดุมีผลึกที่บริสุทธิ์ คุณภาพสูงและมีค่านำไฟฟ้ามากที่สุด และ 3) เมื่อทดสอบประสิทธิภาพทางไฟฟ้าเคมี พบว่าความจุเริ่มต้นในการอัดและคายประจุเท่ากับ 108.88 และ 112.23 mAh/g ที่อัตรา 1C-rate ตามลำดับ, ค่า columbic efficiency เท่ากับ 97.01% และค่า capacity retention เท่ากับ 99.99% หลังการอัดและคายประจุครบ 20 รอบ และมีค่าความหนาแน่นพลังงานเริ่มต้นเท่ากับ 336.68 Wh/kg จึงสามารถสรุปได้ว่าวัสดุแคโทดสำหรับแบตเตอรี่ลิเทียมไอรอนฟอสเฟตที่สังเคราะห์ด้วยกระบวนการไมโครเวฟช่วยวิธีโซลิดสเตตร่วมกับไคติน มีประสิทธิภาพทางไฟฟ้าที่ดี สามารถนำไปพัฒนาและต่อยอดในการผลิตเชิงพาณิชย์ต่อไป

คำสำคัญ: แบตเตอรี่ลิเทียมไอรอนฟอสเฟส, ไมโครเวฟร่วมกับโซลิดสเตต, คาร์บอนเคลือบ

Thesis Title   Microwave-assisted Solid State Synthesis of Cathode Materials Incorporating Chitin for Lithium Iron Phosphate Batteries

Author   Mr. Ekawat Ratchai

Major Program   Sustainable Energy Management

Academic Year   2022

ABSTRACT

Cathode materials have long been recognized as an important component for lithium iron phosphate (LFP) batteries due to their low production costs, high safety, non-toxicity, and environmental friendliness. However, cathode materials made from lithium iron phosphate have the disadvantage of poor electrical conductivity and low energy density. Such disadvantages can be improved by synthesis methods and carbon coating methodologies on the cathode material. This thesis therefore aims to improve cathode efficiency for lithium iron phosphate batteries. A microwave-assisted solid-state method with chitin (LFPM) was used to synthesize cathode materials for lithium iron phosphate batteries. The results revealed that the carbon element from chitin-coated LFPM material is 19.80 wt%, which can be homogeneously mixed for LFPM material and has an average particle size of ~380 nm. The optimal time for the synthesis of the LFPM cathode material by the microwave-assisted solid-state method is 5 minutes, resulting in a phase pure, high-quality crystalline, and the most electrical conductivity. Regarding the electrochemical performance, the initial charge and discharge capacities were 108.88 and 112.23 mAh/g at 1C-rate, respectively, the columbic efficiency was 97.01%, and the capacity retention was 99.99% after 20 charge and discharge cycles. The initial energy density was 336.68 Wh/kg. It can be concluded that the cathode material for lithium iron phosphate batteries synthesized by the microwave-assisted solid-state method coated with carbon derived from chitin has good electrical performance, which can be manufactured on a large scale and is commercially feasible.

Keywords: Lithium Iron Phosphate Batteries, Microwave-assisted Solid State Synthesis, Carbon Coating

ACKNOWLEDGEMENT

CONTENTS

CONTENTS (CONTINUED)

LIST OF TABLES

LIST OF FIGURES

LIST OF FIGURES (CONTINUED)

LIST OF FIGURES (CONTINUED)

LIST OF ABBREVIATIONS

Abbreviation	Description
C	Carbon
C_3H_6O	Acetone solution
C_2H_5OH	Ethanol solution
CNT	Carbon nanotubes
Co	Cobalt
CoO_6	Cobalt (III) oxide
CV	Cyclic voltammetry
DMC	Dimethyl carbonate
EC	Ethylene carbon
EDX	Energy dispersive X-ray analysis
EIS	Electrochemical impedance spectroscopy
Fe	Iron
FeO_6	Iron (II) oxide (Ferrous oxide)
Fe_2O_3	Iron (III) oxide (Ferric oxide)
$FePO_4$	Iron phosphate
H	Hydrogen
HCl	Hydrochloric acid
H_3PO_4	Phosphoric acid
Lead-acid	Lead acid batteries
LFP	Lithium iron phosphate battery
LFPM	Microwave irradiation on cathode material
LFPM5	Microwave irradiation on cathode material of 5 minutes
LFPM10	Microwave irradiation on cathode material of 10 minutes
LFPM15	Microwave irradiation on cathode material of 15 minutes
LFPM20	Microwave irradiation on cathode material of 20 minutes
Li	Lithium
$LiAsF_6$	Lithium hexafluororoarsenate
$LiBF_4$	Lithium tetrafluoroborate

LIST OF ABBREVIATIONS (CONTINUED)

Abbreviation	Description
LiC_6	Lithium carbide
Li_2CO_3	Lithium carbonate
$LiCF_3SO_3$	Lithium trifluoromethanesulfonate
$LiCoO_2$	Lithium cobalt oxide
$LiCoPO_4$	Lithium cobalt phosphate
Li-ion	Lithium-ion batteries
LiO_6	Lithium octahedra
$LiMPO_4$	Lithium metal phosphate
$LiMn_2O_4$	Lithium manganese oxide
$LiPF_6$	Lithium hexafluorophosphate
Li-Po	Lithium polymer battery
$LiFePO_4$	Lithium iron phosphate
$LiFePO_4/C$	Carbon coatings on lithium iron phosphate
$LiMnPO_4$	Lithium manganese phosphate
$LiNiPO_4$	Lithium nickel phosphate
Li_3PO_4	Lithium phosphate
M	Early transition metal
Mn	Manganese
Mo	Molybdenum
MnO_6	Manganese lactates
Ni	Nickel
Ni-Cd	Nickel cadmium batteries
Ni-MH	Nickel metal hydride batteries
NMP	N-Methyl-2-pyrrolidone
O	Oxygen
P	Phosphorus
PC	Propylene carbonate
PEG	Polyethylene glycol

LIST OF ABBREVIATIONS (CONTINUED)

Abbreviation	Description
pH	Potential of hydrogen
PO_4	Phosphate ion
PVDF	Poly (vinylidene fluoride)
S	Sulfur
SEM	Scanning electron microscopy
Si	Silicon
V	Vanadium
W	Tungsten (Wolfram)
XRD	X-ray diffraction

LIST OF SYMBOLS

Symbol	Description
n	an integer
λ	the incident wave's wavelength
d	the distance between the planes in the atomic lattice
θ	the angle between the incident ray and the scattering planes

CHAPTER 1

INTRODUCTION

1.1 Energy storage batteries

Energy and environmental issues have emerged as major concerns in the twenty-first century, potentially altering the course of life on Earth [1]. Climate change, toxic pollution, acid deposition, and diminishing energy supplies are all frightening difficulties straightforwardly related to technological advancement [2]; thus, the search for alternative energy sources continues. Currently, the energy economy, which is primarily based on fossil fuels, is under threat due to the depletion of nonrenewable resources and the ever-increasing demand for energy [3]. Since the dawn of time, one of the most challenging questions and societal challenges has been the production and storage of energy, with far-reaching implications for the environment, human health, and the global economy [4].

Conventional forms of energy (coal, oil, and natural gas) that took millions of years to form are depleting and non-renewable [5], and thereby generating regional and worldwide controversy and environmental degradation. As a result, we should strive to achieve a sustainable, environmentally friendly, and low-cost energy supply at present by incorporating renewable energy sources (solar energy, wind power, geothermal energy, biomass and biofuel, hydropower) with mobile energy storage devices that can rapidly obtain and release energy [6, 7]. However, even though sustainable energy sources keep changing during the present time, adopting sustainable energy for electricity generation necessitates the implementation of proportionately appropriate energy storage devices [8].

A battery is a type of power source that converts chemical energy into electrical energy [9]. Batteries are classified into two types: primary and secondary batteries [10]. Primary batteries (such as zinc-carbon, alkaline zinc-manganese dioxide, and metal-air-depolarized batteries) are often non-rechargeable and

disposable. After usage, primary batteries are discarded or chemically recycled if legally (environmentally) required or for material cost savings [11]. As a result, when discharged, they are first discarded since the materials used in primary batteries may not return to normal form due to the chemical reaction being difficult to reverse.

Lead acid batteries (Lead-acid), nickel cadmium batteries (Ni-Cd), nickel metal hydride batteries (Ni-MH), and lithium-ion batteries are examples of secondary batteries (Li-ion). The term "rechargeable batteries" refers to the fact that they can be recharged multiple times after each discharge by using an electric current to reverse the chemical reaction that occurs during discharging, thereby making the battery reusable [12]. There have been various materials and procedures used in the manufacture of rechargeable batteries. However, various studies show that the lithium-ion battery is the best rechargeable battery technology in terms of gravimetric energy density, as shown in Figure 1.1.
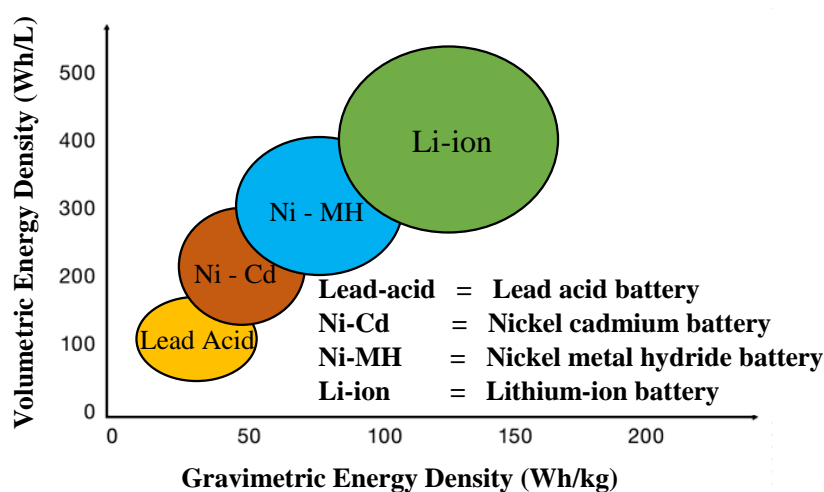
Figure 1.1 A comparison of different rechargeable battery technologies

1.2 Lithium iron phosphate batteries

Table 1.1 summarizes the most important electrochemical performance parameters of lithium-ion batteries that can be compared to other types of rechargeable batteries. It demonstrates that the performance of various rechargeable

lithium-ion batteries (Li-ion) outperforms all other types of batteries. It also has a low self-discharge, a short charge time, and short-cycle durability.

Table 1.1 A comparison of the performance of different rechargeable batteries

Types of batteries	Energy density (Wh/kg)	Cycle durability (Cycle)	Self-discharge (Per month; %)	Cell voltage (V)	Charge time (h)
Ni-MH	30 - 80	500 - 1,000	25 - 30	1.2	2 - 4
Ni-CD	40 - 60	1,500	10 - 20	1.25	1
Lead-acid	30 - 40	600 - 800	5 - 20	2.1	8 - 16
Li-ion	100 - 170	1,200	5 - 12	3.5	1 - 3

Furthermore, the lithium-ion battery has almost no memory effect and can thus be recharged at any time [13]. Given these characteristics, lithium-ion battery devices can provide a dependable rechargeable system to meet the demand for electrochemical performance and high efficiency [14].

More research is needed to improve the performance of commonly used lithium-ion batteries in order to achieve high performance batteries, particularly in terms of electrochemical performance [13]. Many factors, such as anode, cathode, and electrolyte components, can have an impact on the performance of lithium-ion batteries. However, the cathode material is now the most important determining factor for energy density in lithium-ion batteries because it has a lower specific capacity than the graphite anode material [15]. Furthermore, the main rate-limiting step in a lithium-ion battery system is Li transport/diffusion on the cathode [16].

As shown in table 1.2, there are three main types of materials used to form cathode polarity currently. The first kind of material is one with a layered structure, such as $LiCoO_2$ (Lithium cobalt oxide). The second is a spinel structure, similar to $LiMn_2O_4$ (Lithium manganese oxide). The last type is the olivine structure, which is found in $LiFePO_4$ (Lithium iron phosphate). Because of its high energy density, $LiCoO_2$ is the most important cathode material in lithium-ion batteries used

in portable devices [17]. Co, on the other hand, is hard to come by. The main disadvantages are the cost and the lack of safety [18].

Table 1.2 A comparison of the performance of various lithium-ion batteries materials

Types of materials	Voltage average (V)	Advantages	Disadvantages
$LiCoO_2$	3.6-3.7	- high efficiency	- low capacity - expensive - toxicity
$LiMn_2O_4$	3.7-3.8	- high voltage - high efficiency - low cost	- low capacity - low life cycle
$LiFePO_4$	3.3	- low toxicity - low cost - high security	- low capacity - low voltage

Spinel structure or LiMn2O4 is frequently used in work requiring high safety and a large amount of material, such as electric cars and energy storage from renewable energy sources. Because of this property, $LiMn_2O_4$ uses Mn instead of Co, making it less expensive, safer, and more environmentally friendly than $LiCoO_2$ [19]. However, spinel structure has a complex structure and phase shift mechanism when working with complex and unstable material above 50 °C [20, 21]. Despite the fact that the olivine structure or $LiFePO_4$ can store less energy than spinel and layered structures [22], it is a low-cost material because Fe is not only easier to find but also cheaper than Co. Furthermore, it is environmentally friendly, stable, and safe. Consequently, $LiFePO_4$ is appropriate for high-risk equipment or innovation, such as electric vehicles [23]. $LiFePO_4$ is also suitable for work that requires a large amount of material at a low cost, such as electric energy storage from renewable energy sources [24].

That is to say, $LiFePO_4$ has outstanding properties such as low cost, non-toxicity, high durability, and easy temperature control, the ability to store electronic energy, high stability at high temperatures, high security, and environmental friendliness. It does, however, have some disadvantages, such as inadequate ionic diffusion and poor electrical conductivity, which limit its application

in devices and its ability to work at low charge and discharge current densities [25, 26]. These are the main challenges in this thesis. As a result, optimizing the morphology, particle size, carbon coating, and transition metal doping is expected to improve the performance of those materials at higher current rates [27-30]. To improve the electrochemical performance of $LiFePO_4$, many researchers have examined particle size reduction and carbon coating methodologies.

A carbon coating is typically formed during the synthesis of $LiFePO_4$ by carbonization of organic/polymeric compounds or by mixing with carbon materials [31, 32]. Aside from the good performance of carbon coating, organic carbon coated with electrodes has been developed to improve the electrochemical properties of lithium-ion batteries. For example, it was found that superior electrochemical performance is due to decreased size and high polarity, which provide enlarged Li^+ diffusion channels and increased electronic conductivity [33, 34]. When first coated with carbon, $LiFePO_4$ was said to have a capacity of 160 mAh/g at 1C-rate at 80 °C. Carbon can also be coated on the surface of the $LiFePO_4$ thin-film, demonstrating good cyclic performance and rate capability [35-38].

The organic carbon (sucrose) was also coated on $LiFePO_4/C$ to improve the performance of battery cathode materials, demonstrating capacity retention of 94% of the initial discharge capacity after 30 cycles and good electrochemical performance [39]. Rate performance of 163.4 mAh/g at 0.2C-rate was also demonstrated, as was cycling stability of 99.3% capacity retention after 300 cycles at 0.2C-rate [40]. Recently, there has been much more interest in chitin (an organic carbon) for energy-storage applications, specifically the preparation of nitrogen-doped (porous) carbons such as porous carbon fibers and nanofibrous microspheres with hierarchical porosity.

Chitin-derived porous carbon electrode materials for energy storage applications have received attention because of their wide accessibility, high porosity, low weight, natural biodegradability, renewability, and eco-friendliness [41, 42]. When hard carbons from chitin (shrimp shell) were prepared as an electrode material for Na-ion batteries, they were discovered to have a 44.00wt%, an initial specific

charge of 280 mAh/g at 0.1C-rate, and a high columbic efficiency of 97.03% [41]. Interestingly, chitin is an organic carbon found in living things as a biopolymer, and it can be used as an alternative raw material in the modified synthesis of $LiFePO_4$ materials.

To address the drawbacks mentioned earlier of LiFePO4, these various fabrication approaches can be broadly classified into three categories, based on which three general approaches to improving LiFePO4's electrochemical performance can be derived: 1) to enhance electronic conductivity by incorporating conductive additives, such as coating carbon during the synthesis of $LiFePO_4$/C composites, or dispersing copper, silver, and other metals into the solution during synthesis [28, 43-45]; 2) to manage particle size and grow homogeneous composite materials $LiFePO_4$ nanoparticles by improving the synthesis conditions [46-48]; and 3) to selectively dope [49, 50]. However, novel $LiFePO_4$ synthesis methods should be developed to improve its electrochemical performance. To prepare $LiFePO_4$, various synthesis routes such as solid state, hydrothermal, sol-gel, co-precipitation, and microwave processes have been proposed. However, solid-state reaction synthesis is still the most common and traditional method of producing $LiFePO_4$ [51].

The solid-state synthesis approach entails chemical decomposition reactions in which a combination of solid reactants is heated to make a new solid composition and gases, which are the most commonly, used method due to its simple procedure, short reaction time, and high efficiency [52-54]. The disadvantages of the solid-state method are that it takes time and energy. Unlike conventional heating, microwave heating, the preparation of $LiFePO_4$ cathode material, is a self-heating process that occurs over a short period through the absorption of electromagnetic energy, resulting in energy savings and a reduction in manufacturing costs [55, 56].

Therefore, the $LiFePO_4$/C was prepared using a microwave irradiation method. An electrode's excellent rate capability, high discharge capacity, and good electrochemical reversibility were discovered [57]. $LiFePO_4$/C was also prepared using a microwave-assisted solid-state method. The results revealed a straightforward and efficient method with high crystallinity and a narrow particle size distribution

[58]. Rapid microwave irradiation has recently received attention due to the advantages of low cost and super-fast volumetric heating [59]. Simultaneously, a highly crystalline $LiFePO_4/C$ phase was successfully synthesized in 4 minutes [60]. In contrast, 3 minutes of microwave calcination resulted in the smallest particle size (mostly between 100 and 150 nm) and the highest electrochemical operation for the Li-ion intercalation process [61].

Therefore, to achieve high electrochemical performance, the development of cathode materials properties coated with organic carbon (chitin) using the microwave-assisted solid-state synthesis of cathode materials for lithium iron phosphate batteries was investigated in this thesis.

1.3 Thesis objectives

The objectives of the present thesis are three folds:

1. to synthesize cathode materials for lithium iron phosphate batteries with solid-state method and microwave-assisted synthesis,

2. to investigate the best conditions for cathode materials for lithium iron phosphate batteries in terms of electrochemical performance, and

3. to describe the performance of cathode materials for lithium iron phosphate batteries based on physical characterization and electrochemical measurements.

CHAPTER 2

BACKGROUND AND LITURATURE REVIEW

For decades, lithium metal has been the most appealing and suitable material used as the cathode in lithium-ion batteries (Li-ion) [62]. Due to their high energy density, lithium-ion batteries are becoming increasingly popular for use in electric vehicles, hybrid electric vehicles, renewable energy storage applications, and consumer electronics [63]. Figure 2.1 represents various commercial batteries that typically display the gravimetric energy density relationship between various energy efficiency devices. Obviously, Li-ion outperforms Lead-acid, Ni-Cd, Ni-MH, and Li-Po in terms of its high energy efficiency and gravimetric energy density.
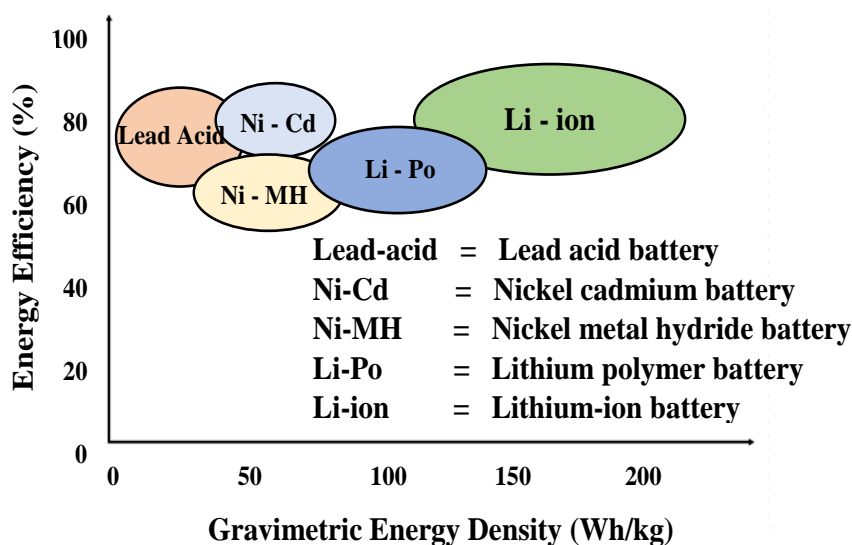
Figure 2.1 A comparison of various commercially available batteries

2.1 Lithium-ion batteries

There is currently an abundance of competing lithium-ion batteries on the market, each with its own set of advantages and disadvantages when compared to one another. Table 2.1 compares the cathode materials used in different types of lithium-ion batteries. While all modern lithium-ion batteries use the same materials for the anode and electrolyte, the cathode material varies greatly and is usually

classified primarily by cathode material [64]. The three most common types of lithium-ion batteries are lithium cobalt oxide ($LiCoO_2$), lithium manganese oxide ($LiMn_2O_4$), and lithium iron phosphate ($LiFePO_4$) [65].

Table 2.1 A comparison of the cathode materials used in various lithium-ion batteries

Chemical Name	Material	Specific capacity (mAh/g)	Voltage (V)	Notes
Lithium Cobalt Oxide	$LiCoO_2$	170	3.7	High capacity, low-rate capability
Lithium Manganese Oxide	$LiMn_2O_4$	120-140	3.9	Most safe, lower capability, high power
Lithium Iron Phosphate	$LiFePO_4$	130	3.3	Low capacity, high-rate capability, flat discharge

As shown in Table 2.1, lithium manganese oxide (manganese-based compounds (Spinels structure: $LiMn_2O_4$)) is now of main interest to battery manufacturers because manganese is the safest, high-power, and voltage source [66-68]. Unfortunately, the use of lithium manganese spinel is constrained by several operational issues, the most serious of which is manganese dissolution into the electrolyte during cycling in lithium cells, resulting in a shorter lifespan than lithium cobalt oxide [69].

Another cathode material with high specific energy and capacity for devices is lithium cobalt oxide (cobalt-based compounds (layered structure: $LiCoO_2$)) [70]. However, for several reasons, this material cannot be used for the next generation of energy storage: production of $LiCoO_2$ is expensive, Co is toxic, and batteries based on $LiCoO_2$ would be highly polluting [71-73]. Currently, the lithium iron phosphate cathode material, which has a high-rate capability and flat discharge, is getting more attention (Olivine structure: $LiFePO_4$). Its additional benefits include low cost, environmental friendliness, and abundance of elements [74]. However, the voltage is slightly lower than in the other chemistries, and the energy is relatively low [75]. As a result, depending on the application for which lithium-ion batteries are

required, the decisions about active materials must be made to determine which one is the most appropriate.

The olivine structure, $Li_xM_y (XO_4)_z$ (M = metal, X = P, S, Si, Mo, W), is now considered the most suitable cathode material for future lithium-ion batteries [76]. Since its discovery, lithium iron phosphate ($LiFePO_4$) has received the most attention. Since its first synthesis in Goodenough's group in 1997, $LiFePO_4$ has been one of the most widely used and researched cathode materials for lithium-ion batteries [77]. $LiFePO_4$ has been recognized for characteristics such as a high reversible capacity of 170 mAh/g at 3.45 V, a potentially low cost of production, being one of the most abundant metals on earth, environmental compatibility, long cycle ability, and high safety [26, 78, 79].

Presently, research is being conducted to enhance lithium-ion battery cathode materials' stability and electrochemical performance [80]. Excellent cathode materials should also have the following properties: 1) high redox potential; 2) high reversibility; 3) high lithium ion hosting to provide sufficient capacity; 4) high specific surface area to increase reduction/oxidation reaction rates; 5) high electronic conductivity to transfer electron instantly and reduce heat generation; 6) high ionic conductivity to verify small polarization and high capability; 7) low volume structure change during Li^+ insertion/extraction to confirm cycling stability [15, 69, 81].

Furthermore, the nature of the interfaces between the electrodes and electrolyte affects the cycle-life and lifetime of lithium-ion batteries, whereas safety is determined by the stability of the electrodes and electrode/electrolyte interfaces [82]. Thus, new cathode materials contribute significantly to developing better lithium-ion batteries with high electrochemical performance, long life, small size, low cost, and environmentally friendly compatibility [83-86]. Typically, the basic properties of cathode materials should: 1) be a reducible/oxidizable ion, including a transition metal; 2) intercalate lithium reversibly and without considerable structural change; 3) react with lithium with high free energy for high voltage; 4) react with lithium instantly during insertion/removal for output efficiency; 5) be an excellent electrochemical conductor, and 6) be the least expensive and sustainable [87-89].

Since there is a strong interest in further developing this type of cathode material, this thesis aims at describing novel synthetic routes to produce LiFePO$_4$ cathode material for lithium-ion batteries.

2.2 Components of lithium-ion batteries

In general, cathode materials (positive electrode), anode materials (negative electrode), and electrolytes serve as conductors in lithium-ion batteries [90]. The cathode is composed of metal oxide, while the anode is composed of porous carbon [91]. Throughout discharge, ions flow from the anode to the cathode through the electrolyte and separator. On the other hand, ions flow from the cathode to the anode during charge [32]. Ions transfer between the cathode and anode once the cell charges and discharges. The anode oxidizes, or loses electrons, during discharge, whereas the cathode reduces, or gains electrons [22]. Charge, as shown in figure 2.2, reverses the movement.
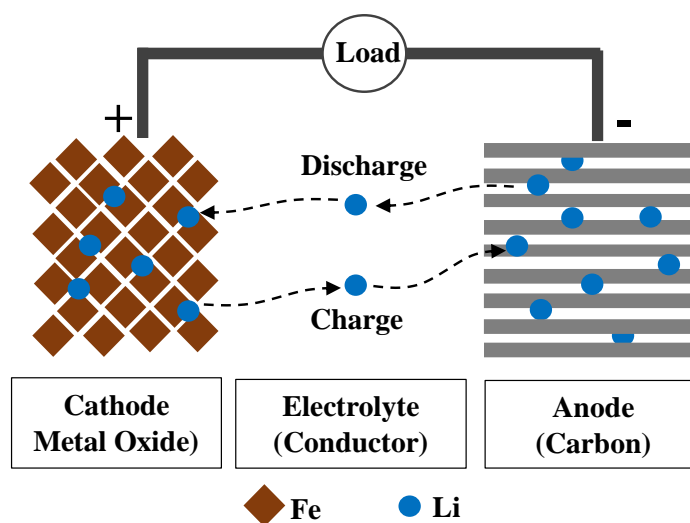
Figure 2.2 The charge and discharge principle for lithium-ion batteries

2.2.1 Anode

During the electrochemical discharge reaction, the anode is the negative electrode that releases electrons to the external circuit and oxidizes [92]. To use carbon material in an anode to create high energy density batteries, the anode carbon

material's lithium storage capability must be improved [93, 94]. There are five types of carbon anode materials: 1) graphite, 2) carbon nanotubes (CNT), 3) amorphous carbon materials, 4) mesoporous carbon materials, and 5) carbon materials derived from biomass [95].

1) Graphite is one of the most commonly used anode materials in commercial lithium-ion batteries. It also corresponds to the formation of LiC_6 and is commonly used the active material in negative electrodes due to the ability to place Lithium-ions between its many layers reversibly [96]. On the other hand, the high cost of synthetic graphite production serves as a significant economic force for the development of new natural graphite sources for energy conversion and storage devices in general [97].

2) Carbon Nanotube (CNT), one of several carbon allotropes, has been approved as an additive or substitute in the anode of lithium-ion batteries because of its chemical stability, large surface area, powerful mechanical properties, and high electrical conductivity [98]. However, a drawback of CNT-based anodes is the loss of a voltage plateau during the discharge process.

3) Amorphous Carbon consists of soft carbon materials and hard carbon materials. During lithiation/delithiation, soft carbon materials exhibit a faster lithium-ion diffusion co-efficiency and a more stable charge/discharge platform. Hard carbon materials, on the other hand, maintain a disordered structure indefinitely regardless of temperature [99]. They are typically produced through the pyrolysis of polymers such as resins and organic polymers. Because of their pore structure and excellent electrolyte compatibility, they are a potential storage material. However, during the beginning of the charging process, hard carbon materials demonstrate significant irreversible capacity degradation [100].

4) Mesoporous Carbon Materials have various advantages, including a high surface area, many active sites for lithium-ion adsorption and storage, and pore sizes ranging from nanometers to microns [101].

5) Carbon Materials Derived from Biomass are primarily composed of C, H, and O elements. Producing carbon materials from biomass materials is theoretically feasible. Furthermore, biomass materials are renewable, abundant, and environmentally friendly resources, making them appealing to use [102]. Nowadays, constructing the relationship between the structure and properties of biomass-derived carbon to guide the progress of material characteristics (such as morphology, porosity, and surface chemistry properties) and accomplishing manageable material preparation is important for the development of biomass carbon materials.

2.2.2 Cathode

There are three major types of cathode materials currently available: layered structure ($LiCoO_2$), spinel structure ($LiMn_2O_4$), and olivine structure ($LiFePO_4$) [103]. Other types of cathodes, such as conjugated organics, sulfur, air, and conversion cathodes, i.e., transition metal fluorides, have also been proposed but have yet to be commercialized. The three major cathode material types are as follows:

1) Layered structure

In the 1980s, the layered form of lithium transition metal oxide was discovered and studied [104]. The layered oxides share a general formula of $LiMO_2$, where M can be one or more transition metals (M = Ni, Co, V, Mn).
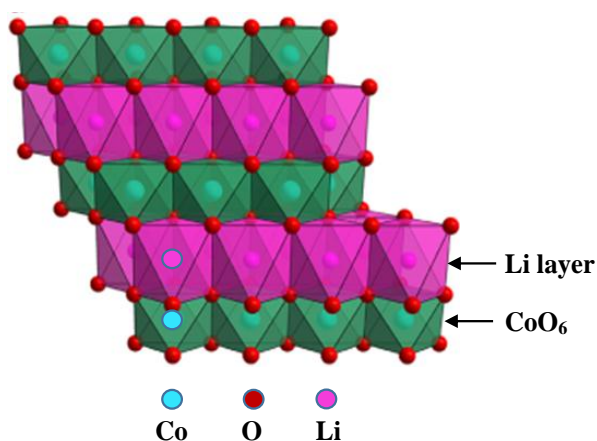
Figure 2.3 The layered crystalline structure of $LiCoO_2$ [105]

The layered $LiCoO_2$ is the most common layered oxide used as a cathode in commercial lithium-ion batteries [17]. Since its first successful usage in commercial lithium-ion batteries by SONY Company in 1991, $LiCoO_2$ has been the most popular cathode material for portable electronics [106]. Despite having a theoretical capacity of 274 mAh/g, $LiCoO_2$ has a practical capacity of 130-150 mAh/g and a working voltage of 3.5-4.2 V [107]. On the other hand, cobalt (Co) is toxic and expensive because a change in the crystal structure occurs when more than half of the Li is removed [62], resulting in irreversible capacity loss. Consequently, there has been an attempt to explore additional transition metals to replace Co [108, 109]. Various approaches have been considered to overcome these difficulties, including coating with metal oxide and reducing the amount of Co [110].

2) Spinel structure

The first spinel used as a cathode for lithium-ion batteries was $LiMn_2O_4$, proposed by Thackeray and Goodenough in 1983 [68]. It was originally introduced as a cathode material with a theoretical capacity of 148 mAh/g. The Mn ion, with a potential of 4.1 V, also provides high power capability and stability [111]. Furthermore, the spinel structures provide three-dimensional pathways for lithium migration, making spinel a high-power cathode material [112].
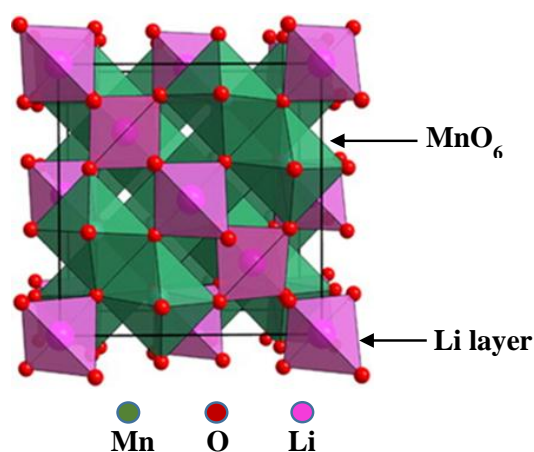
Figure 2.4 The crystalline spinel structure of $LiMn_2O_4$ [105]

On the other hand, cathodes with a spinel structure have a lower capacity by definition. Also, the dissolution of Mn is the main issue in spinel

structured cathode systems compared to olivine structured $LiMPO_4$ cathode systems [113, 114]. Substituting Mn with other metal ions has proven to be an effective method for improving the cycling performance of spinel materials. Although $LiMn_2O_4$ is a promising cathode material with excellent electrochemical properties that can be improved, its discharge capacity is low due to its inherent structure [115].

3) Olivine structure

Since Padhi et al. (1997) introduced olivine-type $LiMPO_4$ (M= Fe, Co, Mn, or Ni) as cathode materials in lithium-ion batteries, these compounds have caught the interest of researchers and developers [116]. A typical phosphate material is $LiFePO_4$, which has an orthorhombic unit cell, as shown in Figure 2.5, and has some advantages, such as low cost, non-toxicity, excellent thermal stability, low capacity fading; high cycle ability, relatively high specific capacity, and low-capacity fade [45, 62, 117, 118]. At 3.4 V, $LiFePO_4$ illustrates a flat discharge plateau and a capacity close to its theoretical capacity of 170 mAh/g [119].
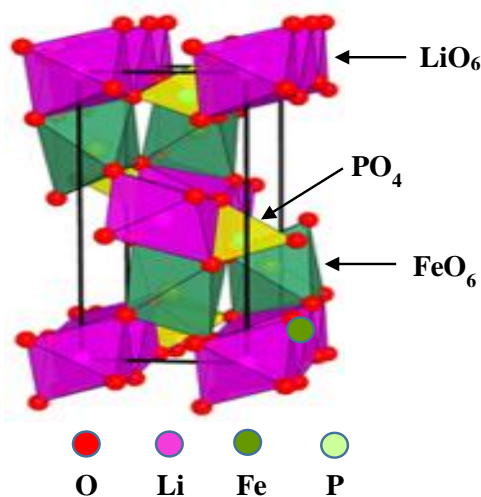
Figure 2.5 The crystalline of olivine structure of $LiFePO_4$ [105]

Other stable olivine phases with different transition metals, such as $LiMnPO_4$, $LiNiPO_4$, and $LiCoPO_4$, are also generated [120]. Because of the wide availability of Mn and its low cost, $LiMnPO_4$ material with a high operation potential of 4.1 V can be an excellent choice [121]. However, several studies have revealed that the conductivity of $LiMnPO_4$ material is lower than that of $LiFePO_4$, resulting in poor

rate capability [122]. The operation potentials of $LiNiPO_4$ and $LiCoPO_4$ materials with olivine structures are 5.1 V and 4.8 V vs. Li/Li^+, respectively [123].

The advantages of $LiNiPO_4$ include its high stability, low cost, and environment friendly. Despite their advantages, one of the major drawbacks of olivine-phased compounds is low electrical conductivity [124]. $LiCoPO_4$ materials have not been widely used in practical applications due to a number of issues, including low electronic conductivity, poor Li^+ diffusion, and limited electrolyte stability at high voltage [125, 126]. Electrolytes that had been well-developed, on the other hand, had to be stable at these high potentials. Moreover, the increased costs and environmental concerns associated with Co and Ni have made their commercial application regretful. As a result, $LiFePO_4$ will be considered the primary material in this thesis. Table 2.2 summarizes the advantages and disadvantages of three main types of cathode materials.

Table 2.2 A summary of the advantages and disadvantages of cathode materials

Crystal structure	Voltage (V)	Specific capacity (mAh/g) Theoretical/ Practical	Thermal stability	Cycling stability/ capacity retention
Layered	3.5-4.5	274/ 130-150	Moderate (Stable below 200 °C)	Moderate/ 80-95%
Spinel	4	148/ 110-120	Moderate (Stable below 200 °C)	Poor/ 58%
Olivine	3.4-3.5	170/ 160	Excellent (Stable below 400 °C)	Excellent/ 80-95%

2.2.3 Electrolyte

The electrolyte is the ionic conductor that serves as a medium for ion transfer between the anode and cathode [127]. The electrolyte must be ionic but not electronically conductive, resulting in internal short-circuiting [128]. The anode and

cathode electrodes should be physically separated by the electrolyte but electronically isolated in the cell to prevent internal short-circuiting.

Commercial lithium battery electrolytes currently use organic liquid electrolytes composed of lithium salts, for example, lithium hexafluorophosphate ($LiPF_6$), lithium tetrafluoroborate ($LiBF_4$), lithium trifluoromethanesulfonate ($LiCF_3SO_3$), and lithium hexafluororoarsenate ($LiAsF_6$) dissolved in appropriate organic solvent combinations, such as propylene carbonate (PC), ethylene carbonate. At ambient conditions, liquid electrolytes have the highest ionic conductivity (10^{-2} S/cm) [129], allowing the use of these electrolytes to realize high-performance batteries. The electrolyte in this thesis was a solution of 1 mol/L $LiPF_6$ in ethylene carbon (EC)/dimethyl carbonate (DMC) (1:1 w/w) (Sigma Aldrich: Japan).

2.3 Structure of $LiFePO_4$

$LiFePO_4$'s ordered olivine structure has the orthorhombic space group Pnma [130]. Figure 2.5 represents the crystal structure of $LiFePO_4$, which is composed of FeO_6-octahedra and PO_4-tetrahedra connected by oxygen vertices [131]. The FeO_6-octahedra then connects to other PO_4-tetrahedra via a shared edge. The PO_4-tetrahedra are not in contact with one another. As a result, phosphorus atoms occupy tetrahedral sites, iron and lithium atoms occupy octahedral sites, and oxygen atoms occupy a slightly distorted, hexagonal close-packed array [132].

$LiFePO_4$ is a stable compound due to its structure. Furthermore, because the oxygen atoms in the $(PO_4)^{3-}$ clusters are strongly covalently bonded by phosphorus atoms, the structures of $LiFePO_4$ and $FePO_4$ are stable in both oxygen and nitrogen atmospheres [123]. As a result, $LiFePO_4$ has excellent operational safety.
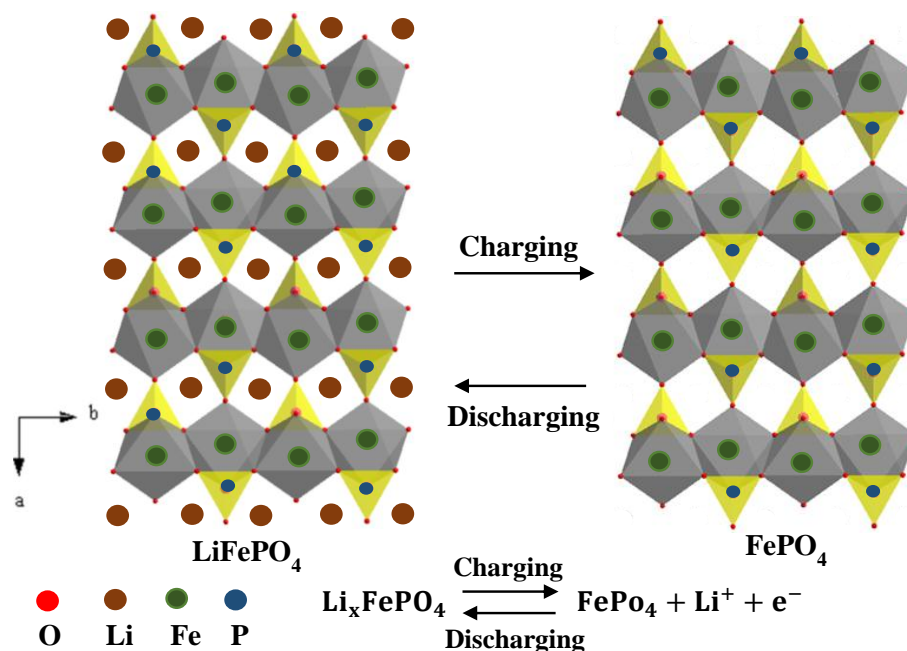
Figure 2.6 The schematic representation of LiFePO$_4$ [133]

The charge-discharge process of LiFePO$_4$ is supported by the extraction/insertion interaction between the two phases of LiFePO$_4$ and FePO$_4$ [134]. As illustrated in Figure 2.6, Li$^+$ is extracted from the structure of LiFePO$_4$ and changed to the structure of FePO$_4$ during the charge process, whereas Li$^+$ is put into the structure of FePO$_4$ and transformed to the structure of LiFePO$_4$ during the discharge process [135]. These procedures can be described as follows:

$$Li_xFePO_4 \; \rightarrow \; FePo_4 + xLi^+ + xe^- \quad \text{(Charge process)} \qquad (1)$$

$$FePO_4 \; + \; xLi^+ + \; xe^- \rightarrow \; Li_xFePO_4 \; \text{(Charge process)} \qquad (2)$$
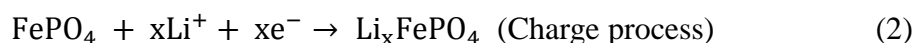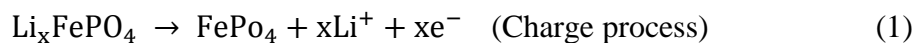
The observed structural similarities between LiFePO$_4$ and FePO$_4$ help in avoiding capacity degradation caused by severe volume changes during the charge-discharge process in cathodes and may also effectively compensate for volume changes in carbon anodes. As a result, the LiFePO$_4$/FePO$_4$ structure meets the requirements for excellent battery cycle ability. However, LiFePO$_4$ has the disadvantage of poor rate performance due to diffusion limitation (10^{-14} cm^2/s), and

low electrical conductivity (10^{-9} S/cm) [116, 136]. Its poor electrical conductivity is the main issue preventing its use in commercial production [26]. Research groups have used various methods to overcome these barriers, such as particle size reduction and carbon coating.

A reduction in grain size can result in faster reactions due to easier diffusion of intercalation ions by shortening the diffusion path, resulting in higher ion diffusion [45]. The poor electrical conductivity of $LiFePO_4$ is overcome by coating the particles' surfaces with conductive carbon films or grinding them with carbon powder [137]. Furthermore, carbon coating could protect electrode materials from electrolyte dissolution, particularly in the case of nanostructured materials due to the large solid/liquid interface, and indicating good cyclic stability [62, 138, 139]. However, the excessive coating reduces capacity and volumetric energy. Because the addition of carbon reduces the cathode material's particle density, increasing the cell's volumetric capacity is difficult [26]. As a result, the carbon coating must be optimized.

Carbon content and particle size must be optimized concurrently. Because small particles have a large surface area, a large amount of carbon is required to coat the particles. A large amount of carbon, on the other hand, reduces the material's energy density. This tends to limit electron transfer through the material, necessitating the use of additional electronically conductive material as an additive to improve the kinetics of $LiFePO_4$ electrochemical reactions. Various approaches and combinations were used to address the ionic and electronic conductivity problems in $LiFePO_4$ used as a lithium-ion battery cathode material, as follows [107];

1) Coating the surface of cathode materials with a thin layer of metal or metal oxides, such as carbon, or conductive polymers has been shown to significantly improve the electrical conductivity of the active material in most cases. Carbon coating has been extensively researched as a coating material due to its low cost, high conductivity even at low concentrations (0.52wt%), and simple coating procedures during or after the synthesis of active materials.

2) Aside from surface coating, one of the most effective and widely used approaches is to reduce the particle size of active materials. The electrode particle size was reduced primarily to achieve two goals: (1) to shorten the ion diffusion and (2) to increase the surface area of the active material. Reducing particle size results in a significant increase in rate capability. By reducing particle size, the diffusion route for lithium ions to reach the cathode materials' interior areas was considerably reduced, greatly enhancing the cathode materials' rate capabilities.

3) Additionally, metal ion doping proved important in changing the crystallographic and electronic environment of phosphate-based polyanion cathodes to improve their electronic and ionic conductivities.

2.4 Chitin

Chitin materials can be formed as the second most abundant biopolymer on earth after cellulose. [140]. Chitin has been applied to synthesise hydrogels in a wide range of applications caused of its nontoxicity, biodegradability, and biocompatibility [141, 142]. Chitin materials have always been prepared as hydrogels from native chitin, nano chitin, and chitin derivatives via chemical or physical procedures. Many publications also discussed how the electric field, magnetic field, pH, temperature, composition, and other parameters impact chitin-based hydrogel as a specific material release carrier [142-144]. Carboxymethyl chitin (CMChit) has been synthesised and has the potential to be used as a solid polymer electrolyte (SPE) due to its ionic conductivity in self-standing membranes on the order of 10^{-6} S/m [145]. This aqueous battery electrolyte was investigated in symmetric cells based on Zn/SPE/Zn and has shown obvious potential and excellent reversibility for operation in proton-conducting batteries [146].

There has recently been a shift in interest in chitin for energy-storage applications, specifically the preparation of nitrogen-doped (porous) carbons such as porous carbon fibers and nanofibrous microspheres with hierarchical porosity. Because of their broad accessibility, high porosity, low weight, natural biodegradability, renewability, and eco-friendliness, chitin-derived porous carbon

electrode materials for energy storage applications have received significant attention in recent years [41, 42].

The nitrogen-doped amorphous carbon nanofibers (NACF) generated by direct pyrolysis of chitin were used as the anode material in sodium-ion batteries (SIBs), and the NACF electrode produced a high reversible capacity of 320.6 mAh/g with great rate capability and extended cycle ability [147]. When chitin was pyrolyzed with lignosulfonate, its capacitive characteristics increased significantly, delivering a high reversible specific capacity of up to 644.5 mAh/g at a current density of 50 mA/g. After 300 cycles at a current density of 100 mA/g, the specific capacity remained at 350.7 mA/g. As a result, this anode material demonstrated excellent electrochemical performance, rate capability, and cycle stability [148].
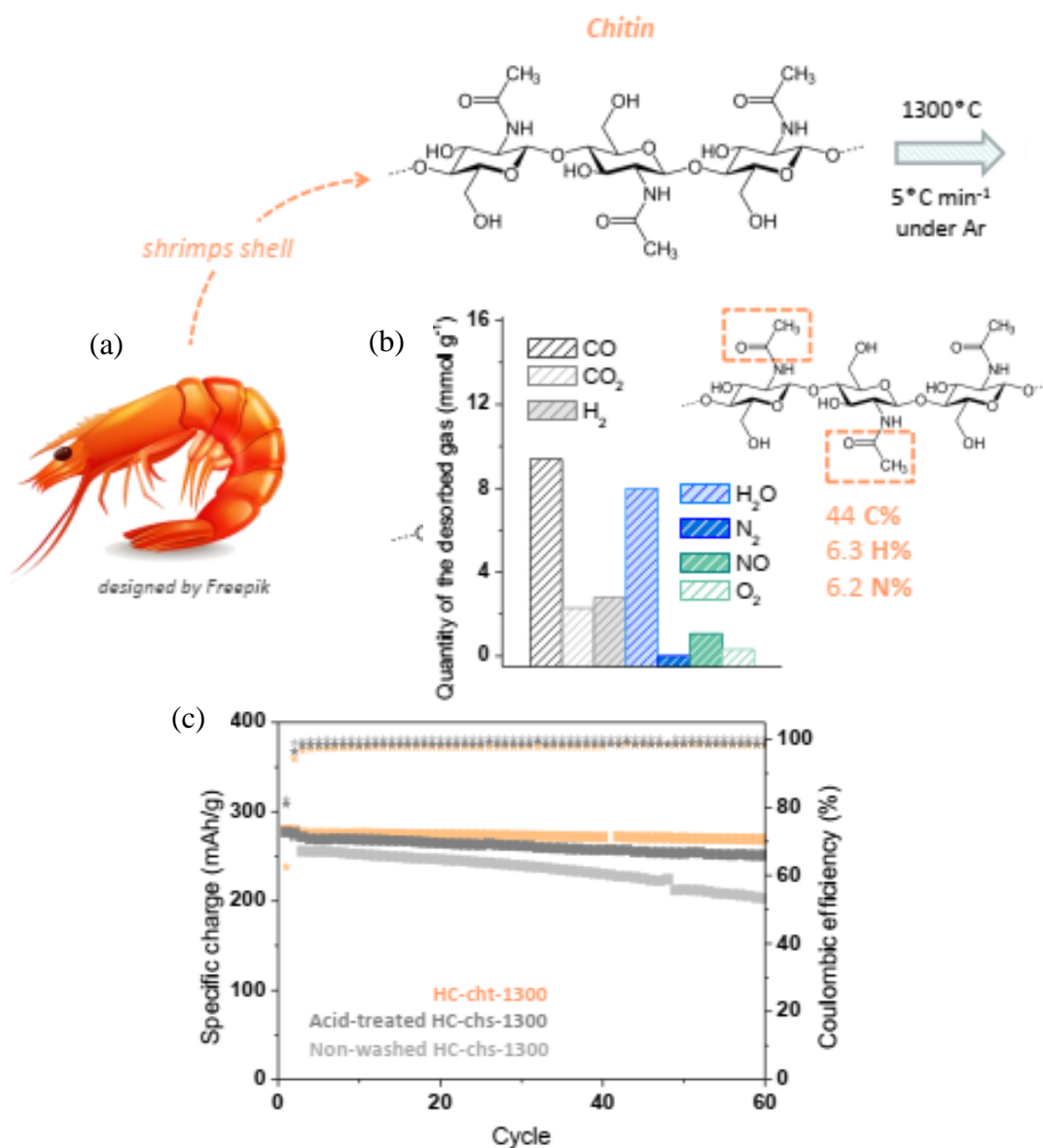
Figure 2.7 The electrode material for Na-ion batteries: (a) preparation of hard carbons from chitin (shrimps shell), (b) composition of quantities of the element desorbing from the surface of chitin, and (c) specific charge and coulombic efficiency of the electrodes based on chitin-derived HC [41]

N-doped carbon (NC) composite is prepared using biopolymer chitin a carbon precursor. After 100 cycles at 0.5C-rate, the assembled $SiO_x@TiO_2@NC/LiFePO_4$ full cells can retain a discharge capacity of 121 mAh/g, maintaining 90% of the third capacity [149]. Hard carbons from chitin (shrimp shell) were prepared as electrode material for Na-ion batteries as shown in Figure 2.7. The

hard carbon (HC) from chitin was discovered to have a 44.00wt%, an initial specific charge of 280 mAh/g at 0.1C-rate, and a high columbic efficiency of 97.03% [41].

Chitin can be used as electrode material in lithium iron phosphate batteries because it converts into non-graphitizable or hard carbons. Therefore, chitin-derived carbon coating cathode materials for lithium iron phosphate batteries are investigated in this thesis.

2.5 Synthesis of LiFePO$_4$

Many synthesis methods have been developed to prepare the LiFePO$_4$ cathode material. These methods are briefly discussed in this section.

2.5.1 Solid-state synthesis

Solid-state synthesis is a common technique for creating polycrystalline materials from solid reagents. To enable the reaction, a very high temperature is usually used. Chemical and morphological properties of the reagents, such as reactivity, surface area, and free energy, change with the solid-state reaction, as do other reaction conditions such as temperature, pressure, and reaction environment [87, 150]. The simplicity and large-scale production of solid-state synthesis are two of its advantages [151]. It was reported that enhanced ammonium sulfate leaching was used to extract and separate Fe and Ti from extracted vanadium residue, as well as the synthesis of LiFePO$_4$/C for lithium-ion batteries. The Ti-doped LiFePO$_4$/C was synthesized solid-state using ammonium jarosite as the Fe source, and its initial discharge specific capacity was 141.6 mAh/g at 0.1C-rate [152].

The electrochemical performance and synthesis of LiFePO$_4$/ graphene composites by solid-state reaction were also reported. The initial discharge capacity of the LiFePO$_4$/graphene composites was 161 mAh/g at 0.1C-rate, and the capacity was retained at 70 mAh/g even at a high rate of 50C-rate. The composites have great potential as cathode materials in high-power lithium-ion batteries for electric and hybrid vehicles [153]. A modified two-step solid-state reaction was also used to create LiFePO$_4$/carbon composites with widely different amounts of carbon. Carbon coatings were formed on the olivine particles as the mixed precursors and

were heated at three different initial-step temperatures of 200, 300, and 400 °C, followed by second-step annealing at 700 °C. The LiFePO$_4$/carbon composite calcined at an initial step temperature of 300 °C demonstrated the highest discharge capacity and rate capability in the voltage range of 2.5–4.2 V [154].
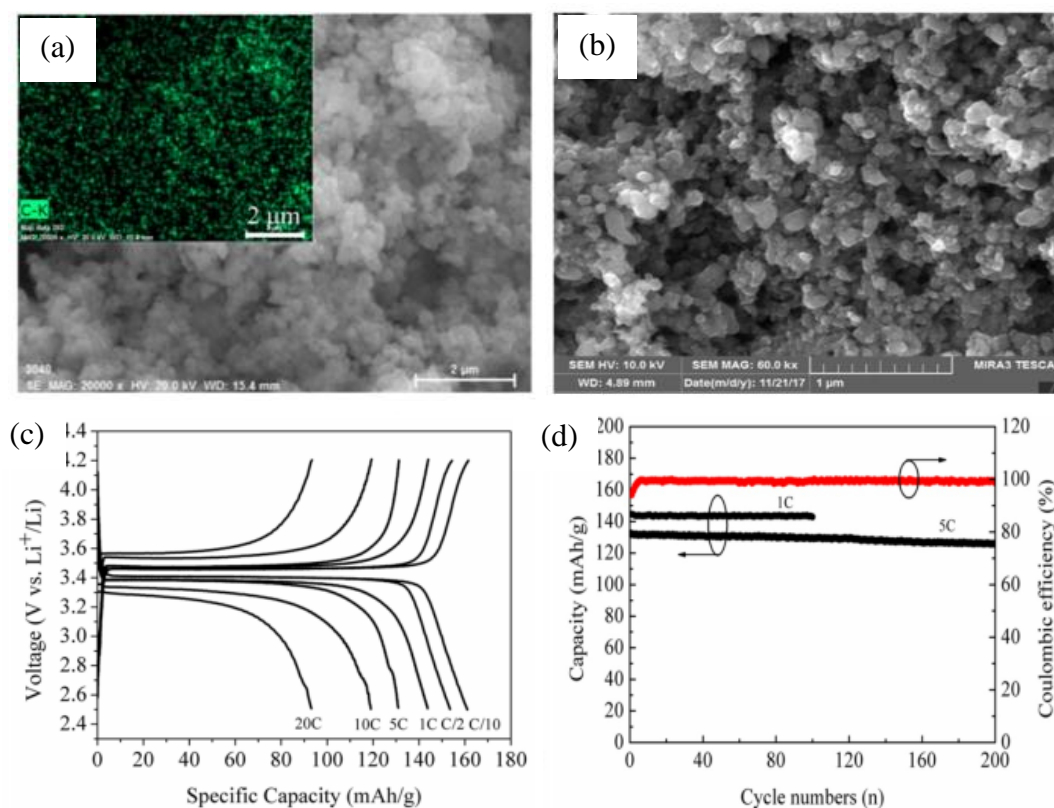
Figure 2.8 The LiFePO$_4$/C composite: (a) EDS mapping of C in the LiFePO$_4$/C composite, (b) SEM image of LiFePO$_4$/C composite, (c) charge and discharge profiles of LiFePO$_4$/C composite, and (d) cycling performance combined with coulombic efficiency at 1 and 5C-rate [155]

The green route was developed to synthesize the LiFePO$_4$/C composite using iron (III) oxide (Fe$_2$O$_3$) nanoparticles, lithium carbonate (Li$_2$CO$_3$) powder, glucose powder, and phosphoric acid (H$_3$PO$_4$) solution as presented in Figure 2.8. EDS mapping is used to estimate the carbon element composition distribution in the LiFePO$_4$/C composite, which has a discharge capability of 161 mAh/g at 0.1C-rate, 119 mAh/g at 10C-rate, and 93 mAh/g at 20C-rate, as well as cycling stability of

98.0% capacity retention at 1C-rate after 100 cycles and 95.1% at 5C-rate after 200 cycles [155].

As a result, solid-state synthesis, thought to be an efficient and scalable method, became widely used and accepted as the primary method to produce the cathode material for Li-ion batteries [107]. The general advantages of solid-state synthesis include ease of purification; rapid generation; pollution reduction; low costs; and handling simplicity [52, 156].

2.5.2 Microwave-assisted synthesis

The microwave method has caught the interest of many scientists in recent years due to its quick synthesis time and homogeneous properties [59]. Traditional heating mechanisms used in a variety of industrial fields typically take a long time (up to 10 hours) to complete a reaction, resulting in a high time and energy cost [115]. Under microwave irradiation, however, the reaction is completed in a relatively short time (a few minutes), which is a breakthrough in the industry because large-scale production can be accomplished with much higher efficiency and lower cost. Meanwhile, a microwave-assisted solid-state reaction was used to generate $LiFePO_4$. The product obtained at the microwave calcination time of 3 minutes yielded the best results in terms of particle size (majority in the range of 100-150 nm), the crystallographic pattern of $LiFePO_4$ and some by-products, and a voltammetric profile characteristic of $LiFePO_4$.

As a consequence, the synthesis methodology presented here implies a significant reduction in processing time while producing $LiFePO_4$ nanoparticles with good electrochemical activity for the Li-ion intercalation process [61]. Therefore, microwave synthesis of $LiFePO_4$ has received much attention, and it may become the preferred method in the future. Microwave irradiation has several advantages over traditional heating methods, including homogeneous and fast heating (deep internal heating), remarkable reaction accelerations as a result of heating rate, and specific heating [116].

Figure 2.9 shows a microwave-assisted solid-state synthesis using various organic carbon sources that were fast, simple and environmentally friendly. The samples were microwave-irradiated for 8 minutes at 2.45 GHz and 136 W, and they were named LF-1 (citric acid) and LF-2 (sucrose). The results demonstrated that the LiFePO$_4$/C nanoparticles prepared from sucrose as a carbon source have good crystallinity and a higher percentage of graphitic carbon, and they provided an initial discharge capacity of 145.6, 140.5, and 122.4 mAh/g at 0.1, 0.5, and 1.0C-rate, respectively. These benefits, combined with the effective and simple preparation method, make LiFePO$_4$/C nanoparticles appealing for practical and large-scale applications [157].
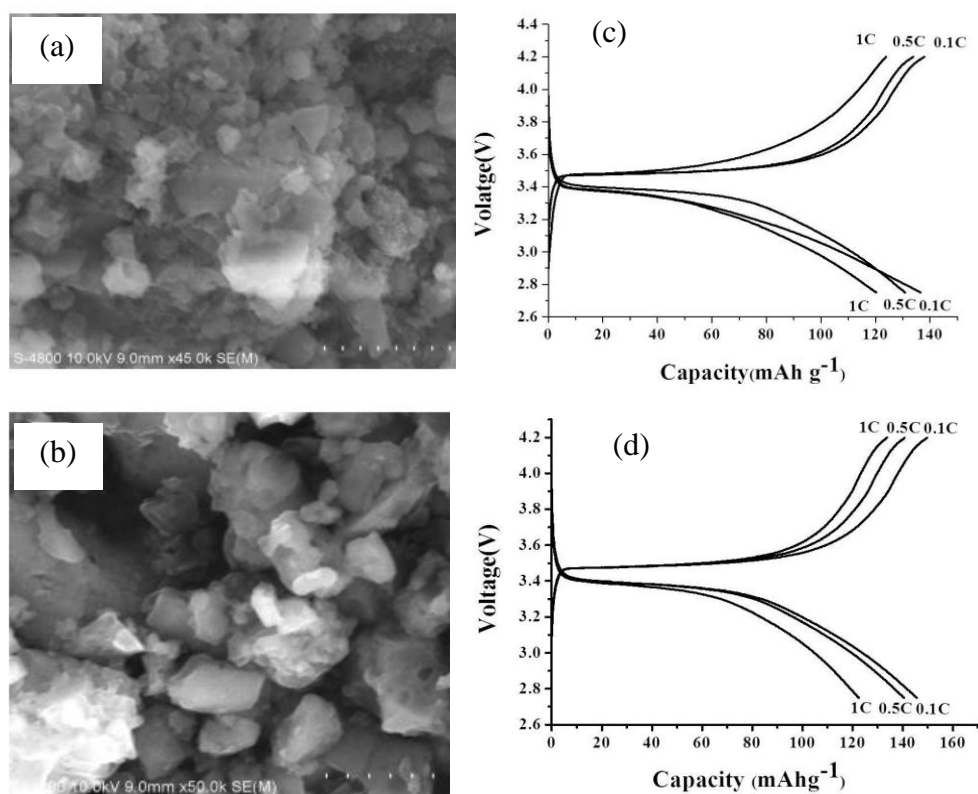
Figure 2.9 A microwave-assisted solid-state synthesis; SEM micrographs of LiFePO$_4$/C: (a) LF1, (b) LF2, initial charge and discharge curves of LiFePO$_4$/C at different charging rates, (c) LF1, and (d) LF2 [157]

2.5.3 Sol-gel synthesis

The sol-gel process, which is a method for producing solid materials from small molecules, is another technique used for catalyst synthesis. This method involves the mixing of several precursor solutions rather than powders, implying that the final product can be mixed evenly and uniformly. It generates high-quality materials with high homogeneity and purity at lower temperatures than traditional methods [158]. The $LiFePO_4/C$ nanocomposite for lithium-ion batteries was synthesized using a gelatin-based sol-gel procedure. The product as-synthesized has a narrow particle size distribution (100–300 nm) and a tap density of 1.42 g/cm^3. The $LiFePO_4/C$ nanocomposite cathode is found to have excellent cycle ability, with capacity retention of 95.2% at 0.2C-rate after 100 cycles. Furthermore, the battery's performance has improved, with the cathode's discharge capacity reaching 128 mAh/g at 5C-rate [159].

The electrochemical performance of $LiFePO_4/C$ as a cathode for aqueous lithium-ion batteries synthesized by the sol-gel method was then proved. At 0.1C-rate, the $LiFePO_4/C$ composites have a high reversible capacity of 163.5 mAh/g. In addition, $LiFePO_4/C$ has an excellent rate and cycling capability [160]. As a result, it is a low-temperature (200–600 °C) process that is simple, cost-effective, and efficient for producing high-quality coatings. The disadvantages of this method, on the other hand, include a lengthy processing time and high raw material, drying, and sintering costs.

2.5.4 Co-precipitation synthesis

The chemical co-precipitation method can be realized by using the kinetics of nucleation and growth in a homogeneous solution [161]. To create ordered nanostructures, it is necessary to understand super saturation, nucleation, growth, and post-growth (Ostwald ripening). Temperature, pressure, concentration, pH, stirring speed, reaction time, and the nature of the precursors, as well as the presence of surfactants or other growth inhibitors, all play important roles in controlling the final nanostructures' size, shape, and size distribution [162]. Although co-precipitation is

one of the most common wet chemical methods for producing cathode materials, it is challenging to produce controlled nanostructures using this method.

Consequently, $FePO_4 \cdot H_2O$ was synthesized using a co-precipitation method in order to fabricate submicrometer-structured $LiFePO_4/C$. The discharge capacities of the $LiFePO_4/C$ fabricated from as-synthesized $FePO_4$ were 162.5, 147.3, 133.0, 114.7, 97.2, 91.3, and 88.5 mAh/g, respectively, at rates of 0.1C, 0.2C, 0.5C, 1C, 2C, 3C, and 4C-rate, with satisfactory capacity retention [163]. Similarly, the synthesis of F-doped $LiFePO_4/C$ cathode materials for high-performance lithium-ion batteries using a co-precipitation method with a hydrofluoric acid source demonstrated the best high-rate performance, cycling life, and capacity retention. At 0.1C, 1C, 3C, 5C, 10C, 20C, and 30C-rates, the discharge capacities are 165.7, 161.1, 155.3, 150.8, 140.3, 129.8 and 115.7 mAh/g, respectively. As a result, by increasing electronic conductivity, accelerating the Li^+ ion diffusion coefficient, and increasing structural stability, F doping can improve the inherent flaws of $LiFePO_4$ materials [161].

The advantages of the co-precipitation method seem to include no solid waste, effective and proven technologies, and no daily use of chemicals [164]. On the other hand, the method's disadvantages, include the need for a trained person for maintenance and regeneration, toxic liquid waste (pH readjustment may be required), and monitoring of breakthroughs.

2.5.5 Solvothermal/ Hydrothermal synthesis

The solvothermal method uses the solubility of the precursors in a solvent at high temperatures and pressures to crystallize nanostructures from the solvent [165]. The hydrothermal method is named after the solvent used, which is water [166]. A variety of synthesis parameters, such as reaction temperature, pressure, time, and solvent type, influence the solubility and reactivity of the precursors in the solvent as well as their transformation into nanostructures at high temperatures [167]. As a result, the parameters can be tuned to achieve a high nucleation rate and a good

size distribution, providing good control over the size, crystallinity, and shape distribution of cathode metal oxide nanostructures.

To control the particle size and shape, $LiFePO_4$/C powders were synthesized using a solvothermal method with L-Lysine as a surfactant. Obviuosly, the $LiFePO_4$/C powder produced by 50 mmol L-Lysine had the highest specific capacity of 96 mAh/g at 1C-rate and the highest capacity retention of 95.6% after a 650 cycle [168]. Following that, the synthesis of $LiFePO_4$ cathode material and its reaction mechanism during the solvothermal method are presented. It has an excellent initial discharge capacity of 156.9 mAh/g at 1C-rate of 25 °C, and high-temperature behavior of 147.1 and 126.8 mAh/g at 1C and 2C-rate of 55 °C [169].

Furthermore, the enhancement of electrochemical properties of a platinum doped $LiFePO_4$/C cathode material synthesized using a hydrothermal method demonstrated the charge/discharge performance of the $LiFePO_4$/C cell with 117, 104, 83, 63, and 47 mAh/g at 0.1, 0.2, 1C, 5C, and 10C-rate, respectively [170]. The electrochemical properties of the $LiFePO_4$/graphene cathode nanocomposite prepared using a one-step hydrothermal method were then enhanced. As a result, the initial discharge capacity of the $LiFePO_4$/graphene active material (LFP/G) was 157 mAh/g at 0.2C and 114 mAh/g at 5C-rate. The results were compared to LFP, which has capacities of up to 120 mAh/g at 0.1C-rate and 50 mAh/g at 5C-rate [171]. However, the solvothermal method has the disadvantage that the particle size is relatively large compared to other methods.

For all of these reasons, the cathode material for lithium iron phosphate batteries was synthesized in this thesis using microwave-assisted solid-state synthesis. Due to their high power, best rate capability, good crystallinity, and good electrochemical performance, lithium iron phosphate batteries have a high potential for use as cathode materials.

2.6 Physical characterization

2.6.1 X-ray diffraction

By providing peak positions and cell dimensions, XRD is a useful technique for identifying the phase of crystalline material. The principle of operation is based on the constructive interference of monochromatic X-rays and a crystalline sample. When matter, such as metal, is irradiated with fast-moving accelerated electrons, X-rays are produced. As shown in Figure 2.10, the interaction between the samples and the X-rays results in constructive interference, which satisfies the condition of Bragg's Law ($n\lambda = 2d\sin\theta$).

Incident plane wave

θ

2θ

$2d\sin\theta$

d

θ θ

Constructive interference

When $n\lambda = 2d\sin\theta$

$d\sin\theta$
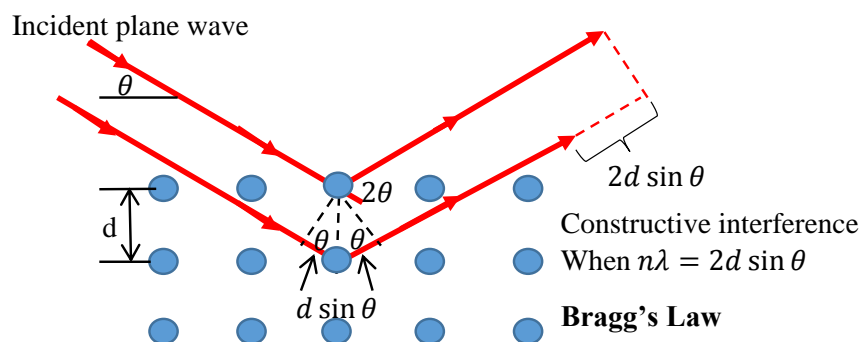
Bragg's Law

Figure 2.10 The bragg's law schematic diagram

In this thesis, PANalytical Empyrean used XRD to identify the crystalline phases present in a material and thus reveal chemical composition information through the study of the crystal structure.

2.6.2 Scanning Electron Microscopy

Scanning Electron Microscopy (SEM) is a type of electron microscope used to reveal a material's morphology, chemical composition, and crystal orientation. At the top of the equipment is an electron gun, which uses a voltage to direct an electron beam towards the sample. SEM, as the name implies, primarily displays surface information about a substance. Secondary, backscattered, and Auger electrons are produced when electrons interact with samples. Inside the equipment,

various detectors collect and analyze the signal. The secondary electrons collected, for example, primarily provide information for high spatial resolution images. SEM was performed in this thesis using a SEM-Quanta 400 (Thermo Fisher Scientific Quanta), which provides high-resolution imaging useful for evaluating various materials for surface fractures, flaws, contaminants, or corrosion.

2.6.3 Energy dispersive X-ray spectroscopy

Energy dispersive X-ray spectroscopy (EDX) is used to determine the composition of a sample, especially its chemical elements. When an electron beam from a SEM strikes a sample, X-rays with characteristic energies for each element are produced, providing a qualitative analysis of the elements present as well as the quantitative composition with further analysis.

2.7 Electrochemical performance analysis

Electrochemical impedance spectroscopy (EIS), cyclic voltammetry (CV), and galvanostatic charge-discharge testing were used to measure and analyze electrochemical performance.

2.7.1 Electrochemical Impedance Spectroscopy

Electrochemical Impedance Spectroscopy (EIS) is a useful technique for revealing resistance, chemical side reactions, and capacitance by applying different frequencies to coin cells and recording their responses. The Autolab Electrochemical was used to carry out the experiment, with the cathode side serving as the working electrode and the Li metal serving as the counter and reference electrodes. The freshly made (fully discharged) and cycled (fully discharged) cells were tested at frequencies ranging from 0.01 Hz to 1 MHz, with an amplitude of 5 mV. The Autolab electrochemical (Metrohm, PGSTAT302N) was used in this thesis to determine the electrical response of chemical systems in a nondestructive manner.

2.7.2 Cyclic Voltammetry

The technique of cyclic voltammetry (CV) is widely used to investigate the properties of electrochemical systems. The current is measured when a cyclic linear potential sweep is delivered to the electrode. A current peak occurs at a specific potential within the potential scanning range, indicating the occurrence of an electrode reaction. If the electrode reaction is reversible, a peak will be visible when scanning in the opposite direction. The Autolab Electrochemical (Metrohm, PGSTAT302N) between 2.0-4.2 V at a scan rate of 0.1-0.5 mV/s at room temperature was used in this thesis.

2.7.3 Galvanostatic charge-discharge testing

Galvanostatic is an electrochemical technique used to measure corrosion rate and electrochemical reactions by applying a constant current (charging) and recording the potential as a function of time or total charge passing through the system. The Autolab electrochemical (Metrohm, PGSTAT302N) tests were performed at room temperature.

2.8 Literature review

Table 2.3 summarizes the microwave-assisted solid-state synthesis of LiFePO$_4$, including the advantages, electrochemical performance, and appropriate processing time.

Table 2.3 A summary of the microwave-assisted solid-state synthesis of the LiFePO$_4$

Advantages of synthesis method	Reference
- Simple and effective preparation method	[157], [58], [126]
- Low cost	[157], [172]
- Environmentally friendly	[157], [58]
- Smallest particle size (100–150 nm)	[61]
- high phase purity and crystallinity	[126]
Electrochemical performance	
- Good cycling stability	[157], [58], [126]
- High discharge capability	[157], [126]
- High charge/discharge capacity	[173], [174]
- Excellent capacity retention	[157], [172], [126], [174]
- Excellent reversible capacity	[172], [61], [174]
- Excellent electrochemical performance	[61]
- Good activity for the Li ion intercalation process	[174]
Appropriate time for synthesis processing	
- 2.45 GHz, 136 W for 8 minutes	[157]
- 3.0 GHz, 750 W for 15 minutes	[58]
- 2.45 GHz, 800 W for 3 minutes	[61]
- 2.45 GHz, 1,500 W for 10 minutes	[126]
- 2.45 GHz, 600 W for 15 minutes	[174]

To summarize, the main benefits of microwave heating are its controllability, uniform selective heating, short processing time (3–15 minutes), low energy consumption, and low cost. Furthermore, microwave heating is a low-temperature, repeatable process.

CHAPTER 3

EXPERIMETAL APPARATUS AND PROCEDURES

3.1 General procedure

To explore the electrochemical properties of lithium iron phosphate batteries, cathode materials properties were synthesized using solid-state synthesis and microwave heating. Figure 3.1 describes the methodologies and techniques used in this thesis.

```
┌─────────────────────────────────────────────┐
│ 1. Preparation of LFP and LFPM materials     │
└─────────────────────────────────────────────┘
                    │
                    ▼
        ┌─────────────────────────────────────────────┐
        │ 2. The procedure for producing cathode materials │
        └─────────────────────────────────────────────┘
┌───────────────────────────────────────┐
│ 3. Physical characterizations          │
│   - X-ray diffractometer (XRD)         │
│   - Scanning electron microscope (SEM) │
│   - Energy dispersive x-ray analysis (EDX) │
└───────────────────────────────────────┘
            ┌─────────────────────────────────────────┐
            │ 4. Electrochemical measurements          │
            │   - Impedance spectroscopy               │
            │   - Cyclic voltammetry                   │
            │   - Charge-discharge characterization    │
            └─────────────────────────────────────────┘
```
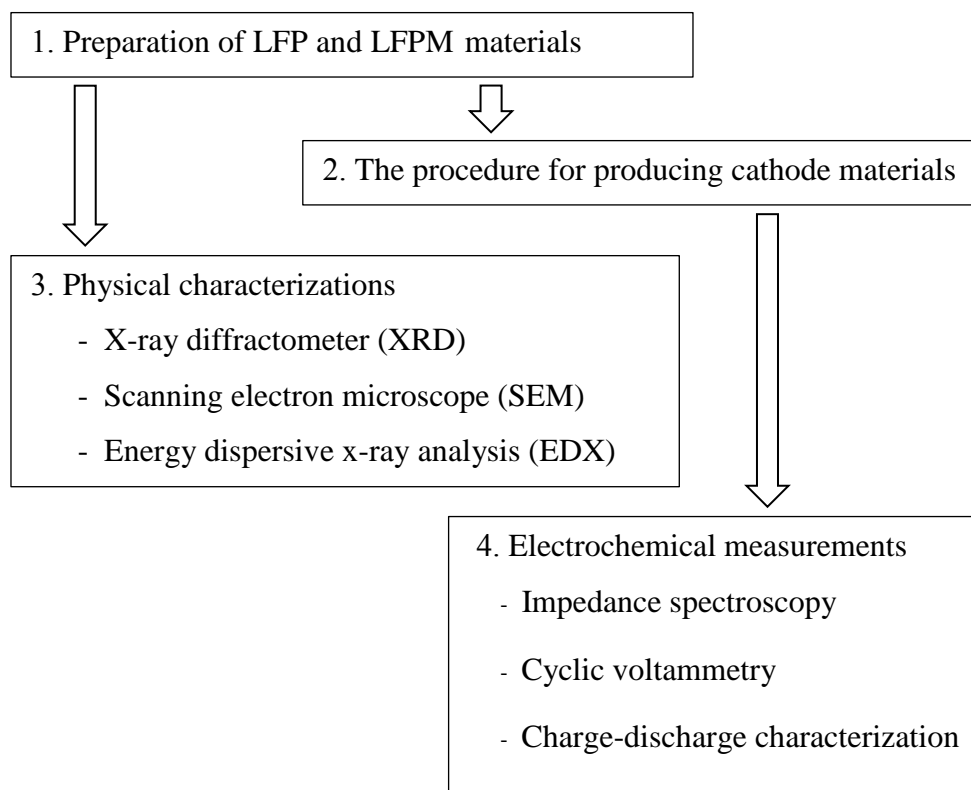
Figure 3.1 Procedures and techniques for the experiments

3.2 Materials and equipment

The key chemicals, materials, tools, and equipment used in this thesis are listed in Table 3.1 and 3.2.

Table 3.1 A list of chemicals and materials

Name	Formula	Supplier
1. Iron (III) oxide	Fe_2O_3	Sigma Aldrich (Japan)
2. Phosphoric acid	H_3PO_4	Sigma Aldrich (Japan)
3. Lithium carbonate	Li_2CO_3	Sigma Aldrich (Japan)
4. Acetone solution (Dimethyl ketone)	C_3H_6O	Anantanara CO., LTD., (Thailand)
5. Hydrochloric acid	HCl	RCL Labscan (Thailand)
6. Ethanol solution	C_2H_5OH	RCL Labscan (Thailand)
7. Poly (vinylidene fluoride) (PVDF)	$(CH_2CF_2)_n$	Alfa Aesar (USA)
8. N-methyl-2-pyrrolidone (NMP)	C_5H_9NO	Loba Chemie (India)
9. 1 mol/L $LiPF_6$ in ethylene carbon (EC)/dimethyl carbonate (DMC) (1:1 w/w)	1 mol/L $LiPF_6$ in (EC)/(DMC) (1:1 w/w)	Sigma Aldrich (Japan)
10. Chitin	-	-
11. Aluminum foil and copper plates	-	-

Table 3.2 A list of tools and equipment

Tools and equipment	Brand/Model
1. X-ray diffractometer (XRD)	PANalytical empyrean
2. Scanning electron microscope (SEM)	SEM-quanta 400 (Thermo fisher scientific quanta)
3. Energy dispersive x-ray analysis (EDX)	Oxford
4. Autolab electrochemical	Metrohm PGSTAT302N
5. Tube furnace	Pyrotron TF3Z1200
6. Drying oven	Laboratory drying oven- 99200-3
8. Analytical balance	KERN ABS-N analytical balance
9. Ball mill manufacturer	Delhi scientific
10. Ultrasonic bath	Grant ultrasonic bath
11. Microwave oven	ER-SM20(W)TH 800W

3.3 Preparation of cathode material

The applied procedures and techniques for preparation of the LFP material are described as follows:

3.3.1 Preparation of the $FePO_4 \cdot 2H_2O$ precursor

A typical procedure was formed the $FePO_4 \cdot 2H_2O$ precursor, which used the iron (III) oxide (Fe_2O_3) powder and phosphoric acid (H_3PO_4) solution (85%), added with deionized water (DW), where the ratio of the Fe/P/DW was 2 g:1.8 mL: 2.5 mL in a flask followed by ultrasonic dispersion at room temperature for 30 minutes. The mixtures were transferred into a horizontal ball mill for 9 hours, heating up at 90 °C for 5 hours to form a suspension and cooling down at room temperature.
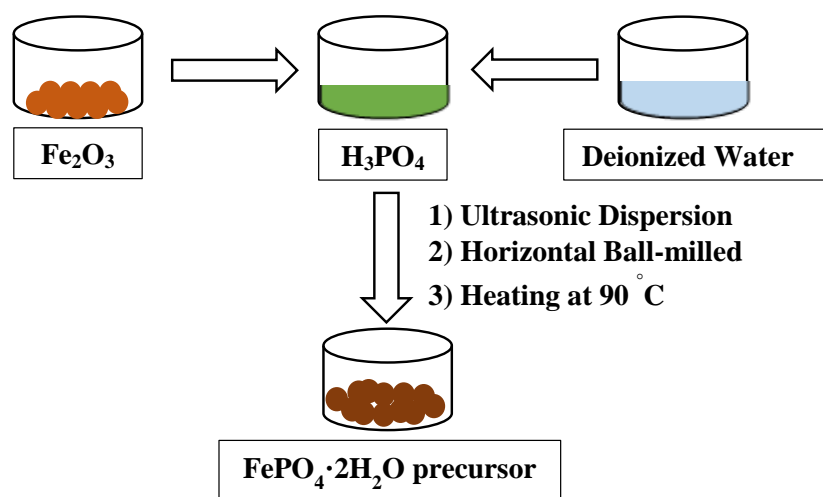
Figure 3.2 The schematic illustrations for the $FePO_4 \cdot 2H_2O$ precursor

3.3.2 Preparation of the chitin

In order to form chitin, 10 g of ground shrimp shell were mixed with 20 mL of acetone (Dimethyl Ketone) solution before gradually adding 200 mL of hydrochloric acid (HCl; 37%), stirring in an ice tank until completely dissolved, and storing at 4 °C for 24 hours. After 24 hours, a 600 mL ethanol solution (50%) was added to the precursors and continuously stirred while waiting for precipitation and draining out the top layer of the water. The deionized water was then added in the

same amount as the drained water. After that, the pH balance was determined to be 7.0. The precursors were centrifuged at 5,000 rpm for 10 minutes before being steamed in an autoclave at 120 °C for 15 minutes and then kept at 10 °C.
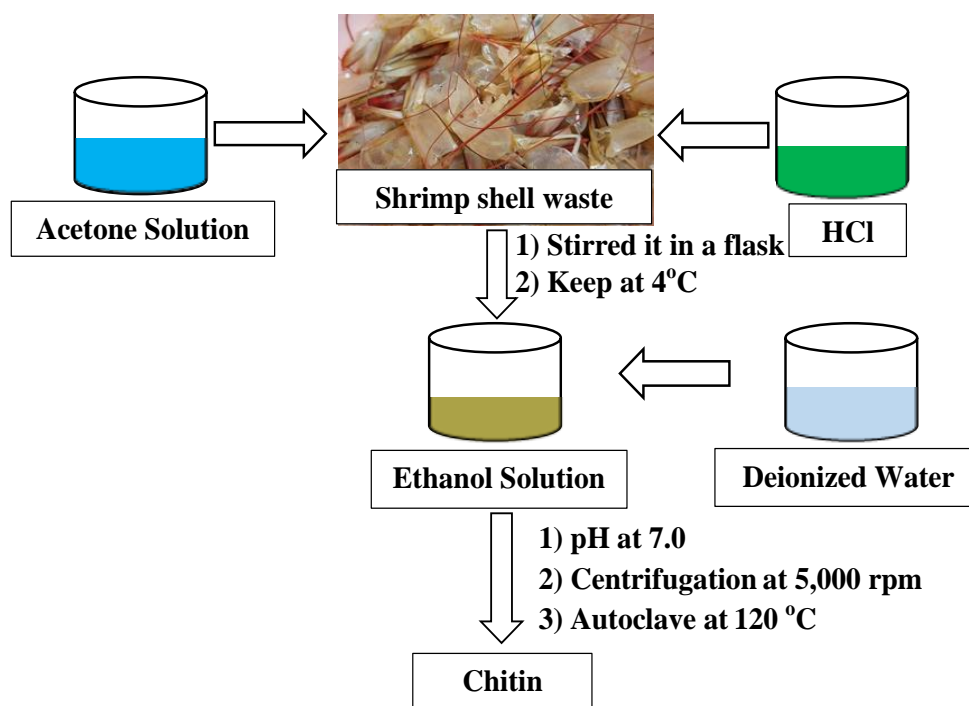
Figure 3.3 The schematic illustrations for preparation of the chitin

3.3.3 Preparation of the LFP material

The $FePO_4 \cdot 2H_2O$ precursor, lithium carbonate (Li_2CO_3) synthesis from Sigma Aldrich (Japan), chitin, and deionised water (DW) were used to create the LFP material. At room temperature, the $FePO_4 \cdot 2H_2O$ precursor, Li_2CO_3, chitin, and deionised water were mixed in the following proportions: 1 g: 0.485 g: 0.1 g: 32 mL. The mixtures were then placed in ultrasonic dispersion for 30 minutes. The mixed slurries were then dried in an 85 °C oven for 24 hours. To obtain LFP material, the mixture was sintered for 10 hours at 650 °C in a tube furnace with a 3 °C/min argon flow.

1) Ultrasonic Dispersion
2) Horizontal Ball-milled
3) Autoclave at 120 $^{\circ}$C

Chitin

🔵 **Shrimp shell waste**
⚫ **Acetone solution**
🟣 **Hydrochloric acid**
🟡 **Ethanol solution**

FePO$_4$·2H$_2$O precursor

Li$_2$CO$_3$

1) Ultrasonic Dispersion
2) Horizontal Ball-milled
3) Drying at 85 $^{\circ}$C
4) Heating at 650 $^{\circ}$C
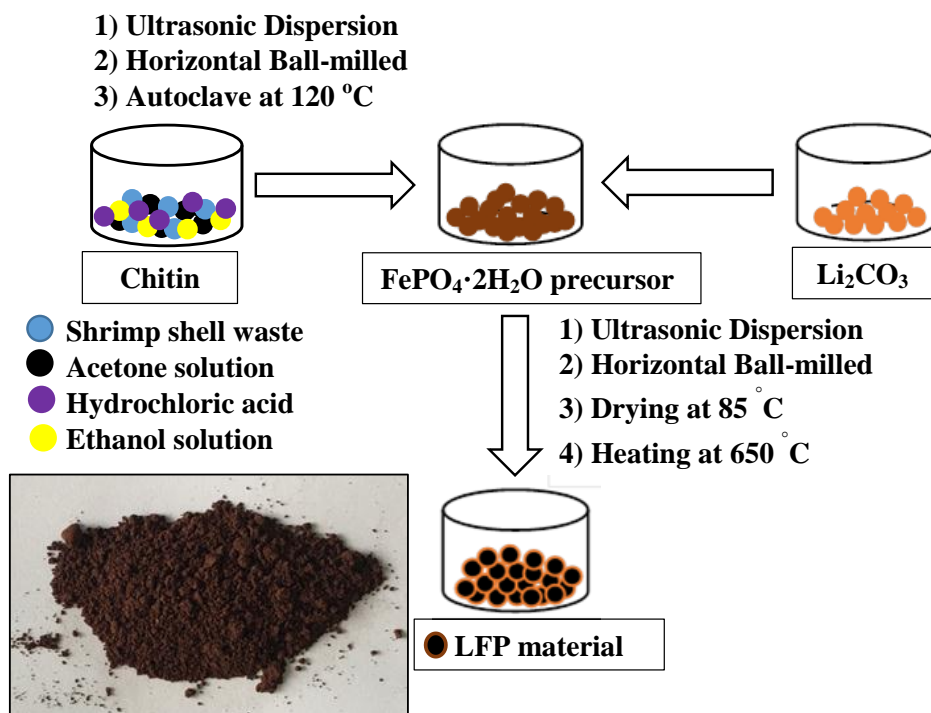
⚫ **LFP material**

Figure 3.4 The schematic illustrations for the preparation of the LFP material

3.3.4 Preparation of the LFPM material

In this thesis, LFP, LFPM5, LFPM10, LFPM15, and LFPM20 materials were microwave-irradiated in a specially designed single-mode microwave furnace at 2.45 GHz and 800 W for 5, 10, 15, and 20 minutes, respectively. Following that, the electrical conductivity of the five samples mentioned above (LFP, LFPM5, LFPM10, LFPM15, and LFPM20) was measured at room temperature, as shown in Figure 3.5.
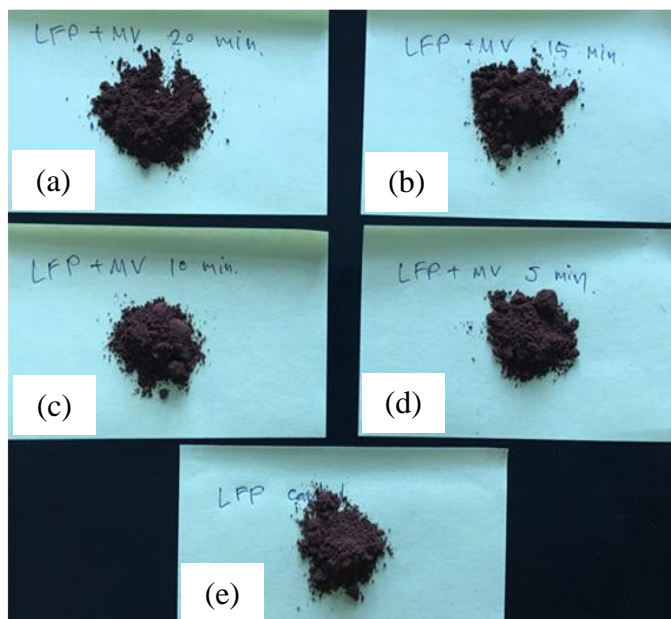
Figure 3.5 The schematic illustrations for the preparation of the LFPM material:
(a) LFPM20, (b) LFPM15, (c) LFPM10, (d) LFPM5, and (e) LFP

3.4 Procedure for producing cathode materials

The forming process of cathode materials, which used the LFP and LFPM materials and polyvinylidene fluoride (PVDF), was added with acetylene black in an 80:10:10 ratios into a horizontal ball mill for 1 hour. It was coated by doctor-blade on aluminum foil and dried for 12 hours at 120 °C. The weight and loading levels were ~4.3 mg and 1.0 cm^2, respectively. The acetylene black coated by doctor-blade on copper plates was used as the counter and reference electrode, as shown in Figure 3.6.

(a) Cathode and anode materials

(b) LFP and LFPM materials
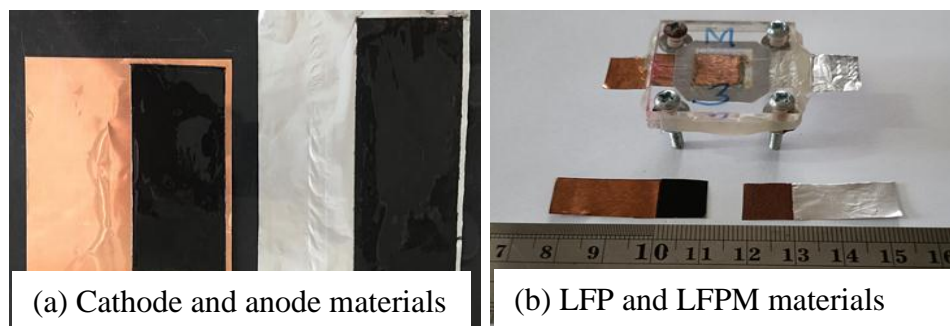
Figure 3.6 The schematic illustrations for the cathode materials: (a) Cathode and anode materials, and (b) LFP and LFPM materials

3.5 Physical characterizations

As shown in Figure 3.7, there are two pieces of equipment for investigating the physical characteristics of LFP and LFPM materials. Firstly, X-ray diffraction (XRD; PANalytical Empyrean) is used to define the crystal structure of the LFP and LFPM materials. Secondly, the scanning electron microscope (SEM-quanta 400; Thermo fisher scientific quanta) coupled with energy dispersive X-ray analysis (EDX; Oxford) is a type of electron microscope that creates images by scanning a subject's surface with a concentrated beam of electrons.

(a) X-ray diffraction   (b) SEM-quanta 400
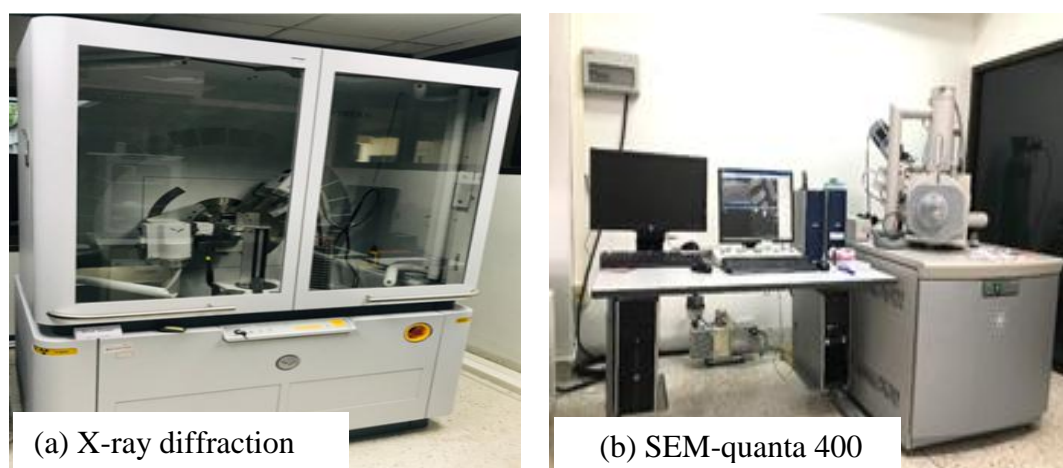
Figure 3.7 The equipment for investigating the physical characteristics of LFP and LFPM materials: (a) X-ray diffraction (XRD), and (b) SEM-quanta 400

3.6 Electrochemical measurements

Preparing the cathode material, the LFP and LFPM material, chitin, and poly- (vinylidene fluoride) (PVDF) solution were mixed in an 80:10:10 weight ratio before being mixed into a various slurry in N-methyl-2-pyrrolidone (NMP). The mixture was coated with aluminum foil and dried in a vacuum at 100 °C for 5 hours. This composition was dried and formed into a film, which was loaded at the level of ~4.3 mg/cm^2 and used as the cathode. LFP and LFPM cathode materials were used as

cathode materials, whereas copper plates were used as counter and reference electrodes, electrolyte, and cathode materials. The electrolyte consisted of a solution of 1 mol/L LiPF$_6$ in ethylene carbon (EC)/dimethyl carbonate (DMC) (1:1 w/w)

Figure 3.8 The Autolab electrochemical for electrochemical measurements

The cell was measured at room temperature using Autolab electrochemical as galvanostatic charged-discharged between 2.0 and 4.2 V at a scan rate of 0.1–0.5 mV/s. Electrochemical impedance spectra (EIS) were also characterized by Autolab electrochemical adjusting frequency range of 0.01–1000 kHz.

CHAPTER 4

RESULTS AND DISCUSSIONS

4.1 Physical Characterization

4.1.1 Measurement of the conductivity

To measure the conductivity, microwave irradiation was used to irradiate LFP, LFPM5, LFPM10, LFPM15, and LFPM20 materials, in a specially designed single-mode microwave furnace at 2.45 GHz and 800 W for 5, 10, 15, and 20 minutes, respectively. Afterwards the conductivity of the five samples (LFP, LFPM5, LFPM10, LFPM15, and LFPM20) was measured using a resistivity meter (Mitsubishi Resistivity Meter Loresta GX MCP-T700).
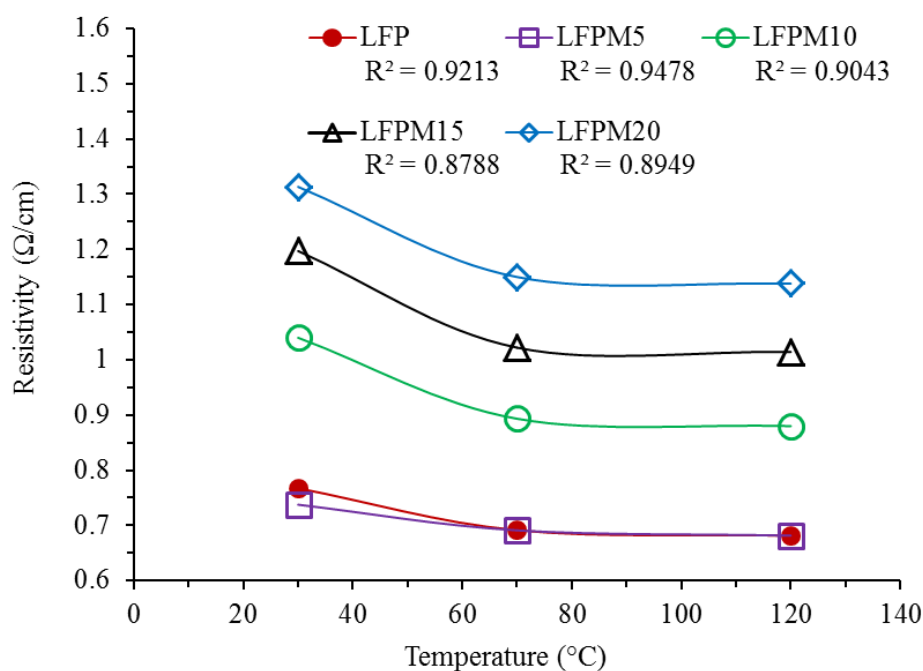
Figure 4.1 The resistivity plots of cathode materials (LFP, LFPM5, LFPM10, LFPM15, and LFPM20) at the temperatures of 30, 70, and 120 °C

For the internal resistance measurement, the samples were compressed into cylindrical pallets with a 12 mm diameter and a 2 mm thickness through a hydraulic press. The four-probe method was used to test resistivity at 30, 70, and 120 °C. The values of the five samples' resistivity are shown in Figure 4.1. As can be seen, all samples' resistivity values drop as temperature rises, which is consistent with other studies [175, 176]. It is interesting to note that LFPM5 had the lowest resistivity of all the materials, with a value of 0.77 Ω/cm at 30 °C, followed by values of 0.69 Ω/cm at 70 °C and 0.68 Ω/cm at 120 °C. Additionally, with a correlation value of R^2 = 0.9478, the average experimental power function approximation of resistivities and temperatures represents the best condition. Therefore, the low resistivity denotes strong conductivity [177], which will lead to excellent efficiency in lithium iron phosphate batteries.
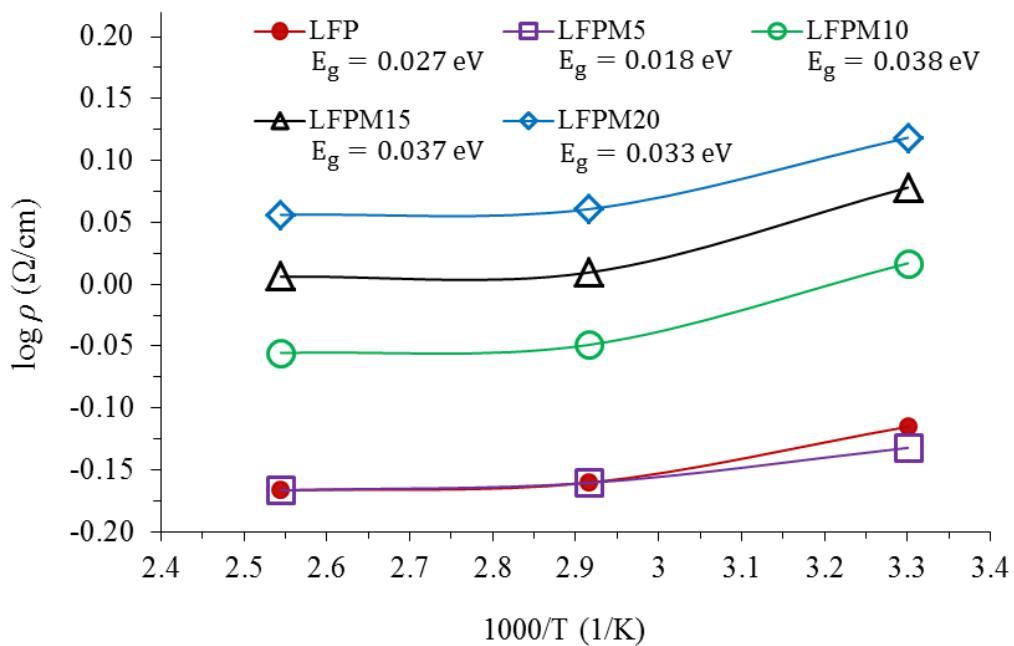
Figure 4.2 The resistivity plots of cathode materials (LFP, LFPM5, LFPM10, LFPM15 and LFPM20) as a function of inverse temperature

Figure 4.2 shows the resistivity of LFP, LFPM5, LFPM10, LFPM15, and LFPM20 as a function of inverse temperature. It is clear that the band gap energy of LFPM5 is 0.018 eV, which is the lowest value of band gap energy. The

lower band gap energy suggests better conductivity [178], and microwave irradiation can significantly increase cathode materials' conductivity. The best conductivity was discovered after 5 minutes. As a result, LFPM5 was selected as the best condition to use in this thesis, and the term LFPM is now used to refer to LFPM5.

4.1.2 X-Ray Diffractometer (XRD) measurements
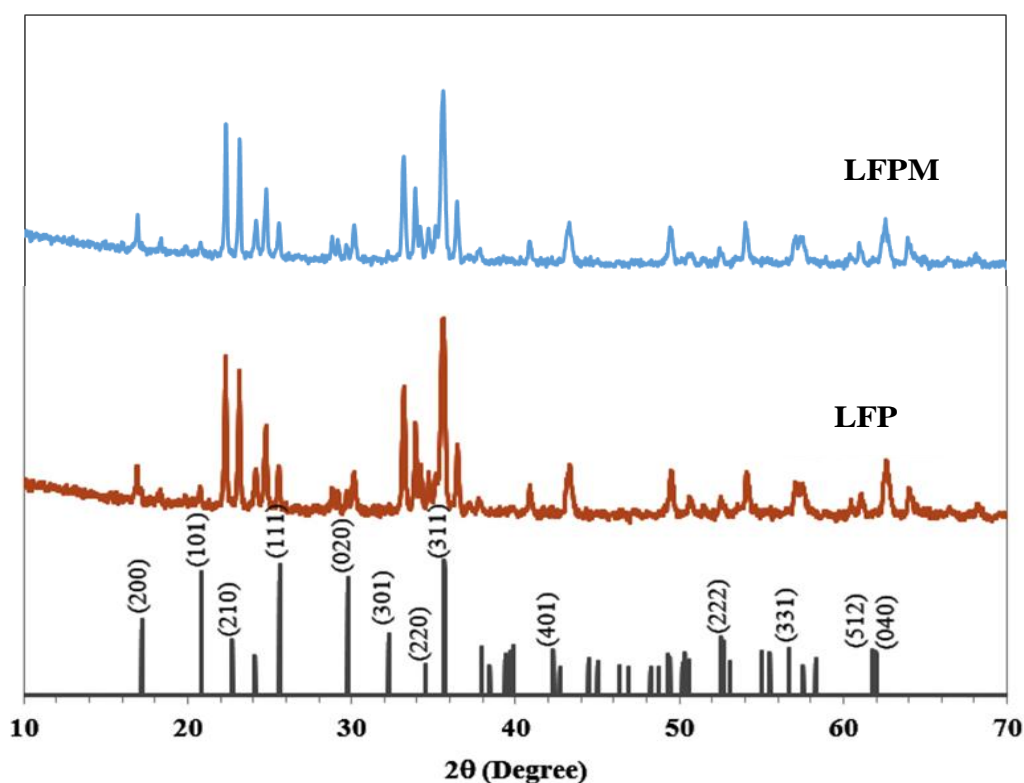
Figure 4.3 The XRD patterns of LFP and LFPM materials compared with standard LiFePO$_4$

Figure 4.3 compares the XRD patterns of LFP and LFPM materials to standard LiFePO$_4$. There is no noticeable difference between the LFP and LFPM materials. This implies that the LFP and LFPM materials were kept in good condition during the preparation process. All sharp diffraction peaks in the regions 17.16, 20.80, 22.69, 25.58, 29.74, 32.24, 34.72, 35.62, 42.31, 52.57, 56.67, 61.75, 61.76 correspond to the planes (200), (101), (210), (111), (020), (301), (220), (311), (401), (222), (331), (512), and (040). As can be seen, all XRD peaks correspond to the standard data

JCSD (Inorganic Crystal Structure Database) card No. 200155, demonstrating the formation of $LiFePO_4$ with an orthorhombic structure (Pnma, 62). The lattice parameters are a = 10.3254 Å, b = 6.0035 Å, and c = 4.6879 Å, in that order. The main XRD peaks for both LFP and LFPM materials are strong and sharp, indicating good crystallinity and purity, and no excess impurity peaks are identified.

Furthermore, no obvious impurity peaks can be seen in the diffraction patterns of the two materials, indicating that the purity of the material is relatively high. At the same time, the carbon diffraction peak could not be found in the spectra, which could be due to the very low carbon content dispersed in the materials [44, 179]. This indicates that both materials were well prepared and organized during their preparation processes, which increased the crystallinity and purity of the product.

4.1.3 Scanning Electron Microscope (SEM) images

SEM images of LFP and LFPM materials are shown in Figure 4.4. The morphology is regular in shape and has a fairly smooth surface; therefore, the mechanical activation process is particularly efficient for synthesizing small particles with homogeneous morphology [38]. It is beneficial in terms of shortening the diffusion path of Li-ion for batteries.

LFP and LFPM materials both have a large number of particles with particle sizes ranging from 170-400 nm to 250-500 nm. The average particle size of LFP materials was noticeably smaller (~300 nm) than LFPM materials (~380 nm), with a more intimate particle connection in the LFPM materials. This could be due to the carbon coating layer's importance in particle size control. Furthermore, carbon coating can prevent particle growth and decrease particle agglomeration [180], which corresponds to the carbon content of LFP materials being 36.60wt %. It is higher than the carbon content of LFPM materials being 19.80wt % as shown in Figures 4.5 and 4.6, respectively.
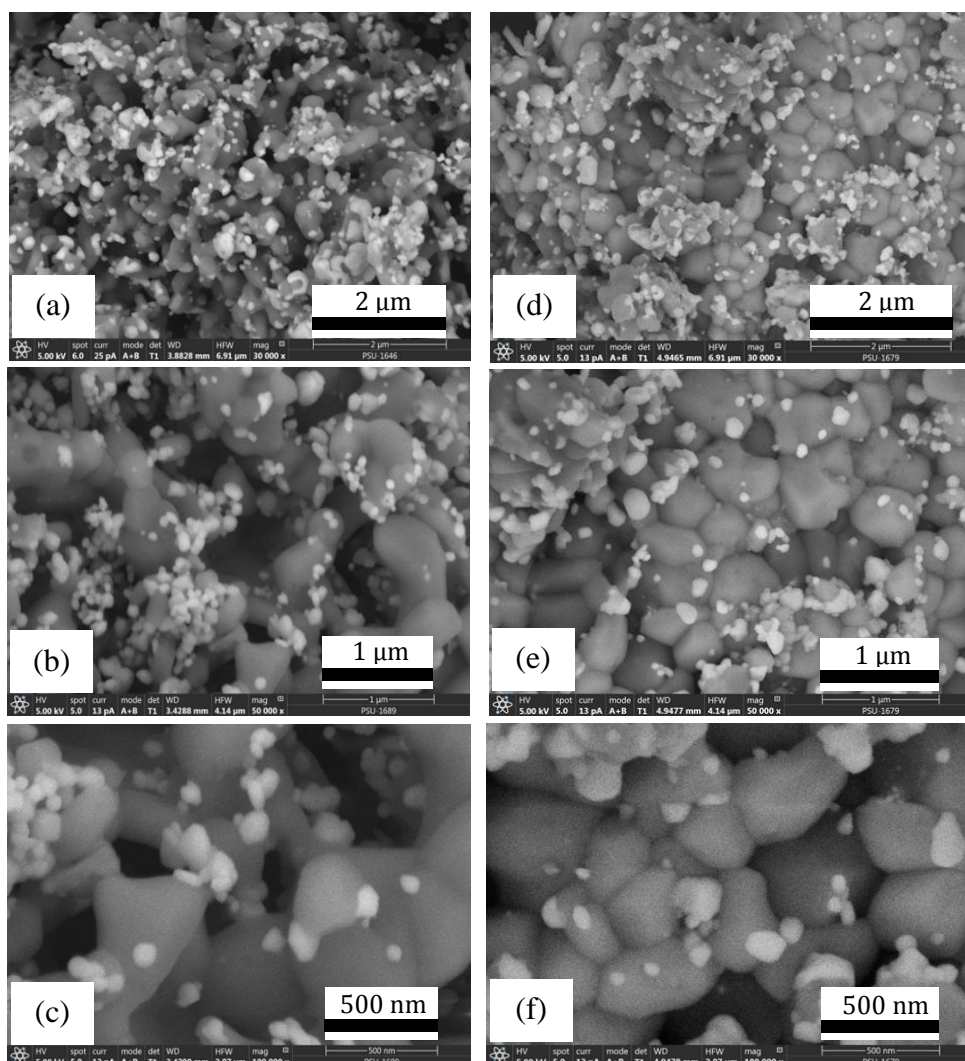
Figure 4.4 The SEM images of LFP and LFPM materials: (a) LFP, scale bar: 2 μm, (b) LFP, scale bar: 1 μm, (c) LFP, scale bar: 500 nm, (d) LFPM, scale bar: 2 μm, (e) LFPM, scale bar: 1 μm, and (f) LFPM, scale bar: 500 nm

Consequently, the small particle sizes benefit in shortening the migration paths of lithium ions and electrons during the lithiation/delithiation process and, as a result, efficiently improve the electrochemical performance of LFP [155]. Higher carbon content is advantageous because it results in a LiFePO$_4$ that is well-carbon coated and has uniformly ornamented pores. The electrochemical performance of the material should improve as the number of carbon increases. The conductivity of the LiFePO$_4$ material is determined by the amount of carbon deposited on it.

4.1.4 Energy dispersive X-ray spectrometer (EDX mapping)

EDX mappings are shown in Figures 4.5 and 4.6 to estimate the elemental mappings of the films. The films show that the elements C, O, P, and Fe are homogeneously distributed in the LFP and LFPM materials (Li cannot be detected due to its relatively small molecular mass) [181, 182], indicating a well-interconnected conducting framework and that the carbon network interconnected channel structure is evenly distributed among the particles of the LFP and LFPM materials[183, 184]. Therefore, uniformly coating carbon material on cathodes is critical for improving battery electrical conductivity and electrochemical performance.

As can be seen, the carbon is uniformly distributed across the entire surface, which benefits the conductivity properties of $LiFePO_4$ and improves the electrochemical performance of lithium-ion batteries [87]. Furthermore, the C and O are derived from the organic compounds found in chitin [185, 186], while the P and Fe are derived from the procedure used to create the LFP materials. Al impurity can be found in very small amounts in LFP and LFPM materials. Al_2O_3 substrates are produced during the sintering process and can be identified as a source of Al impurity [187].

Figures 4.5 and 4.6 demonstrate the EDX map of LFP and LFPM materials containing carbon particles derived from chitin. The elements are 45.10 and 48.90wt% oxygen (O), 36.60 and 19.80wt% carbon (C), 10.60 and 19.20wt% iron (Fe), and 5.20 and 10.10wt% phosphor (P), respectively. When microwave heating is applied to LFPM materials, the element carbon (C) decreases while oxygen (O), iron (Fe), and phosphor (P) increase. This could be due to the reason that carbon materials generally are excellent microwave absorbers. This property enables them to be transformed by microwave heating, resulting in new carbons with tailored properties; to be used as microwave receptors to heat other materials indirectly; or to act as catalysts and microwave receptors in various heterogeneous reactions [188, 189]. Because of the presence of LFP and LFPM materials, the carbon was uniformly distributed across the entire surface, benefiting the batteries' conductivity and electrochemical performance.
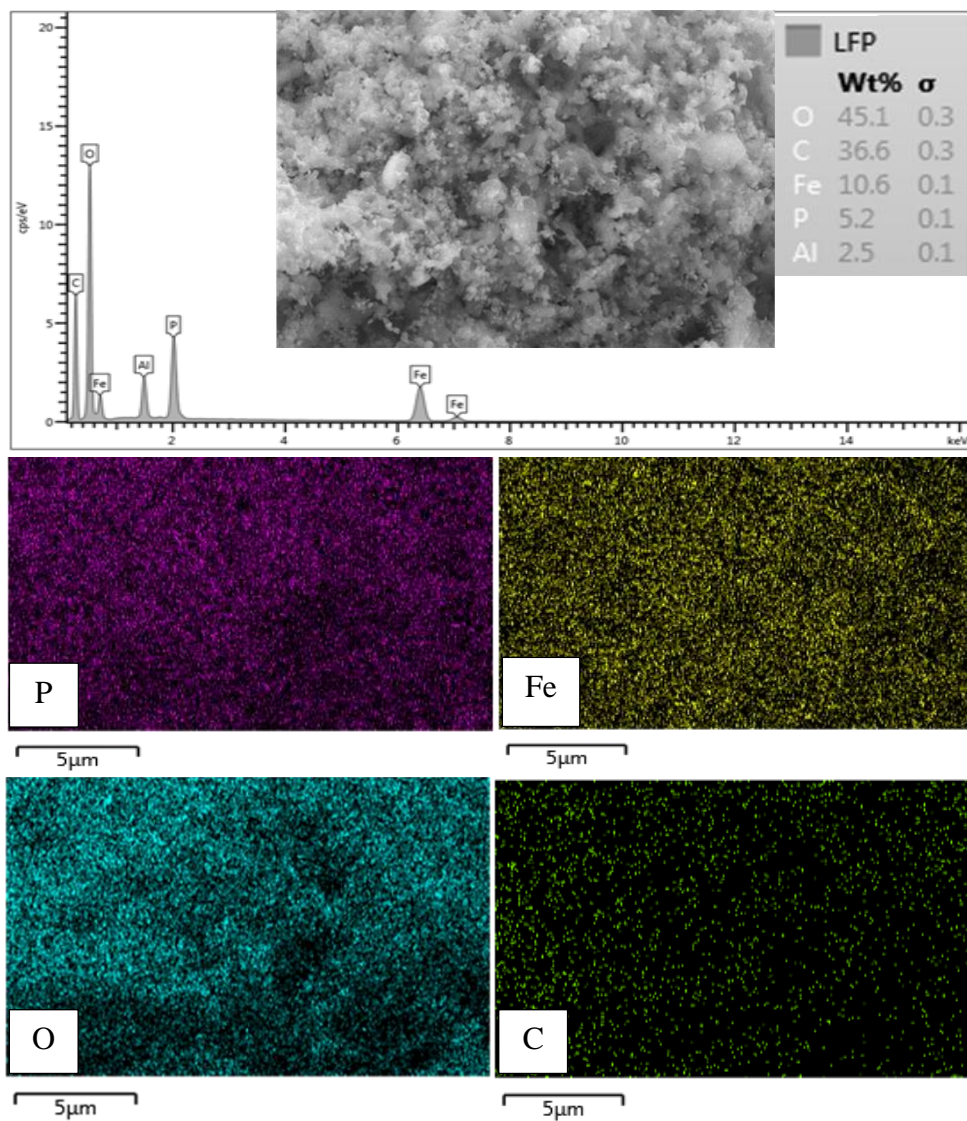
Figure 4.5 The EDX maps of LFP material for the elemental mappings
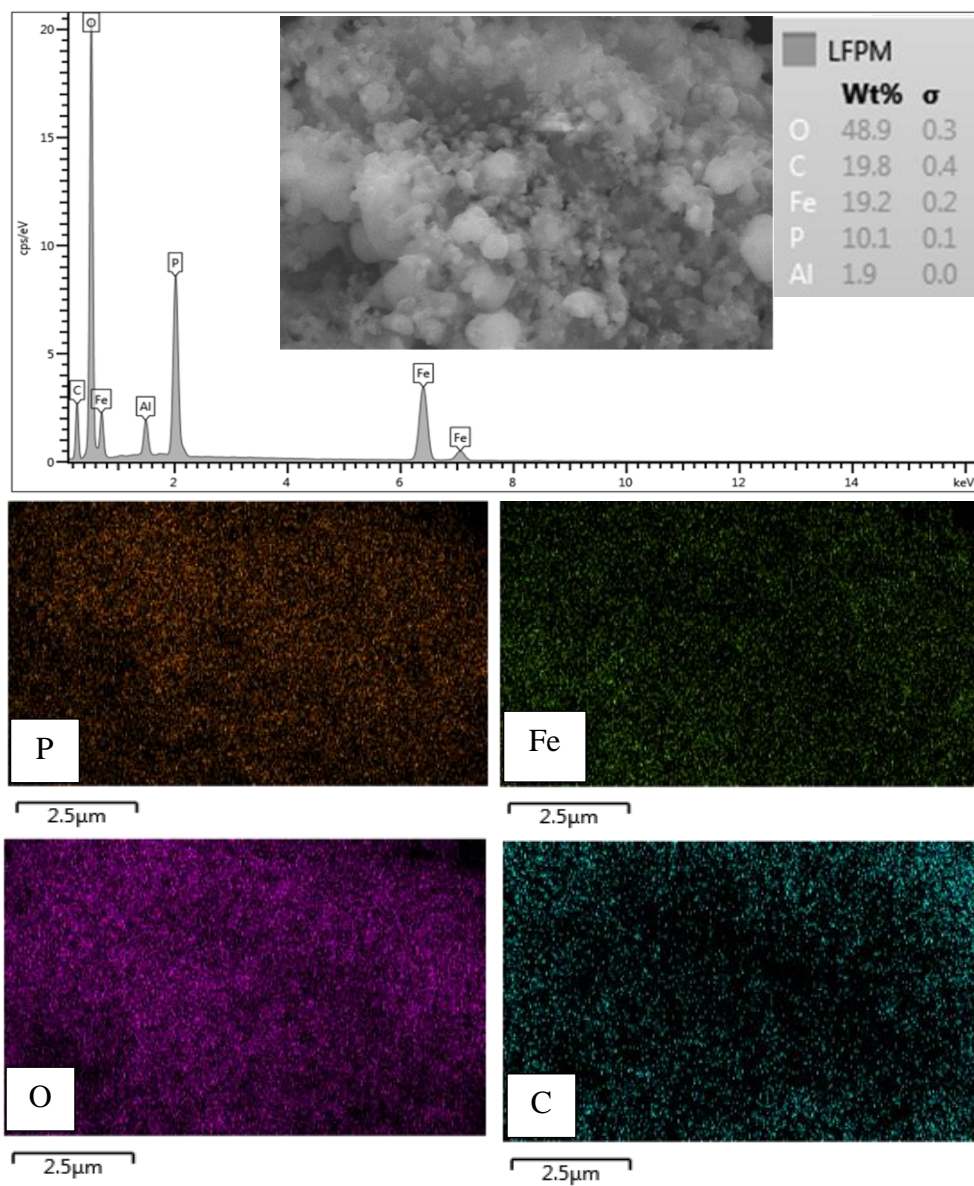
Figure 4.6 The EDX maps of LFPM material for the elemental mappings

4.2 Electrochemical Characterizations

4.2.1 Electrochemical Impedance Spectroscopy (EIS)

Figure 4.7 represents Nyquist plots of LFP electrochemical impedance spectra curves at 2.6 V, 3.1 V, and 3.4 V. A depressed semicircle in the high-frequency region corresponds to the charge transfer resistance (R_{CT}), whereas an inclined line in the low-frequency region corresponds to Warburg impedance or lithium-ion diffusion resistance [150, 190]. As seen in the spectrum, the high-frequency impedance of the LFP material electrode decreases as Li deintercalation progresses. High-frequency impedance is approximately 46, 48, and 51 at potentials of 2.6 V, 3.1 V, and 3.4 V, respectively.
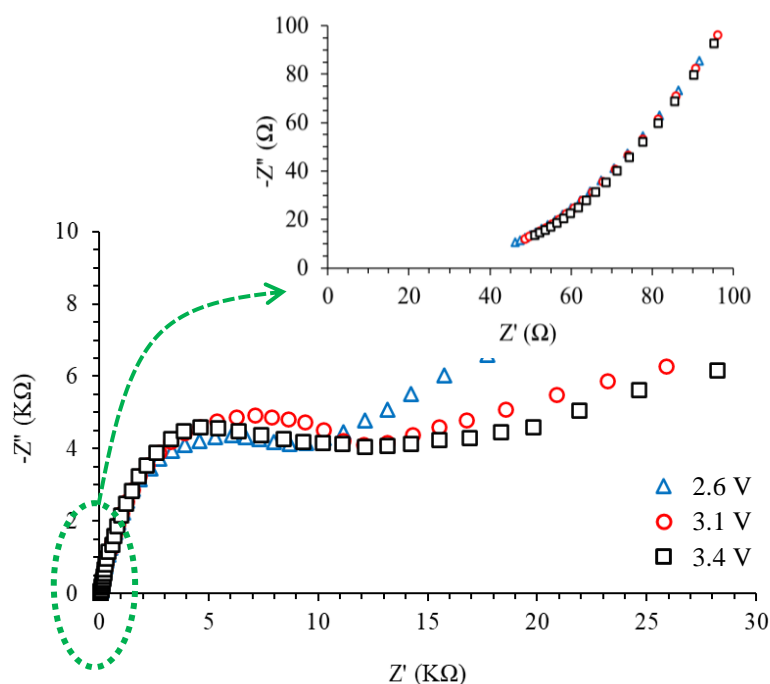
Figure 4.7 The Nyquist plots of electrochemical impedance spectra curves of LFP material at 2.6 V, 3.1 V and 3.4 V

Figure 4.8 illustrates Nyquist plots of LFPM electrochemical impedance spectra curves at 2.5 V, 3.0 V, and 3.3 V. All spectra have a depressed semicircle, which corresponds to the charge transfer resistance (R_{CT}), and an inclined line in the low frequency region, which represents Warburg impedance or lithium-ion diffusion resistance. As shown in the spectrum, the high-frequency impedance of the

LFPM material electrode decreases as Li deintercalation increases. At 5 V, 3.0 V, and 3.3 V potentials, high frequency impedance is at about 71, 75, and 79, respectively.
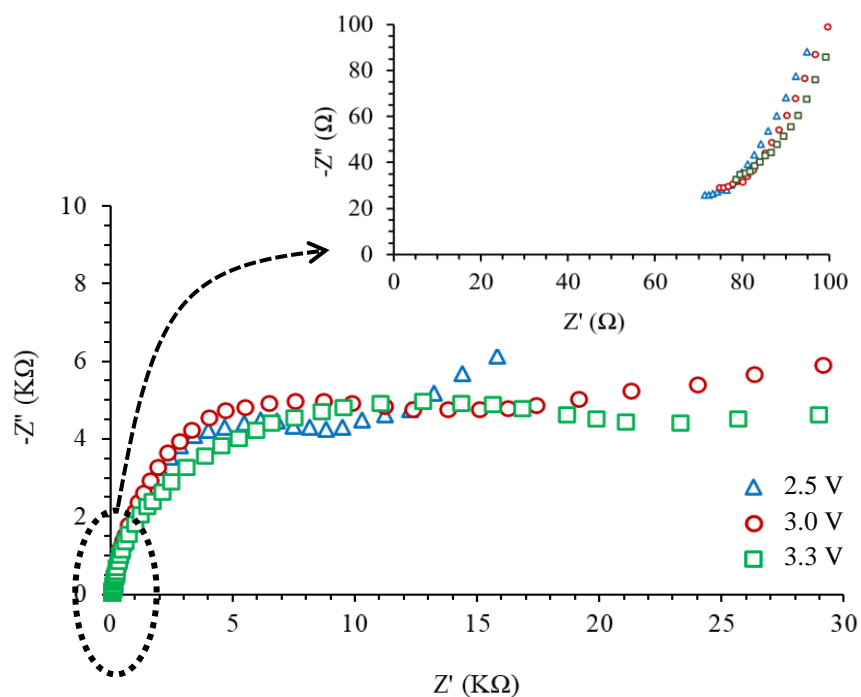
Figure 4.8 The Nyquist plots of electrochemical impedance spectra curves of LFPM material at 2.5 V, 3.0 V and 3.3 V

The high-frequency response of impedance spectroscopy is higher than expected for LFP and LFPM materials, as shown in figures 4.7 and 4.8. The reasons could be the poor distribution of carbon on the surface of LFP and LFPM materials, as well as the quality of carbon used in slurry preparation [150]. Furthermore, the high impedance is caused by the $LiPF_6$ electrolyte used during electrochemical measurements. The high frequency (HF) trend in $LiPF_6$ can result in the formation of surface LiF films. These films are resistant to Li-ion migration, and their presence likely increases the positive electrode's charge transfer resistance [150, 191]. The high resistance protects the batteries from high currents and extends battery life because less current is drawn.

4.2.2 Cyclic voltammetry (CV)

Figures 4.9 and 4.10 represents the CV curves of LFP and LFPM materials measured at room temperature and at a scan rate of 0.1 mV/s, respectively.
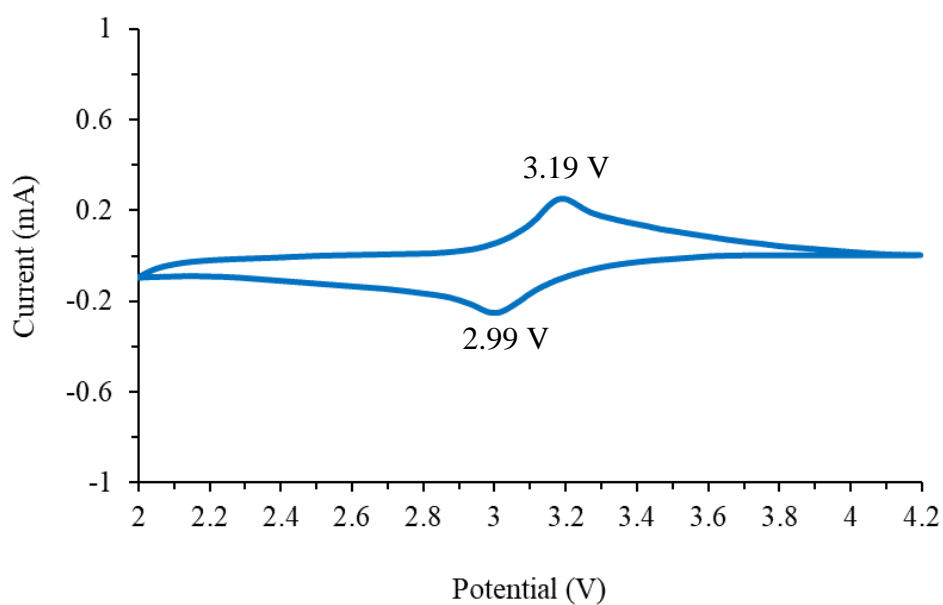
Figure 4.9 The CV curves of LFP material at scan rate of 0.1 mV/s
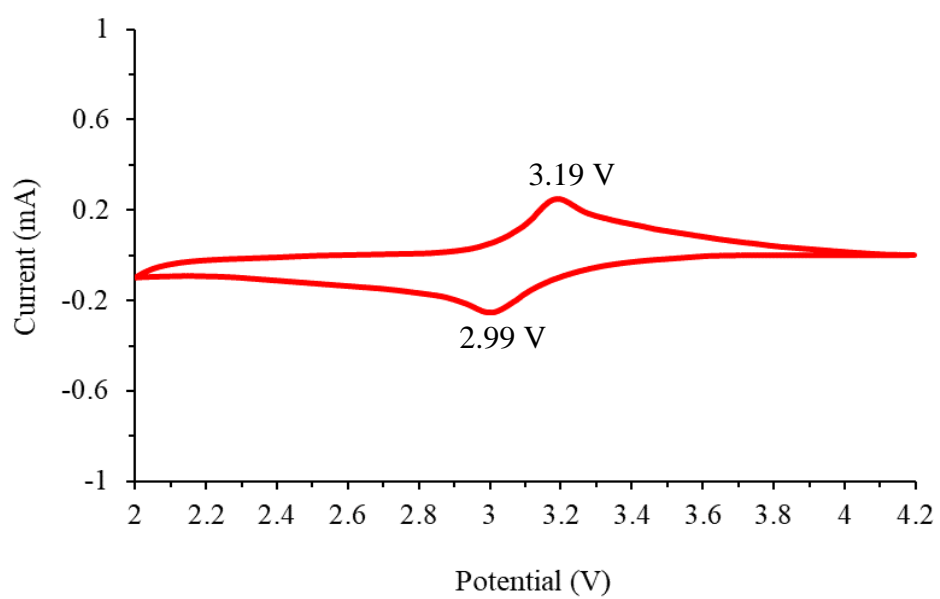
Figure 4.10 The CV curves of LFPM material at scan rate of 0.1 mV/s

The sharp oxidation and reduction peaks' symmetry confirms the good reversibility of lithium extraction-insertion reactions in LFP and LFPM materials. LFP and LFPM materials have oxidation and reduction peaks of 3.19 and 2.99 V vs. Li/Li$^+$, respectively. The symmetrical has a good symmetric and poignant shape, and a small potential separation (0.20 V). The narrow peak separation indicates that the electrodes are polarized, indicating that the electrochemical reverse reaction of Fe^{3+} to Fe^{2+} during the Li$^+$ insertion-desertion process is simple [155, 179], and that the batteries have good electrochemical performance. These redox reaction peaks correspond to lithium-ion insertion (discharge reaction) and extraction (charge reaction) from LFP and LFPM materials. The ratio of oxidation to reduction peak currents is close to 1, suggesting that lithium intercalation into and deintercalation from LiFePO$_4$/C batteries is reversible [150, 192]. The ability of lithium-ion batteries to be completely reversible during the charge and discharge process is a key feature.

Figures 4.11 and 4.12 illustrates the effect of the potential scanning rate on the CV curves of LFP and LFPM materials measured at 0.1, 0.3, and 0.5 mV/s, respectively. In both cases, the shapes of the oxidation and reduction peaks were nearly symmetrical. It is clear that increasing the scan rate leads to increased polarization, as indicated by the increase in separation between the reduction and oxidation peaks [193, 194], implying that the electrode material becomes more polarized with increasing scan rates [136]. Due to the low kinetics mechanism of lithium extraction and insertion in the LiFePO$_4$ crystal structure, the oxidation and reduction peaks increased as the scan rate increased. A possible reason could be the presence of some impurities [150, 191], or it could be due to an increase in the cell's internal impedance during charge and discharge cycling [195]. Most electrode materials demonstrate quasi-reversible processes in which the peak potential increases with increasing scan rate.
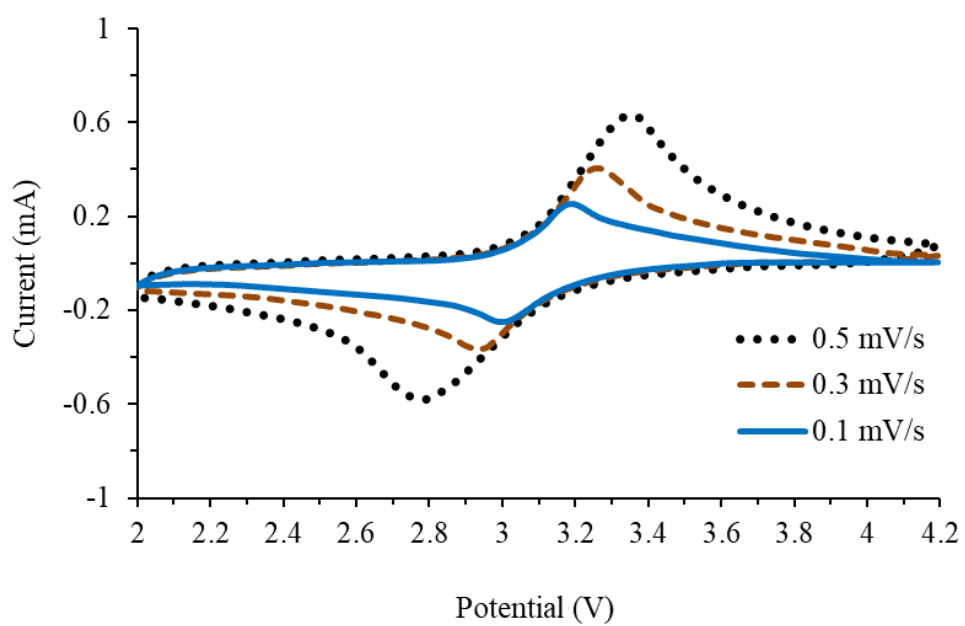
Figure 4.11 The CV curves of LFP material at scan rate of 0.1, 0.3, and 0.5 mV/s
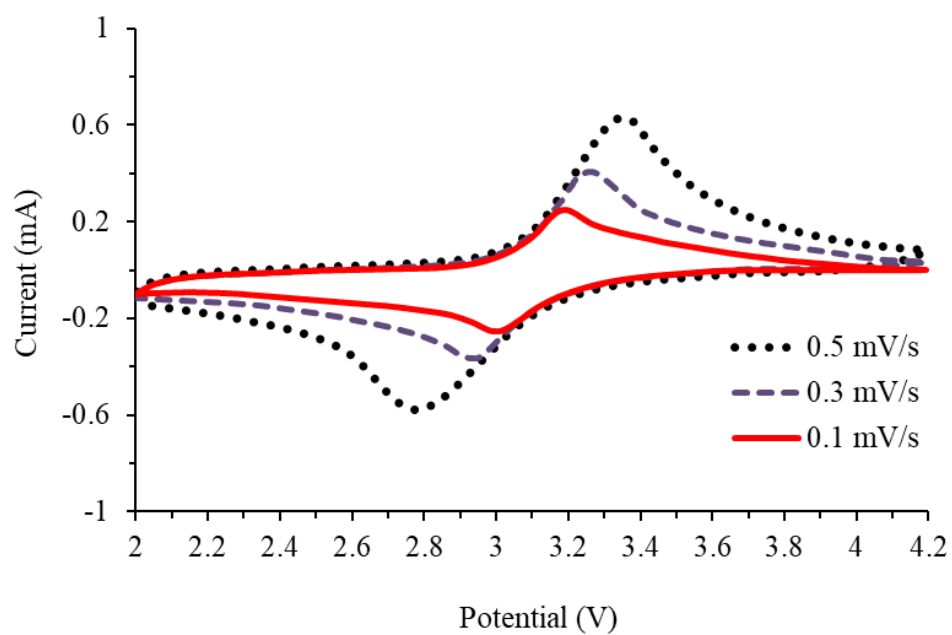
Figure 4.12 The CV curves of LFPM material at scan rate of 0.1, 0.3, and 0.5 mV/s

4.2.3 Galvanostatic charge–discharge capacity

Figures 4.13 and 4.14 illustrates the initial charge and discharge performance of cells using the LFP and LFPM materials at 1C-rate in the 2.0 to 4.2 V voltage range, respectively.
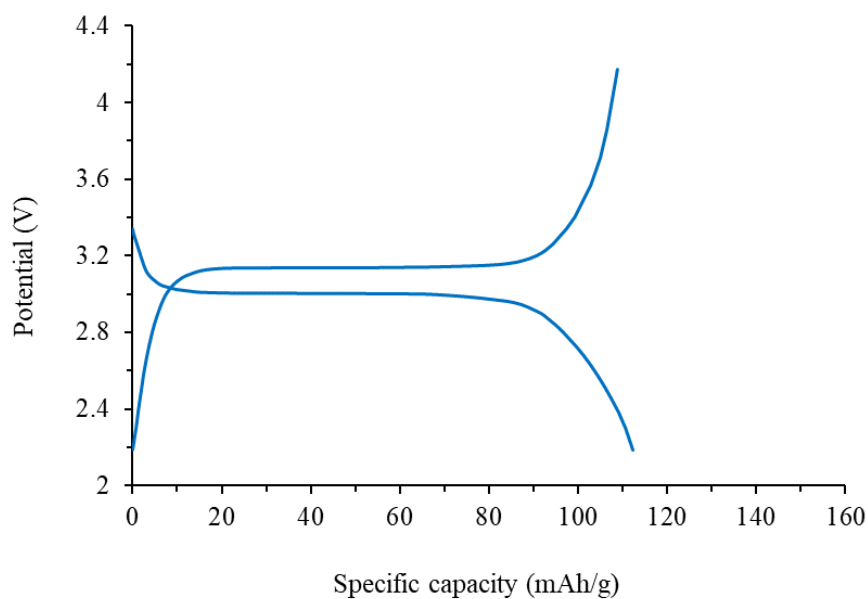
Figure 4.13 The initial charge and discharge curves of LFP material
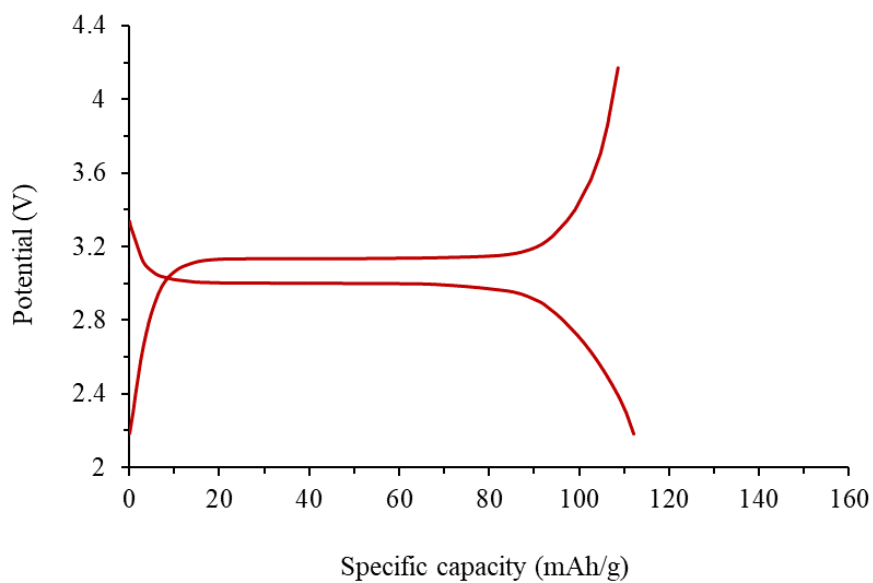
Figure 4.14 The initial charge and discharge curves of LFPM material

The LFP and LFPM materials had a flat voltage plateau at 3.04 V, indicating the two-phase nature of the lithium-ion extraction and insertion reaction between $LiFePO_4$ and $FePO_4$, which was lower than the theoretical value of 3.45 V [194, 196]. It obviously shows that LFP and LFPM materials have a lower polarization, which would be highly advantageous in practical applications. At 1C-rate, the initial charge and discharge capacities of LFP and LFPM materials were 108.72, 112.22 mAh/g and 108.77, 112.22 mAh/g, respectively. The difference between charge and discharge potential is minimal, i.e., 0.13 V and 0.12 V, respectively, indicating low polarization of the electrode and good redox reaction kinetics [38]. The cyclic curves in Figures 4.11 and 12 confirm this.

4.2.4 Specific capacity and cycle number

Figures 4.15 and 4.16 demonstrate the charge and discharge capacity curves of LFP and LFPM materials at 1C-rate. The cycling performance was also measured and plotted in Figure 4.15. The LFP materials had an initial discharge capacity of 112.22 mAh/g and, after cycling, up to 20 cycles of 107.10 mAh/g, with capacity retention of approximately 95.43%. Figure 4.16 shows that the LFPM materials had an initial discharge capacity of 112.23 mAh/g and after cycling up to 20 cycles of 112.22 mAh/g, with capacity retention of approximately 99.99%, indicating that both have excellent cycling performance with no noticeable fade [197]. This is demonstrated by microwave irradiation of activated carbon for porous structure preservation and high regeneration efficiency after many cycles [189, 198]. The cycling performance of batteries is determined by the number of charges and discharge cycles a battery can complete before losing performance.
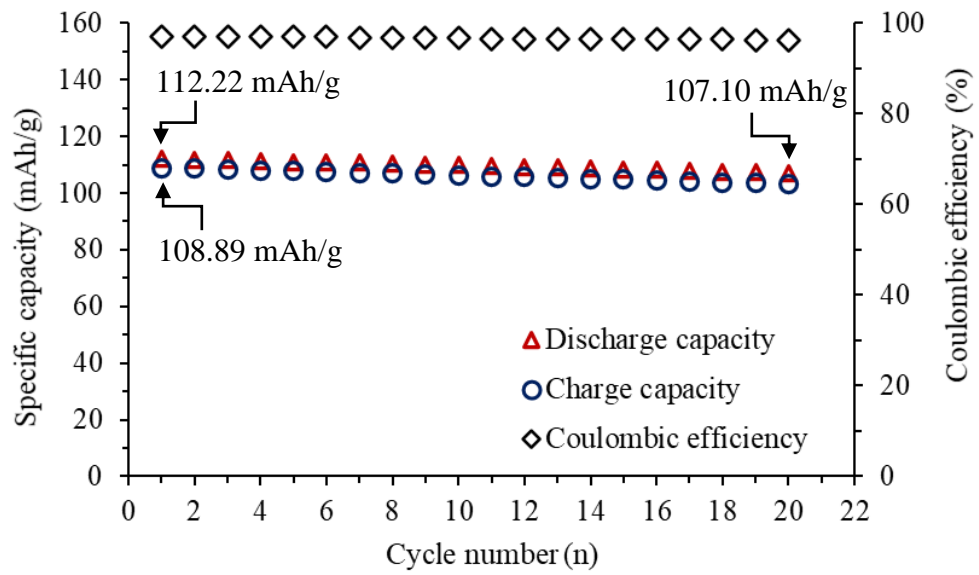
Figure 4.15 The charge and discharge capacity curves of LFP material
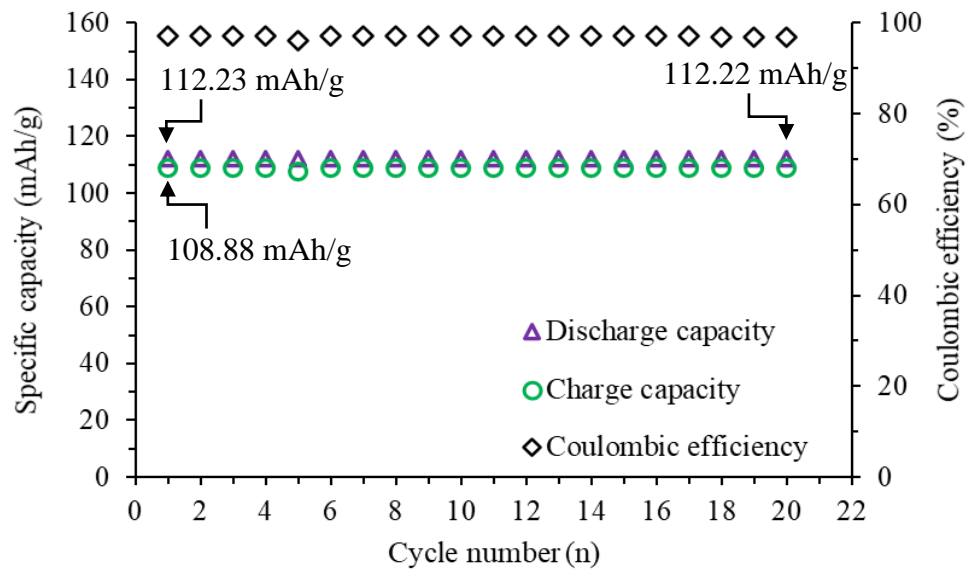
Figure 4.16 The charge and discharge capacity curves of LFPM material

The LFP materials had a reversible initial discharge capacity of 112.22 mAh/g and a charge capacity of 108.89 mAh/g with a high coulombic efficiency of 97.03%. Also, the LFPM materials demonstrated a reversible initial discharge and charge capacity of 112.23 mAh/g, and 108.88 mAh/g, respectively with a high coulombic efficiency of 97.01%. It confirms excellent electrochemical reversibility [159].

Another essential point is that the charge and discharge profiles did not change and were hardly even polarized until the final cycle. Both charge and discharge values show good reversible capacity, with a capacity retention rate of more than 97% after 20 cycles in both cases, implying excellent cyclic reversibility [159]. Batteries have a high electrochemical reaction due to their good cyclic reversibility.

4.2.5 Discharge capacity and energy density

The energy density curve and cycle number for the LFP and LFPM materials at 1C-rate of 20 cycles are shown in Figure 4.17. At the early stage and 20 cycles, the energy density of the LFP materials was 336.67 Wh/kg and 321.29 Wh/kg, respectively, whereas the LFPM demonstrated 336.68 Wh/kg and 336.66 Wh/kg, respectively. The LFPM materials have a slightly higher energy density than LFP materials. There are two main reasons for this. First, as shown in Figures 4.15 and 4.16, the energy density of batteries is normally determined by the specific capacity of the active material; the discharge capacity of LFPM materials is greater than that of LFP materials.
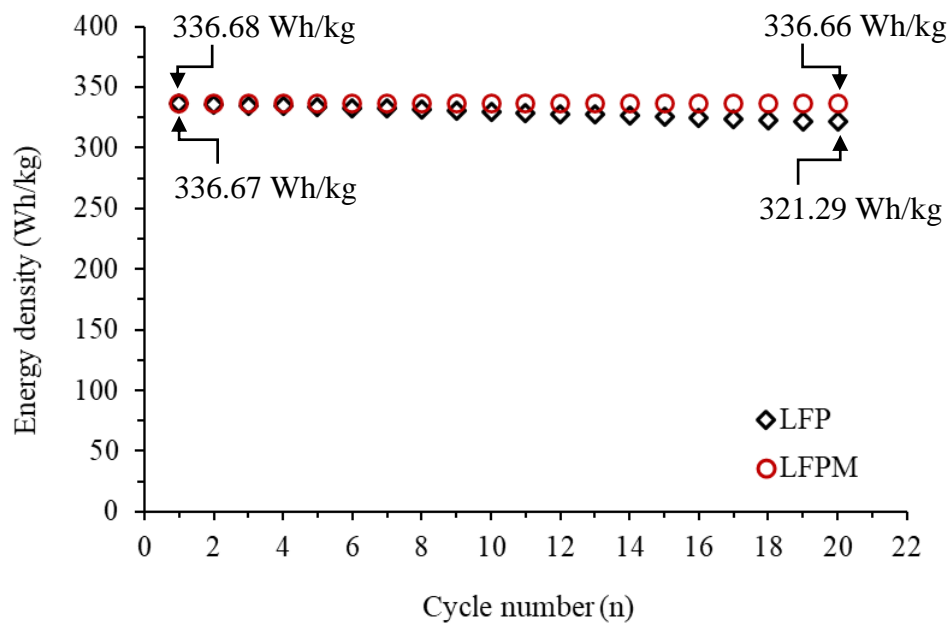
Figure 4.17 The energy density curves with cycle number for the LFP and LFPM materials

Another reason is that the conductivity of LiFePO$_4$ is a significant limiting factor in the capacity of an electrochemical power system [199, 200], which is consistent with the data in Figures 4.1 and 4.2. The conductivity of LFPM materials is greater than that of LFP materials. It suggests that the more energy stored in a given system or region of space per unit volume, the higher the energy density.

CHAPTER 5

CONCLUSIONS AND FUTURE WORK

5.1 Conclusions

As previously mentioned, the cathode material is not only the crucial component of lithium iron phosphate batteries but is also well known for its low cost, non-toxicity, safety characteristics, and environmental friendliness. On the other hand, the disadvantages are poor electronic conductivity and lower energy density. However, the synthesis method, and carbon coating methodologies can be used to improve the performance of the cathode materials. In this thesis, the microwave-assisted solid-state synthesis of cathode materials was performed using chitin, an organic carbon source for lithium iron phosphate batteries. X-ray diffraction (XRD), scanning electron microscopy (SEM), energy dispersive X-ray spectrometer (EDX), and electrochemical characterization measurements were used to investigate the physical and chemical characterization of cathode materials. The results yielded the following conclusions:

1) Solid state synthesis for cathode materials (LFP)

The element carbon from chitin was used to coat LFP materials, revealing an element of 36.60wt% carbon (C) that can be homogeneously mixed for LFP materials with an average particle size of ~300 nm. With initial charge and discharge capacities of 108.89 and 112.22 mAh/g at 1C-rate, it indicated good rate capability. Furthermore, it had a high columbic efficiency of 97.03%, and an initial energy density of 336.67 Wh/kg after cycling up to 20 cycles.

2) Microwave-assisted solid-state synthesis for cathode materials (LFPM)

The carbon element generated from chitin was used to coat LFPM materials, revealing a carbon (C) element of 19.80wt.% that can be homogeneously mixed for LFPM material, as well as an average particle size of ~380 nm. The microwave-assisted solid-state method for 5 minutes is the most appropriate time that

reveals the production of phase pure, high-quality crystalline, and the most electrical conductivity for the optimal synthesis of LFPM materials using microwave heating. The initial charge and discharge capacities of 108.88 and 112.23 mAh/g at 1C-rate, respectively, demonstrate a high columbic efficiency of 97.01%, as well as capacity retention of 99.99 % after 20 cycles and an initial generated energy density of 336.68 Wh/kg.

This thesis used a simple method of microwave-assisted solid-state synthesis of cathode materials to investigate the performance of chitin used in lithium iron phosphate batteries due to its low cost, non-toxicity, and environmental friendliness. The results show that cathode materials coated with carbon derived from chitin have greater energy storage, high cycling stability, excellent reversibility, and good electrochemical performance, all of which can be fabricated on a large scale and are commercially feasible.

5.2 Future Work

To better understand the effects of the nature of the carbon coating on the electrochemical properties of these materials, the synthesis of LFP material by carbon coating from other organic materials should be investigated. Furthermore, to improve electrochemical performance, it would be interesting to develop LFP cathode materials that are low-cost, non-toxic, and environmentally friendly, such as $LiFePO_4$.

REFERENCES

[1]   E. W. Chu and J. R. Karr, "Environmental impact: concept, consequences, measurement," *Encyclopedia of Biodiversity*, vol. 3, pp. 278-296, 2013, doi:10.1016/B978-0-12-384719-5.00253-7.

[2]   P. A. Owusu and S. Asumadu-Sarkodie, "A review of renewable energy sources, sustainability issues and climate change mitigation," *Cogent Engineering,* vol. 3, no. 1, pp. 1167990, 2016, doi:10.1080/23311916.2016.1167990.

[3]   N. E. Benti *et al.*, "The current status, challenges and prospects of using biomass energy in ethiopia," *Biotechnology for Biofuels,* vol. 14, no. 1, pp. 209, 2021, doi:10.1186/s13068-021-02060-3.

[4]   K. R. Smith *et al.*, "Energy and human health," *Annual Review Public Health,* vol. 34, pp. 159-188, 2013, doi:10.1146/annurev-publhealth-031912-114404.

[5]   M. Hannon and R. Bolton, "Energy innovation and the sustainability transition," in *Handbook of Energy Economics and Policy: Fundamentals and Applications for Engineers and Energy Planners*, A. Rubino, A. Sapio, and M. La Scala ,eds., Academic Press, 2021, ch. 8, pp. 303-362.

[6]   J. S. Basha *et al.*, "Potential of utilization of renewable energy technologies in gulf countries," *Sustainability,* vol. 13, no. 18, pp. 10261, 2021, doi:10.3390/su131810261.

[7]   G. He, J. Michalek, S. Kar, Q. Chen, D. Zhang, and J. F. Whitacre, "Utility-scale portable energy storage systems," *Joule,* vol. 5, no. 2, pp. 379-392, 2021, doi:10.1016/j.joule.2020.12.005.

[8]   A. Z. Al Shaqsi, K. Sopian, and A. Al-Hinai, "Review of energy storage services, applications, limitations, and benefits," *Energy Reports,* vol. 6, pp. 288-306, 2020, doi:10.1016/j.egyr.2020.07.028.

[9]   M. Xiao, L. Wang, F. Ji, and F. Shi, "Converting chemical energy to electricity through a three-jaw mini-generator driven by the decomposition of hydrogen peroxide," *ACS Applied Materials & Interfaces,* vol. 8, no. 18, pp. 11403-11411, 2016, doi:10.1021/acsami.6b00550.

[10] A. R. Afif, B. S. Aprillia, and W. Priharti, "Design and implementation of battery management system for portable solar panel with coulomb counting method," *IOP Conference Series: Materials Science and Engineering,* vol. 771, no. 1, pp. 012005, 2020, doi:10.1088/1757-899x/771/1/012005.

[11] J. Jiang and C. Zhang, "Performance modeling of lithium-ion batteries," in *Fundamentals and Applications of Lithium‑ion Batteries in Electric Drive Vehicles*, Wiley, 2015, ch. 2, pp. 9-42.

[12] A. Riaz, M. R. Sarker, M. H. Saad, and R. Mohamed, "Review on comparison of different energy storage technologies used in micro-energy harvesting, WSNs, low-cost microelectronic devices: challenges and recommendations," *Sensors,* vol. 21, no. 15, pp. 5041, 2021, doi:10.3390/s21155041.

[13] T. Sasaki, Y. Ukyo, and P. Novák, "Memory effect in a lithium-ion battery," *Nature Materials,* vol. 12, no. 6, pp. 569-75, 2013, doi:10.1038/nmat3623.

[14] G. E. Blomgren, "The development and future of lithium ion batteries," *Journal of The Electrochemical Society,* vol. 164, no. 1, pp. A5019-A5025, 2016, doi:10.1149/2.0251701jes.

[15] C. Liu, Z. G. Neale, and G. Cao, "Understanding electrochemical potentials of cathode materials in rechargeable batteries," *Materials Today,* vol. 19, no. 2, pp. 109-123, 2016, doi:10.1016/j.mattod.2015.10.009.

[16] C. Heubner, K. Nikolowski, S. Reuber, M. Schneider, M. Wolter, and A. Michaelis, "Recent insights into rate performance limitations of Li-ion batteries," *Batteries & Supercaps,* vol. 4, no. 2, pp. 268-285, 2021, doi:10.1002/batt.202000227.

[17] Y. Lyu *et al.*, "An overview on the advances of $LiCoO_2$ cathodes for lithium-ion batteries," *Advanced Energy Materials,* vol. 11, no. 2, pp. 2000982, 2021, doi:10.1002/aenm.202000982.

[18] J. Qian *et al.*, "Electrochemical surface passivation of $LiCoO_2$ particles at ultrahigh voltage and its applications in lithium-based batteries," *Nature Communications,* vol. 9, no. 1, pp. 4918, 2018, doi:10.1038/s41467-018-07296-6.

[19]   M. Ryou, S. Hong, M. Winter, H. Lee, and J. W. Choi, "Improved cycle lives of LiMn$_2$O$_4$ cathodes in lithium ion batteries by an alginate biopolymer from seaweed," *Journal of Materials Chemistry A,* vol. 1, no. 48, pp. 15224-15229, 2013, doi:10.1039/C3TA13514D.

[20]   V. Tsurkan, H. Krug von Nidda, J. Deisenhofer, P. Lunkenheimer, and A. Loidl, "On the complexity of spinels: magnetic, electronic, and polar ground states," *Physics Reports,* vol. 926, pp. 1-86, 2021, doi:10.1016/j.physrep.2021.04.002.

[21]   S. Mourdikoudis, R. M. Pallares, and N. T. K. Thanh, "Characterization techniques for nanoparticles: comparison and complementarity upon studying nanoparticle properties," *Nanoscale,* vol. 10, no. 27, pp. 12871-12934, 2018, doi:10.1039/C8NR02278J.

[22]   N. Mohamed and N. K. Allam, "Recent advances in the design of cathode materials for Li-ion batteries," *RSC Advances,* vol. 10, no. 37, pp. 21662-21685, 2020, doi:10.1039/D0RA03314F.

[23]   E. Riviere, A. Sari, P. Venet, F. Meniere, and Y. Bultel, "Innovative incremental capacity analysis implementation for C/LiFePO$_4$ cell state-of-health estimation in electrical vehicles," *Batteries,* vol. 5, no. 2, pp. 37, 2019, doi:10.3390/batteries5020037.

[24]   M. Swierczynski, D. Stroe, A. Stan, R. Teodorescu, and D. U. Sauer, "Selection and performance-degradation modeling of LiMO$_2$/Li$_4$Ti$_5$O$_{12}$ and LiFePO$_4$/C battery cells as suitable energy storage systems for grid integration with wind power plants: an example for the primary frequency regulation service," *IEEE Transactions on Sustainable Energy,* vol. 5, no. 1, pp. 90-101, 2013, doi:10.1109/TSTE.2013.2273989.

[25]   G. Xu, K. Zhong, J. Zhang, and Z. Huang, "First-principles study of structural, electronic and Li-ion diffusion properties of N-doped LiFePO$_4$ (010) surface," *Solid State Ionics,* vol. 281, pp. 1-5, 2015, doi:10.1016/j.ssi.2015.08.013.

[26]   Z. Ahsan *et al.*, "Recent progress in capacity enhancement of LiFePO$_4$ cathode for Li-ion batteries," *Journal of Electrochemical Energy Conversion and Storage,* vol. 18, no. 1, pp. 010801, 2020, doi:10.1115/1.4047222.

[27]   Deswita, S. Sudaryanto, H. Jodi, and E. Kartini, "The improving conductivity of LiFePO$_4$ by optimizing the calendaring process," *IOP Conference Series: Materials Science and Engineering,* vol. 432, no. 1, pp. 012059, 2018, doi:10.1088/1757-899X/432/1/012059.

[28]   S. Sarkar and S. Mitra, "Carbon coated submicron sized-LiFePO$_4$: improved high rate performance lithium battery cathode," *Energy Procedia,* vol. 54, pp. 718-724, 2014, doi:10.1016/j.egypro.2014.07.312.

[29]   H. Raj and A. Sil, "Effect of carbon coating on electrochemical performance of LiFePO$_4$ cathode material for Li-ion battery," *Ionics,* vol. 24, no. 9, pp. 2543-2553, 2018, doi:10.1007/s11581-017-2423-0.

[30]   Y. Gao, K. Xiong, H. Zhang, and B. Zhu, "Effect of Ru doping on the properties of LiFePO$_4$/C cathode materials for lithium-ion batteries," *ACS Omega,* vol. 6, no. 22, pp. 14122-14129, 2021, doi:10.1021/acsomega.1c00595.

[31]   S. Zhao, H. Ding, Y. Wang, B. Li, and C. Nan, "Improving rate performance of LiFePO$_4$ cathode materials by hybrid coating of nano-Li$_3$PO$_4$ and carbon," *Journal of Alloys and Compounds,* vol. 566, pp. 206-211, 2013, doi:10.1016/j.jallcom.2013.03.041.

[32]   Y. A. B and S. I. A, "Carbon coating of electrode materials for lithium-ion batteries," *Surface Innovations,* vol. 9, no. 2-3, pp. 92-110, 2021, doi:10.1680/jsuin.20.00044.

[33]   Y. Lu, Q. Zhang, and J. Chen, "Recent progress on lithium-ion batteries with high electrochemical performance," *Science China Chemistry,* vol. 62, no. 5, pp. 533-548, 2019, doi:10.1007/s11426-018-9410-0.

[34]   X. Yan, L. Xin, H. Wang, C. Cao, and S. Sun, "Synergetic effect of Na-doping and carbon coating on the electrochemical performances of Li$_{3-x}$Na$_x$V$_2$(PO$_4$)$_3$/C as cathode for lithium-ion batteries," *RSC Advances,* vol. 9, no. 15, pp. 8222-8229, 2019, doi:10.1039/C8RA10646K.

[35]   J. Wang and X. Sun, "Understanding and recent development of carbon coating on LiFePO$_4$ cathode materials for lithium-ion batteries," *Energy & Environmental Science,* vol. 5, no. 1, pp. 5163-5185, 2012, doi:10.1039/C1EE01263K.

[36]   E. Mohan and V. Siddhartha, "Urea and sucrose assisted combustion synthesis of LiFePO$_4$/C nano-powder for lithium-ion battery cathode application," *AIMS Materials Science,* vol. 1, pp. 191-201, 2014, doi:10.3934/matersci.2014.4.191.

[37]   J. Hagberg *et al.*, "Lithium iron phosphate coated carbon fiber electrodes for structural lithium ion batteries," *Composites Science and Technology,* vol. 162, pp. 235-243, 2018, doi:10.1016/j.compscitech.2018.04.041.

[38]   H. Kim, G. Bae, S. Lee, J. Ahn, and J. Kim, "Properties of lithium iron phosphate prepared by biomass-derived carbon coating for flexible lithium ion batteries," *Electrochimica Acta,* vol. 300, pp. 18-25, 2019, doi:10.1016/j.electacta.2019.01.057.

[39]   X. Li *et al.*, "Electrochemical property of LiFePO$_4$/C composite cathode with different carbon sources," *Rare Metals,* vol. 37, no. 9, pp. 743-749, 2018, doi:10.1007/s12598-016-0781-9.

[40]   X. Ren *et al.*, "Enhanced rate performance of the mortar-like LiFePO$_4$/C composites combined with the evenly coated of carbon aerogel," *Journal of Alloys and Compounds,* vol. 867, pp. 158776, 2021, doi:10.1016/j.jallcom.2021.158776.

[41]   J. Conder, C. Vaulot, C. Marino, C. Villevieille, and C. M. Ghimbeu, "Chitin and chitosan-structurally related precursors of dissimilar hard carbons for Na-ion battery," *ACS Applied Energy Materials,* vol. 2, no. 7, pp. 4841-4852, 2019, doi:10.1021/acsaem.9b00545.

[42]   R. Vinodh, Y. Sasikumar, H.-J. Kim, R. Atchudan, and M. Yi, "Chitin and chitosan based biopolymer derived electrode materials for supercapacitor applications: a critical review," *Journal of Industrial and Engineering Chemistry,* vol. 104, pp. 155-171, 2021, doi:10.1016/j.jiec.2021.08.019.

[43]   G. Wu, "An efficient carbon coating process applied in different synthetic routes of LiFePO$_4$ cathode materials," *International Journal of Electrochemical Science,* vol. 13, pp. 8006-8021, 2018, doi:10.20964/2018.08.07.

[44] D. Yi, X. Cui, N. Li, L. Zhang, and D. Yang, "Enhancement of electrochemical performance of LiFePO$_4$@C by Ga coating," *ACS Omega,* vol. 5, no. 17, pp. 9752-9758, 2020, doi:10.1021/acsomega.9b04165.

[45] T. V. S. L. Satyavani, A. Srinivas Kumar, and P. S. V. Subba Rao, "Methods of synthesis and performance improvement of lithium iron phosphate for high rate Li-ion batteries: a review," *Engineering Science and Technology, an International Journal,* vol. 19, no. 1, pp. 178-188, 2016, doi:10.1016/j.jestch.2015.06.002.

[46] B. Paul *et al.*, "Nucleation and growth controlled polyol synthesis of size-focused nanocrystalline LiFePO$_4$ cathode for high performance Li-ion batteries," *Journal of the Electrochemical Society,* vol. 161, no. 9, pp. A1468-A1473, 2014, doi:10.1149/2.1191409jes.

[47] Z. Yang and S. Wang, "High cycling performance cathode material: interconnected LiFePO$_4$/carbon nanoparticles fabricated by sol-gel method," *Journal of Nanomaterials,* vol. 2014, pp. 801562, 2014, doi:10.1155/2014/801562.

[48] L. He, W. Zha, and D. Chen, "Crystal growth kinetics, microstructure and electrochemical properties of LiFePO$_4$/carbon nanocomposites fabricated using a chelating structure phosphorus source," *RSC Advances,* vol. 8, no. 6, pp. 3151-3160, 2018, doi:10.1039/C7RA12029J.

[49] X. Zhengrui, L. Gao, Y. Liu, and L. Li, "Review-recent developments in the doped LiFePO$_4$ cathode materials for power lithium ion batteries," *Journal of The Electrochemical Society,* vol. 163, no. 13, pp. A2600-A2610, 2016, doi:10.1149/2.0411613jes.

[50] L. Wang, W. Guo, P. Lu, T. Zhang, F. Hou, and J. Liang, "A flexible and boron-doped carbon nanotube film for high-performance Li storage," *Frontiers in Chemistry,* vol. 7, pp. 832, 2019, doi:10.3389/fchem.2019.00832.

[51] X. Yang, D. Liu, X. Xu, X. He, and J. Xie, "Mechanism and kinetic studies on the synthesis of LiFePO$_4$ via solid-state reactions," *CrystEngComm,* vol. 15, no. 48, pp. 10648-10656, 2013, doi:10.1039/C3CE41063C.

[52]   R. Jamal, F. Xu, W. Shao, and T. Abdiryim, "The study on the application of solid-state method for synthesizing the polyaniline/noble metal (Au or Pt) hybrid materials," *Nanoscale Research Letters,* vol. 8, pp. 117, 2013, doi:10.1186/1556-276X-8-117.

[53]   Y. Ben Smida, R. Marzouki, S. Kaya, s. Erkan, M. Zid, and A. Hamzaoui, "Synthesis methods in solid-state chemistry," in *Synthesis Methods and Crystallization*, R. Marzouki, ed., IntechOpen, London, UK, 2020, ch. 2, pp. 5-21.

[54]   J. Wang, Y. Yang, and X. Liu, "Solid-state fluorescent carbon dots: quenching resistance strategies, high quantum efficiency control, multicolor tuning, and applications," *Materials Advances,* vol. 1, no. 9, pp. 3122-3142, 2020, doi:10.1039/D0MA00632G.

[55]   D. Liu *et al.*, "High-voltage lithium-ion battery using substituted LiCoPO$_4$: electrochemical and safety performance of 1.2 Ah pouch cell," *Materials,* vol. 13, no. 19, pp. 4450, 2020, doi:10.3390/ma13194450.

[56]   S. Singh, D. Gupta, V. Jain, and A. K. Sharma, "Microwave processing of materials and applications in manufacturing industries: a review," *Materials and Manufacturing Processes,* vol. 30, no. 1, pp. 1-29, 2015, doi:10.1080/10426914.2014.952028.

[57]   F. Yu *et al.*, "High electrochemical performance of LiFePO$_4$ cathode material via in-situ microwave exfoliated graphene oxide," *Electrochimica Acta,* vol. 151, pp. 240-248, 2015, doi:10.1016/j.electacta.2014.11.014.

[58]   Y. Huang, L. Wang, D. Jia, S. Bao, and Z. Guo, "Preparation and electrochemical properties of LiFePO$_4$/C nanoparticles using different organic carbon sources," *Journal of Nanoparticle Research,* vol. 15, no. 2, pp. 1459, 2013, doi:10.1007/s11051-013-1459-y.

[59]   J. Wu *et al.*, "Rapid microwave-assisted bulk production of high-quality reduced graphene oxide for lithium ion batteries," *Materialia,* vol. 13, pp. 100833, 2020, doi:10.1016/j.mtla.2020.100833.

[60]   F. Yu *et al.*, "Overwhelming microwave irradiation assisted synthesis of olivine-structured LiMPO$_4$ (M=Fe, Mn, Co and Ni) for Li-ion batteries," *Nano Energy,* vol. 3, pp. 64-79, 2014, doi:10.1016/j.nanoen.2013.10.011.

[61] P. Smecellato, R. Davoglio, S. Biaggio, N. Bocchi, and R. Rocha-Filho, "Alternative route for LiFePO$_4$ synthesis: carbothermal reduction combined with microwave-assisted solid-state reaction," *Materials Research Bulletin,* vol. 86, pp. 209-214, 2016, doi:10.1016/j.materresbull.2016.11.003.

[62] N. Nitta, F. Wu, J. T. Lee, and G. Yushin, "Li-ion battery materials: present and future," *Materials Today,* vol. 18, no. 5, pp. 252-264, 2015, doi:10.1016/j.mattod.2014.10.040.

[63] S. Verma *et al.*, "A comprehensive review on energy storage in hybrid electric vehicle," *Journal of Traffic and Transportation Engineering (English Edition),* vol. 8, no. 5, pp. 621-637, 2021, doi:10.1016/j.jtte.2021.09.001.

[64] S. B. Chikkannanavar, D. M. Bernardi, and L. Liu, "A review of blended cathode materials for use in Li-ion batteries," *Journal of Power Sources,* vol. 248, pp. 91-100, 2014, doi:10.1016/j.jpowsour.2013.09.052.

[65] D. Miranda, A. M. Almeida, S. Lanceros-Méndez, and C. M. Costa, "Effect of the active material type and battery geometry on the thermal behavior of lithium-ion batteries," *Energy,* vol. 185, pp. 1250-1262, 2019, doi:10.1016/j.energy.2019.07.099.

[66] N. Yabuuchi and S. Komaba, "Recent research progress on iron-and manganese-based positive electrode materials for rechargeable sodium batteries," *Science and Technology of Advanced Materials,* vol. 15, no. 4, pp. 043501, 2014, doi:10.1088/1468-6996/15/4/043501.

[67] J. Shin, J. K. Seo, R. Yaylian, A. Huang, and Y. S. Meng, "A review on mechanistic understanding of MnO$_2$ in aqueous electrolyte for electrical energy storage systems," *International Materials Reviews,* vol. 65, no. 6, pp. 356-387, 2020, doi:10.1080/09506608.2019.1653520.

[68] Y. Huang *et al.*, "Lithium manganese spinel cathodes for lithium-ion batteries," *Advanced Energy Materials,* vol. 11, no. 2, pp. 2000997, 2021, doi:10.1002/aenm.202000997.

[69] J. P. Pender *et al.*, "Electrode degradation in lithium-ion batteries," *ACS Nano,* vol. 14, no. 2, pp. 1243-1295, 2020, doi:10.1021/acsnano.9b04365.

[70] D. Deng, "Li-ion batteries: basics, progress, and challenges," *Energy Science & Engineering,* vol. 3, no. 5, pp. 385-418, 2015, doi:10.1002/ese3.95.

[71] N. G. P *et al.*, "Effective and environmentally friendly recycling process designed for LiCoO$_2$ cathode powders of spent Li-ion batteries using mixture of mild organic acids," *Waste Management,* vol. 78, pp. 51-57, 2018, doi:10.1016/j.wasman.2018.05.030.

[72] S. Violaine *et al.*, "Respiratory hazard of Li-ion battery components: elective toxicity of lithium cobalt oxide (LiCoO$_2$) particles in a mouse bioassay," *Archives of Toxicology,* vol. 92, no. 5, pp. 1673-1684, 2018, doi:10.1007/s00204-018-2188-x.

[73] H. Pinegar, R. Marthi, P. Yang, and Y. R. Smith, "Reductive thermal treatment of LiCoO$_2$ from end-of-life lithium-ion batteries with hydrogen," *ACS Sustainable Chemistry & Engineering,* vol. 9, no. 22, pp. 7447-7453, 2021, doi:10.1021/acssuschemeng.0c08695.

[74] S. Dühnen, J. Betz, M. Kolek, R. Schmuch, M. Winter, and T. Placke, "Toward green battery cells: perspective on materials and technologies," *Small Methods,* vol. 4, no. 7, pp. 2000039, 2020, doi:10.1002/smtd.202000039.

[75] B. E. Murdock, K. E. Toghill, and N. Tapia-Ruiz, "A perspective on the sustainability of cathode materials used in lithium-ion batteries," *Advanced Energy Materials,* vol. 11, no. 39, pp. 2102028, 2021, doi:10.1002/aenm.202102028.

[76] E. Antipov, N. Khasanova, and S. Fedotov, "Perspectives on Li and transition metal fluoride phosphates as cathode materials for a new generation of Li-ion batteries," *IUCrJ,* vol. 2, pp. 85-94, 2015, doi:10.1107/S205225251402329X.

[77] P. Xiao and G. Henkelman, "Kinetic monte carlo study of Li intercalation in LiFePO$_4$," *ACS Nano,* vol. 12, no. 1, pp. 844-851, 2018, doi:10.1021/acsnano.7b08278.

[78] S. Liu, P. Yan, H. Li, X. Zhang, and W. Sun, "One-step microwave synthesis of micro/nanoscale LiFePO$_4$/graphene cathode with high performance for lithium-ion batteries," *Frontiers in Chemistry,* vol. 8, pp. 104, 2020, doi:10.3389/fchem.2020.00104.

[79]   X. Ming, R. Wang, T. Li, X. Wu, L. Yuan, and Y. Zhao, "Preparation of micro–nano-structured $FePO_4 \cdot 2H_2O$ for $LiFePO_4$ cathode materials by the turbulent flow cycle method," *ACS Omega,* vol. 6, no. 29, pp. 18957-18963, 2021, doi:10.1021/acsomega.1c02216.

[80]   X. Wu *et al.*, "Safety issues in lithium ion batteries: materials and cell design," *Frontiers in Energy Research,* vol. 7, pp. 65, 2019, doi:10.3389/fenrg.2019.00065.

[81]   Q. Zhang *et al.*, "Incorporation of redox-active polyimide binder into $LiFePO_4$ cathode for high-rate electrochemical energy storage," *Nanotechnology Reviews,* vol. 9, pp. 1350 - 1358, 2020, doi:10.1515/ntrev-2020-0092.

[82]   S. J. An, J. Li, C. Daniel, D. Mohanty, S. Nagpure, and D. L. Wood, "The state of understanding of the lithium-ion-battery graphite solid electrolyte interphase (SEI) and its relationship to formation cycling," *Carbon,* vol. 105, pp. 52-76, 2016, doi:10.1016/j.carbon.2016.04.008.

[83]   J. Li *et al.*, "Toward low-cost, high-energy density, and high-power density lithium-ion batteries," *JOM,* vol. 69, no. 9, pp. 1484-1496, 2017, doi:10.1007/s11837-017-2404-9.

[84]   S. Xia, X. Wu, Z. Zhang, Y. Cui, and W. Liu, "Practical challenges and future perspectives of all-solid-state lithium-metal batteries," *Chem,* vol. 5, no. 4, pp. 753-785, 2019, doi:10.1016/j.chempr.2018.11.013.

[85]   L. Kong, C. Tang, H. Peng, J. Huang, and Q. Zhang, "Advanced energy materials for flexible batteries in energy storage: a review," *SmartMat,* vol. 1, no. 1, pp. 1-35, 2020, doi:10.1002/smm2.1007.

[86]   X. Shen *et al.*, "Advanced electrode materials in lithium batteries: retrospect and prospect," *Energy Material Advances,* vol. 2021, pp. 1205324, 2021, doi:10.34133/2021/1205324.

[87]   R. Liu *et al.*, "Preparation of $LiFePO_4$/C cathode materials via a green synthesis route for lithium-ion battery applications," *Materials,* vol. 11, no. 11, pp. 2251, 2018, doi:10.3390/ma11112251.

[88]   A. Manthiram, "A reflection on lithium-ion battery cathode chemistry," *Nature Communications,* vol. 11, no. 1, pp. 1550, 2020, doi:10.1038/s41467-020-15355-0.

[89]   A. M. Divakaran *et al.*, "Rational design on materials for developing next generation lithium-ion secondary battery," *Progress in Solid State Chemistry,* vol. 62, pp. 100298, 2021, doi:10.1016/j.progsolidstchem.2020.100298.

[90]   D. Zhao and S. Li, "Regulating the performance of lithium-ion battery focus on the electrode-electrolyte interface," *Frontiers in Chemistry,* vol. 8, pp. 821, 2020, doi:10.3389/fchem.2020.00821.

[91]   M. K. Shobana, "Metal oxide coated cathode materials for Li ion batteries-a review," *Journal of Alloys and Compounds,* vol. 802, pp. 477-487, 2019, doi:10.1016/j.jallcom.2019.06.194.

[92]   J. Bisquert, "Voltage, capacitors, and batteries," in *The Physics of Solar Energy Conversion*, CRC Press, Florida, USA, 2020, ch. 3, pp. 33-58.

[93]   H. Cheng, J. G. Shapter, Y. Li, and G. Gao, "Recent progress of advanced anode materials of lithium-ion batteries," *Journal of Energy Chemistry,* vol. 57, pp. 451-468, 2021, doi:10.1016/j.jechem.2020.08.056.

[94]   H. Zhang, L. Wang, H. Li, and X. He, "Criterion for identifying anodes for practically accessible high-energy-density lithium-ion batteries," *ACS Energy Letters,* vol. 6, no. 10, pp. 3719-3724, 2021, doi:10.1021/acsenergylett.1c01713.

[95]   R. Ding *et al.*, "Carbon anode materials for rechargeable alkali metal ion batteries and in-situ characterization techniques," *Frontiers in Chemistry,* vol. 8, pp. 607504, 2020, doi:10.3389/fchem.2020.607504.

[96]   Q. Liu *et al.*, "Kinetically determined phase transition from stage II (LiC_{12}) to stage I (LiC_6) in a graphite anode for Li-ion batteries," *The Journal of Physical Chemistry Letters,* vol. 9, no. 18, pp. 5567-5573, 2018, doi:10.1021/acs.jpclett.8b02750.

[97]   J. Asenbauer, T. Eisenmann, M. Kuenzel, A. Kazzazi, Z. Chen, and D. Bresser, "The success story of graphite as a lithium-ion anode material – fundamentals, remaining challenges, and recent developments including silicon (oxide) composites," *Sustainable Energy & Fuels,* vol. 4, no. 11, pp. 5387-5416, 2020, doi:10.1039/D0SE00175A.

[98] H. Li, D. Yuan, P. Li, and C. He, "High conductive and mechanical robust carbon nanotubes/waterborne polyurethane composite films for efficient electromagnetic interference shielding," *Composites Part A: Applied Science and Manufacturing,* vol. 121, pp. 411-417, 2019, doi:10.1016/j.compositesa.2019.04.003.

[99] R. Borah, F. R. Hughson, J. Johnston, and T. Nann, "On battery materials and methods," *Materials Today Advances,* vol. 6, pp. 100046, 2020, doi:10.1016/j.mtadv.2019.100046.

[100] X. Dou *et al.*, "Hard carbons for sodium-ion batteries: structure, analysis, sustainability, and electrochemistry," *Materials Today,* vol. 23, pp. 87-104, 2019, doi:10.1016/j.mattod.2018.12.040.

[101] M. M. Rahman *et al.*, "Mesoporous carbon: a versatile material for scientific applications," *International Journal of Molecular Sciences,* vol. 22, no. 9, pp. 4498, 2021, doi:10.3390/ijms22094498.

[102] G. Wang, M. Yu, and X. Feng, "Carbon materials for ion-intercalation involved rechargeable battery technologies," *Chemical Society Reviews,* vol. 50, no. 4, pp. 2388-2443, 2021, doi:10.1039/D0CS00187B.

[103] Y. Xie, Y. Jin, and L. Xiang, "Understanding Mn-based intercalation cathodes from thermodynamics and kinetics," *Crystals,* vol. 7, no. 7, pp. 221, 2017, doi:10.3390/cryst7070221.

[104] P. He, H. Yu, D. Li, and H. Zhou, "Layered lithium transition metal oxide cathodes towards high energy lithium-ion batteries," *Journal of Materials Chemistry,* vol. 22, no. 9, pp. 3680-3695, 2012, doi:10.1039/C2JM14305D.

[105] T. Zhang, D. Li, Z. Tao, and J. Chen, "Understanding electrode materials of rechargeable lithium batteries via DFT calculations," *Progress in Natural Science: Materials International,* vol. 23, no. 3, pp. 256-272, 2013, doi:10.1016/j.pnsc.2013.04.005.

[106] C. daniel, D. Mohanty, J. Li, and D. Wood, "Cathode materials review," *AIP Conference Proceedings,* vol. 1597, pp. 26-43, 2014, doi:10.1063/1.4878478.

[107] J. Ling *et al.*, "Phosphate polyanion materials as high-voltage lithium-ion battery cathode: a review," *Energy & Fuels,* vol. 35, no. 13, pp. 10428-10450, 2021, doi:10.1021/acs.energyfuels.1c01102.

[108] L. Leyssens, B. Vinck, C. Van Der Straeten, F. Wuyts, and L. Maes, "Cobalt toxicity in humans-a review of the potential sources and systemic health effects," *Toxicology,* vol. 387, pp. 43-56, 2017, doi:10.1016/j.tox.2017.05.015.

[109] A. Yano, M. Shikano, A. Ueda, H. Sakaebe, and Z. Ogumi, "LiCoO$_2$ degradation behavior in the high-voltage phase transition region and improved reversibility with surface coating," *Journal of The Electrochemical Society,* vol. 164, no. 1, pp. A6116-A6122, 2016, doi:10.1149/2.0181701jes.

[110] S. Kalluri *et al.*, "Feasibility of cathode surface coating technology for high-energy lithium-ion and beyond-lithium-ion batteries," *Advanced Materials,* vol. 29, no. 48, pp. 1605807, 2017, doi:10.1002/adma.201605807.

[111] J. Lu, Z. Liu, K. Lee, and L. Lu, "LiMn$_2$O$_4$ cathode materials with large porous structure and radial interior channels for lithium ion batteries," *Electrochimica Acta,* vol. 212, pp. 553-560, 2016, doi:10.1016/j.electacta.2016.07.013.

[112] R. J. Clément, Z. Lun, and G. Ceder, "Cation-disordered rocksalt transition metal oxides and oxyfluorides for high energy lithium-ion cathodes," *Energy & Environmental Science,* vol. 13, no. 2, pp. 345-373, 2020, doi:10.1039/C9EE02803J.

[113] S. Dou, "Review and prospects of Mn-based spinel compounds as cathode materials for lithium-ion batteries," *Ionics,* vol. 21, no. 11, pp. 3001-3030, 2015, doi:10.1007/s11581-015-1545-5.

[114] N. Tolganbek, Y. Yerkinbekova, S. Kalybekkyzy, Z. Bakenov, and A. Mentbayeva, "Current state of high voltage olivine structured LiMPO$_4$ cathode materials for energy storage applications: a review," *Journal of Alloys and Compounds,* vol. 882, pp. 160774, 2021, doi:10.1016/j.jallcom.2021.160774.

[115] H. Zhao, Y. Li, D. Shen, Q. Yin, and Q. Ran, "Significantly enhanced electrochemical properties of LiMn$_2$O$_4$-based composite microspheres embedded with nano-carbon black particles," *Journal of Materials Research and Technology,* vol. 9, no. 4, pp. 7027-7033, 2020, doi:10.1016/j.jmrt.2020.05.011.

[116] F. Yu, L. Zhang, Y. Li, Y. An, M. Zhu, and B. Dai, "Mechanism studies of LiFePO$_4$ cathode material: lithiation/delithiation process, electrochemical modification and synthetic reaction," *RSC Advances,* vol. 4, no. 97, pp. 54576-54602, 2014, doi:10.1039/C4RA10899J.

[117] L. Bao *et al.*, "Progression of the silicate cathode materials used in lithium ion batteries," *Chinese Science Bulletin,* vol. 58, no. 6, pp. 575-584, 2013, doi:10.1007/s11434-012-5583-3.

[118] S. Sun *et al.*, "Accelerated aging and degradation mechanism of LiFePO$_4$/graphite batteries cycled at high discharge rates," *RSC Advances,* vol. 8, no. 45, pp. 25695-25703, 2018, doi:10.1039/C8RA04074E.

[119] N. Liu *et al.*, "Effect of gelatin concentration on the synthetize of the LiFePO$_4$/C composite for lithium ion batteries," *Journal of Alloys and Compounds,* vol. 599, pp. 127-130, 2014, doi:10.1016/j.jallcom.2014.02.020.

[120] D. H. Snydacker and C. Wolverton, "Transition-metal mixing and redox potentials in Li$_x$(M$_{1-y}$M$'_y$)PO$_4$ (M, M$'$ = Mn, Fe, Ni) olivine materials from first-principles calculations," *The Journal of Physical Chemistry C,* vol. 120, no. 11, pp. 5932-5939, 2016, doi:10.1021/acs.jpcc.6b00575.

[121] P. Xiao, Y. Cai, X. Chen, Z. Sheng, and C. Chang, "Improved electrochemical performance of LiFe$_{0.4}$Mn$_{0.6}$PO$_4$/C with Cr^{3+} doping," *RSC Advances,* vol. 7, no. 50, pp. 31558-31566, 2017, doi:10.1039/C7RA04194B.

[122] Y. Wan, Q. Zheng, and D. Lin, "Recent development of LiMnPO$_4$ as cathode materials of lithium-ion batteries," *Acta Chimica Sinica,* vol. 72, pp. 537, 2014, doi:10.6023/A14010007.

[123] J. Hu, W. Huang, L. Yang, and F. Pan, "Structure and performance of the LiFePO$_4$ cathode material: from the bulk to the surface," *Nanoscale,* vol. 12, no. 28, pp. 15036-15044, 2020, doi:10.1039/D0NR03776A.

[124] K. Vijaya Babu, L. Seeta Devi, V. Veeraiah, and K. Anand, "Structural and dielectric studies of LiNiPO$_4$ and LiNi$_{0.5}$Co$_{0.5}$PO$_4$ cathode materials for lithium-ion batteries," *Journal of Asian Ceramic Societies,* vol. 4, no. 3, pp. 269-276, 2016, doi:10.1016/j.jascer.2016.05.001.

[125] S. Brutti and S. Panero, "Recent advances in the development of LiCoPO$_4$ as high voltage cathode material for Li-ion batteries," *ACS Symposium Series,* vol. 1140, pp. 67-99, 2013, doi:10.1021/bk-2013-1140.ch004.

[126] S. Liu, P. Yan, H. Li, X. Zhang, and W. Sun, "One-step microwave synthesis of micro/nanoscale LiFePO$_4$/graphene cathode with high performance for lithium-ion batteries," *Frontiers in Chemistry,* vol. 8, pp. 104, 2020, doi:10.3389/fchem.2020.00104.

[127] D. Zhang *et al.*, "Research progress and application of PEO-based solid state polymer composite electrolytes," *Frontiers in Energy Research,* vol. 9, pp. 726738, 2021, doi:10.3389/fenrg.2021.726738.

[128] J. Hu, H. Wang, Y. Yang, Y. Li, and Q. Wu, "A highly conductive quasi-solid-state electrolyte based on helical silica nanofibers for lithium batteries," *RSC Advances,* vol. 11, no. 54, pp. 33858-33866, 2021, doi:10.1039/D1RA06803B.

[129] K. Karuppasamy *et al.*, "An efficient way to achieve high ionic conductivity and electrochemical stability of safer nonaflate anion-based ionic liquid gel polymer electrolytes (ILGPEs) for rechargeable lithium ion batteries," *Journal of Solid State Electrochemistry,* vol. 21, no. 4, pp. 1145-1155, 2017, doi:10.1007/s10008-016-3466-2.

[130] S. Kobayashi, A. Kuwabara, C. A. J. Fisher, Y. Ukyo, and Y. Ikuhara, "Microscopic mechanism of biphasic interface relaxation in lithium iron phosphate after delithiation," *Nature Communications,* vol. 9, no. 1, pp. 2863, 2018, doi:10.1038/s41467-018-05241-1.

[131] H. H. Oh and J. Joo, "Colloidal synthesis of monodisperse ultrathin LiFePO$_4$ nanosheets for Li-ion battery cathodes," *Korean Journal of Chemical Engineering,* vol. 38, no. 5, pp. 1052-1058, 2021, doi:10.1007/s11814-021-0772-x.

[132] M. Zheng, Z. Bai, Y. He, S. Wu, Y. Yang, and Z. Zhu, "Anionic redox processes in maricite-and triphylite-NaFePO$_4$ of sodium-ion batteries," *ACS Omega,* vol. 5, no. 10, pp. 5192-5201, 2020, doi:10.1021/acsomega.9b04213.

[133] F. Liu, S. Song, D. Xue, and H. Zhang, "Selective crystallization with preferred lithium-ion storage capability of inorganic materials," *Nanoscale Research Letters,* vol. 7, no. 1, pp. 149, 2012, doi:10.1186/1556-276X-7-149.

[134] Y. Orikasa *et al.*, "Phase transition analysis between LiFePO$_4$ and FePO$_4$ by in-situ time-resolved X-ray absorption and X-ray diffraction," *Journal of the Electrochemical Society,* vol. 160, pp. A3061-A3065, 2013, doi:10.1149/2.012305jes.

[135] I. Takahashi *et al.*, "Irreversible phase transition between LiFePO$_4$ and FePO$_4$ during high-rate charge-discharge reaction by operando X-ray diffraction," *Journal of Power Sources,* vol. 309, pp. 122-126, 2016, doi:10.1016/j.jpowsour.2016.01.077.

[136] Y. Hu *et al.*, "Electrochemical performance of LiFePO$_4$/C via coaxial and uniaxial electrospinning method," *Advances in Chemical Engineering and Science,* vol. 06, pp. 149-157, 2016, doi:10.4236/aces.2016.62017.

[137] A. Mauger and C. M. Julien, "Olivine positive electrodes for Li-ion batteries: status and perspectives," *Batteries,* vol. 4, no. 3, pp. 39, 2018, doi:10.3390/batteries4030039.

[138] J. Wang *et al.*, "Surface aging at olivine LiFePO$_4$: a direct visual observation of iron dissolution and the protection role of nano-carbon coating," *Journal of Materials Chemistry A,* vol. 1, no. 5, pp. 1579-1586, 2013, doi:10.1039/C2TA00521B.

[139] W. Guo, Y. Meng, Y. Hu, X. Wu, Z. Ju, and Q. Zhuang, "Surface and interface modification of electrode materials for lithium-ion batteries with organic liquid electrolyte," *Frontiers in Energy Research,* vol. 8, pp. 170, 2020, doi:10.3389/fenrg.2020.00170.

[140] Q. Ji and H. Li, "High surface area activated carbon derived from chitin for efficient adsorption of grystal violet," *Diamond and Related Materials,* vol. 118, pp. 108516, 2021, doi:10.1016/j.diamond.2021.108516.

[141] R. Kundu, P. Mahada, B. Chhirang, and B. Das, "Cellulose hydrogels: green and sustainable soft biomaterials," *Current Research in Green and Sustainable Chemistry,* vol. 5, pp. 100252, 2022, doi:10.1016/j.crgsc.2021.100252.

[142] J. Liao, B. Hou, and H. Huang, "Preparation, properties and drug controlled release of chitin-based hydrogels: an updated review," *Carbohydrate Polymers,* vol. 283, pp. 119177, 2022, doi:10.1016/j.carbpol.2022.119177.

[143] N. Iglesias, E. Galbis, C. Valencia, M. De-Paz, and J. A. Galbis, "Reversible pH-sensitive chitosan-based hydrogels. Influence of dispersion composition on rheological properties and sustained drug delivery," *Polymers,* vol. 10, no. 4, pp. 392, 2018, doi:10.3390/polym10040392.

[144] S. M. F. Kabir, P. P. Sikdar, B. Haque, M. A. R. Bhuiyan, A. Ali, and M. N. Islam, "Cellulose-based hydrogel materials: chemistry, properties and their prospective applications," *Progress in Biomaterials,* vol. 7, no. 3, pp. 153-174, 2018, doi:10.1007/s40204-018-0095-0.

[145] M. Latifi, A. Ahmad, H. Kaddami, N. Hasyareeda Hassan, R. Dieden, and Y. Habibi, "Chemical modification and processing of chitin for sustainable production of biobased electrolytes," *Polymers,* vol. 12, no. 1, pp. 207, 2020, doi:10.3390/polym12010207.

[146] M. Latifi, A. Ahmad, N. H. Hassan, H. Ben youcef, and H. Kaddami, "Towards the application of carboxymethyl chitin/ionic liquid blend as polymer electrolyte membrane for aqueous batteries," *Carbohydrate Polymers,* vol. 273, pp. 118542, 2021, doi:10.1016/j.carbpol.2021.118542.

[147] R. Hao *et al.*, "Direct chitin conversion to N-doped amorphous carbon nanofibers for high-performing full sodium-ion batteries," *Nano Energy,* vol. 45, pp. 220-228, 2018, doi:10.1016/j.nanoen.2017.12.042.

[148] Q. Jiang *et al.*, "Lignosulfonate for improving electrochemical performance of chitin derived carbon materials as a superior anode for lithium-ion batteries," *Journal of Alloys and Compounds,* vol. 885, pp. 160973, 2021, doi:10.1016/j.jallcom.2021.160973.

[149] D. Liu, Z. Han, X. Yang, S. Cheng, and J. Xie, "Preparation of SiO_x@TiO_2@N-doped carbon composite using chitin as carbon precursor for high-performance lithium storage," *Journal of Alloys and Compounds,* vol. 891, pp. 162076, 2022, doi:10.1016/j.jallcom.2021.162076.

[150] N. Karaman *et al.*, "Solid state synthesis and characterization of LiFePO$_4$/C as cathode material for Li-ion batteries," *Bulletin of the Chemists and Technologists of Bosnia and Herzegovina,* vol. 45, pp. 19-22, 2015.

[151] M. Uddin, P. K. Alaboina, and S. Cho, "Nanostructured cathode materials synthesis for lithium-ion batteries," *Materials Today Energy,* vol. 5, pp. 138-157, 2017, doi:10.1016/j.mtener.2017.06.008.

[152] P. Li *et al.*, "Extraction and separation of Fe and Ti from extracted vanadium residue by enhanced ammonium sulfate leaching and synthesis of LiFePO$_4$/C for lithium-ion batteries," *Separation and Purification Technology,* vol. 282, pp. 120065, 2022, doi:10.1016/j.seppur.2021.120065.

[153] Y. Wang, Z. Feng, J. Chen, and C. Zhang, "Synthesis and electrochemical performance of LiFePO$_4$/graphene composites by solid-state reaction," *Materials Letters,* vol. 71, pp. 54-56, 2012, doi:10.1016/j.matlet.2011.12.034.

[154] J. Gim *et al.*, "A two-step solid state synthesis of LiFePO$_4$/C cathode with varying carbon contents for Li-ion batteries," *Ceramics International,* vol. 40, no. 1, pp. 1561-1567, 2014, doi:10.1016/j.ceramint.2013.07.043.

[155] R. Liu *et al.*, "Preparation of LiFePO$_4$/C cathode materials via a green synthesis route for lithium-ion battery applications," *Materials,* vol. 11, no. 11, pp. 2251, 2018, doi:10.3390/ma11112251.

[156] Y. F. Varela, M. Vanegas Murcia, and M. E. Patarroyo, "Synthetic evaluation of standard and microwave-assisted solid phase peptide synthesis of a long chimeric peptide derived from four plasmodium falciparum proteins," *Molecules,* vol. 23, no. 11, pp. 2877, 2018, doi:10.3390/molecules23112877.

[157] A. Naik, J. Zhou, C. Gao, and L. Wang, "Microwave assisted solid state synthesis of LiFePO$_4$/C using two different carbon sources," *International Journal of Electrochemical Science,* vol. 9, pp. 6124-6133, 2014.

[158] R. Angela, H. Islam, V. Sari, C. Latif, M. Zainuri, and S. Pratapa, "Synthesis of LiFePO$_4$/C composites based on natural iron stone using a sol gel method," *AIP Conference Proceedings,* vol. 1788, no. 1, pp. 030102, 2017, doi:10.1063/1.4968355.

[159] M. Gao *et al.*, "A gelatin-based sol–gel procedure to synthesize the LiFePO$_4$/C nanocomposite for lithium ion batteries," *Solid State Ionics,* vol. 258, pp. 8-12, 2014, doi:10.1016/j.ssi.2014.01.041.

[160] Y. Zhang, P. Xin, and Q. Yao, "Electrochemical performance of LiFePO$_4$/C synthesized by sol-gel method as cathode for aqueous lithium ion batteries," *Journal of Alloys and Compounds,* vol. 741, pp. 404-408, 2018, doi:10.1016/j.jallcom.2018.01.083.

[161] C. Gao, J. Zhou, G. Liu, and L. Wang, "Synthesis of F-doped LiFePO$_4$/C cathode materials for high performance lithium-ion batteries using co-precipitation method with hydrofluoric acid source," *Journal of Alloys and Compounds,* vol. 727, pp. 501-513, 2017, doi:10.1016/j.jallcom.2017.08.149.

[162] P. Xue, Q. Qin, and G. Li, "Construction of E-pH diagram and experimental study on wet synthesis of FePO$_4$ as the precursor of cathode materials," *MATEC Web of Conferences,* vol. 355, pp. 01013, 2022, doi:10.1051/matecconf/202235501013.

[163] Y. Zhu, S. Tang, H. Shi, and H. Hu, "Synthesis of FePO$_4$·xH$_2$O for fabricating submicrometer structured LiFePO$_4$/C by a co-precipitation method," *Ceramics International,* vol. 40, no. 2, pp. 2685-2690, 2014, doi:10.1016/j.ceramint.2013.10.055.

[164] A. Ali *et al.*, "Synthesis, characterization, applications, and challenges of iron oxide nanoparticles," *Nanotechnology, Science and Applications,* vol. 9, pp. 49-67, 2016, doi:10.2147/nsa.S99986.

[165] J. Zhu *et al.*, "Solvothermal synthesis, development, and performance of LiFePO$_4$ nanostructures," *Crystal Growth & Design,* vol. 13, no. 11, pp. 4659-4666, 2013, doi:10.1021/cg4013312.

[166] X. Qin, X. Wang, H. Xiang, J. Xie, J. Li, and Y. Zhou, "Mechanism for hydrothermal synthesis of LiFePO$_4$ platelets as cathode material for lithium-ion batteries," *The Journal of Physical Chemistry C,* vol. 114, no. 39, pp. 16806-16812, 2010, doi:10.1021/jp104466e.

[167] C. Nan, J. B. Lu, C. Chen, Q. Peng, and Y. Li, "Solvothermal synthesis of lithium iron phosphate nanoplates," *Journal of Materials Chemistry,* vol. 21, pp. 9994-9996, 2011, doi:10.1021/cg4013312.

[168] A. Sarmadi, S. M. Masoudpanah, and S. Alamolhoda, "L-Lysine-assisted solvothermal synthesis of hollow-like structure $LiFePO_4$/C powders as cathode materials for Li-ion batteries," *Journal of Materials Research and Technology,* vol. 15, pp. 5405-5413, 2021, doi:10.1016/j.jmrt.2021.11.002.

[169] Y. Li, L. Wang, K. Zhang, Y. Yao, and L. Kong, "Optimized synthesis of $LiFePO_4$ cathode material and its reaction mechanism during solvothermal," *Advanced Powder Technology,* vol. 32, no. 6, pp. 2097-2105, 2021, doi:10.1016/j.apt.2021.04.019.

[170] M. Talebi-Esfandarani and O. Savadogo, "Synthesis and characterization of Pt-doped $LiFePO_4$/C composites using the sol–gel method as the cathode material in lithium-ion batteries," *Journal of Applied Electrochemistry,* vol. 44, pp. 555-562, 2014, doi:10.1007/s10800-014-0675-1.

[171] F. Fathollahi, M. Javanbakht, H. Omidvar, and M. Ghaemi, "Improved electrochemical properties of $LiFePO_4$/graphene cathode nanocomposite prepared by one-step hydrothermal method," *Journal of Alloys and Compounds,* vol. 627, pp. 146-152, 2015, doi:10.1016/j.jallcom.2014.12.025.

[172] C. Chen, G. Liu, Y. Wang, J. Li, and H. Liu, "Preparation and electrochemical properties of $LiFePO_4$/C nanocomposite using $FePO_4 \cdot 2H_2O$ nanoparticles by introduction of $Fe_3(PO_4)_2 \cdot 8H_2O$ at low cost," *Electrochimica Acta,* vol. 113, pp. 464-469, 2013, doi:10.1016/j.electacta.2013.09.095.

[173] M. Islam, M. S. Yoon, Y. M. Park, and S. C. Ur, "Solid state synthesis of $LiFePO_4$/C: using low cost materials," *Journal of Ceramic Processing Research,* vol. 16, pp. 218-222, 2015, doi:10.36410/jcpr.2015.16.2.218.

[174] C. J. Jafta, M. K. Mathe, N. Manyala, W. D. Roos, and K. I. Ozoemena, "Microwave-assisted synthesis of high-voltage nanostructured $LiMn_{1.5}Ni_{0.5}O_4$ spinel: Tuning the Mn^{3+} content and electrochemical performance," *ACS Applied Materials & Interfaces,* vol. 5, no. 15, pp. 7592-7598, 2013, doi:10.1021/am401894t.

[175] M. Alipour, C. Ziebert, F. V. Conte, and R. Kizilel, "A review on temperature-rependent electrochemical properties, aging, and performance of lithium-ion cells," *Batteries,* vol. 6, no. 3, pp. 35, 2020. doi:10.3390/Batteries6030035.

[176] M. Razi, Z. H. Che Daud, Z. Asus, I. Mazali, M. Ardani, and M. Hamid, "A review of internal resistance and temperature relationship, state of health and thermal runaway for lithium-ion battery beyond normal operating condition," *Journal of Advanced Research in Fluid Mechanics and Thermal Sciences,* vol. 88, pp. 123-132, 2021, doi:10.37934/arfmts.88.2.123132.

[177] H. Raj and A. Sil, "PEDOT:PSS coating on pristine and carbon coated $LiFePO_4$ by one-step process: the study of electrochemical performance," *Journal of Materials Science: Materials in Electronics,* vol. 30, pp. 13604-13616, 2019, doi:10.1007/s10854-019-01730-1.

[178] A. Kulka, A. Milewska, W. Zając, K. Świerczek, E. Hanc, and J. Molenda, "Possibility of modification of phospholivine by substitution in Li sublattice," *Solid State Ionics,* vol. 225, pp. 575-579, 2012, doi:10.1016/j.ssi.2012.02.027.

[179] Q. Zhang *et al.*, "Engineering 3D bicontinuous hierarchically macro-mesoporous $LiFePO_4$/C nanocomposite for lithium storage with high rate capability and long cycle stability," *Scientific Reports,* vol. 6, no. 1, pp. 25942, 2016, doi:10.1038/srep25942.

[180] X. Huang, "Effect of carbon coating on the properties and electrochemical performance of $LiFePO_4$/C composites by vacuum decomposition method," *International Journal of Electrochemical Science,* vol. 12, pp. 7183-7196, 2017, doi:10.20964/2017.08.77.

[181] J. A. Österreicher, C. Simson, A. Großalber, S. Frank, and S. Gneiger, "Spatial lithium quantification by backscattered electron microscopy coupled with energy-dispersive x-ray spectroscopy," *Scripta Materialia,* vol. 194, pp. 113664, 2021, doi:10.1016/j.scriptamat.2020.113664.

[182] P. Hovington *et al.*, "Can we detect Li K x-ray in lithium compounds using energy dispersive spectroscopy?," *Scanning,* vol. 38, no. 6, pp. 571-578, 2016, doi:10.1002/sca.21302.

[183] M. Liu *et al.*, "Mild solution synthesis of graphene loaded with LiFePO$_4$-C nanoplatelets for high performance lithium ion batteries," *New Journal of Chemistry,* vol. 39, pp. 1094-1100, 2015, doi:10.1039/c4nj01485e.

[184] C. Li *et al.*, "Optimization of LiFePO$_4$ cathode material based on phosphorus doped graphite network structure for lithium ion batteries," *Ionics,* vol. 25, no. 3, pp. 927-937, 2019, doi:10.1007/s11581-018-2744-7.

[185] G. Cárdenas, G. Cabrera, E. Taboada, and S. P. Miranda, "Chitin characterization by SEM, FTIR, XRD, and ^{13}C cross polarization/mass angle spinning NMR," *Journal of Applied Polymer Science,* vol. 93, no. 4, pp. 1876-1885, 2004, doi:10.1002/app.20647.

[186] H. Rasti, K. Parivar, J. Baharara, M. Iranshahi, and F. Namvar, "Chitin from the mollusc chiton: extraction, characterization and chitosan preparation," *Iranian Journal of Pharmaceutical Research,* vol. 16, no. 1, pp. 366-379, 2017.

[187] A. F. Orliukas *et al.*, "SEM/EDX, XPS, and impedance spectroscopy of LiFePO$_4$ and LiFePO$_4$/C ceramics," *Lithuanian Journal of Physics,* vol. 54, pp. 106-113, 2014, doi:10.3952/physics.v54i2.2919.

[188] J. A. Menéndez *et al.*, "Microwave heating processes involving carbon materials," *Fuel Processing Technology,* vol. 91, no. 1, pp. 1-8, 2010, doi:10.1016/j.fuproc.2009.08.021.

[189] T. Kim, J. Lee, and K. Lee, "Microwave heating carbon-based solid materials," *Carbon letters,* vol. 15, pp. 15-24, 2014, doi:10.5714/CL.2014.15.1.015.

[190] W. Choi, H. Shin, J. M. Kim, J. Choi, and W. Yoon, "Modeling and applications of electrochemical impedance spectroscopy (EIS) for lithium-ion batteries," *Journal of Electrochemical Science and Technology,* vol. 11, no. 1, pp. 1-13, 2020, doi:10.33961/jecst.2019.00528.

[191] M. Koltypin, D. Aurbach, L. Nazar, and B. Ellis, "More on the performance of LiFePO$_4$ electrodes-the effect of synthesis route, solution composition, aging, and temperature," *Journal of Power Sources,* vol. 174, no. 2, pp. 1241-1250, 2007, doi:10.1016/j.jpowsour.2007.06.045.

[192] G. Bajars, J. Smits, J. Kleperis, and A. Lusis, "Characterization of LiFePO$_4$/C composite thin films using electrochemical impedance spectroscopy," *IOP Conference Series: Materials Science and Engineering,* vol. 38, pp. 012019, 2012, doi:10.1088/1757-899X/38/1/012019.

[193] N. Yesibolati *et al.*, "High performance Zn/LiFePO$_4$ aqueous rechargeable battery for large scale applications," *Electrochimica Acta,* vol. 152, pp. 505-511, 2015, doi:10.1016/j.electacta.2014.11.168.

[194] J. Come, P. L. Taberna, S. Hamelet, C. Masquelier, and P. Simon, "Electrochemical kinetic study of LiFePO$_4$ using cavity microelectrode," *Journal of The Electrochemical Society,* vol. 158, no. 10, pp. A1090, 2011, doi:10.1149/1.3619791.

[195] B. Jin, H. Gu, W. Zhang, K. Park, and G. Sun, "Effect of different carbon conductive additives on electrochemical properties of LiFePO$_4$-C/Li batteries," *Journal of Solid State Electrochemistry,* vol. 12, no. 12, pp. 1549-1554, 2008, doi:10.1007/s10008-008-0509-3.

[196] J. Vidal Laveda *et al.*, "Structure-property insights into nanostructured electrodes for Li-ion batteries from local structural and diffusional probes," *Journal of Materials Chemistry A,* vol. 6, pp. 127-137, 2017, doi:10.1039/C7TA04400C.

[197] L. Zhang *et al.*, "Capacity fading mechanism and improvement of cycling stability of the SiO anode for lithium-ion batteries," *Journal of The Electrochemical Society,* vol. 165, no. 10, pp. A2102-A2107, 2018, doi:10.1149/2.0431810jes.

[198] C. O. Ania, J. B. Parra, J. A. Menéndez, and J. J. Pis, "Microwave-assisted regeneration of activated carbons loaded with pharmaceuticals," *Water Research,* vol. 41, no. 15, pp. 3299-3306, 2007, doi:10.1016/j.watres.2007.05.006.

[199] M. S. Park, S. B. Ma, D. J. Lee, D. Im, S. Doo, and O. Yamamoto, "A highly reversible lithium metal anode," *Scientific Reports,* vol. 4, no. 1, pp. 3815, 2014, doi:10.1038/srep03815.

[200] Y. Wang, J. Zhang, J. Xue, X. Ke, and G. Liang, "LiFePO$_4$/C composites with high compaction density as cathode materials for lithium-ion batteries with high volumetric energy density," *Ionics,* vol. 27, no. 11, pp. 4687-4694, 2021, doi:10.1007/s11581-021-04078-x.

VITAE

Name   Mr. Ekawat Ratchai
Student ID   6110930011
Educational Attainment

Degree	Name of Institution	Year of Graduation
B.Sc. Physics	Mahasarakham University	2002
M.Sc. Physics	Mahasarakham University	2006

Scholarship Awards during Enrolment

Scholarship supported by Graduate School, PSU, Hatyai Campus

Scholarship supported by Faculty of Engineering, PSU, Hatyai Campus